ROBUST DAMPING CONTROL OF POWER SYSTEMS WITH FACTS

by

Jingchao Deng

A thesis submitted to
The University of Birmingham
for the degree of
DOCTOR OF PHILOSOPHY

School of Electronic,
Electrical and Computer Engineering
The University of Birmingham
March 2014

To my wife and parents

ACKNOWLEDGEMENTS

Foremost, I would like to express my sincere gratitude to my supervisor Prof. Xiao-Ping Zhang, for his invaluable guidance and enthusiastic support during my PhD study. I appreciate his professionalism and dedication in research studies, and it is a great experience to work under his supervision.

I am also grateful to my colleagues Dr. Gan Li, Dr. Zhou Li, Dr Dechao Kong, Dr. Xuan Yang, Mr. Suyang Zhou, Ms. Rui Shi, Mr. Jianing Li, Mr. Puyu Wang and Ms. Na Deng for their advices and assistance.

I would also like to thank my family for the support they provided me through my entire life and in particular, I must acknowledge my wife and best friend, Can Li, without whose love and encouragement, I would not have finished this thesis.

ABSTRACT

Power systems are under greater stress today due to the rapid growing demand and market-oriented activities. Operation of the existing system networks is gradually approaching their transmission limits and this raises a lot of stability problems which could potentially result in series consequences. The advent of FACTS provides new solutions to the reinforcement of the existing networks. Furthermore, the integration of FACTS also creates additional opportunities for the enhancement of system dynamic stability.

This thesis presents the robust damping control of power systems with FACTS for the purpose of improving system small-signal dynamic stability. A Novel BMI-based methodology is proposed for the design of robust FACTS damping controllers. Different from most of the existing method, the proposed method is capable of managing multiple control objectives under several preselected operating points which could guarantee controller robustness in a broader range. The generality and feasibility of the proposed method is validated by controller designs on a two-area four-generator system and a five-area 16-generator 68-bus system with different FACTS devices.

As an extension of the proposed BMI-based method, a coordinated design approach for multiple FACTS damping controllers is developed to address the damping problem with respect to multiple dominant oscillatory modes in large interconnected power systems. To reduce the adverse interactions between different FACTS devices, multiple SISO controllers are designed in a sequential manner with cautiously selected feedback signals. The coordinated design approach is then applied on a five-area 16-generator 68-bus system with an SVC and a TCSC to evaluate its effectiveness.

TABLE OF CONTENTS

LIST OF FIGURES

LIST OF TABLES

LIST OF ABBREVIATIONS

AVR	Automatic Voltage Regulator
BMI	Bilinear Matrix Inequality
DPFC	Distributed Power Flow Controller
FACTS	Flexible AC Transmission System
HVDC	High Voltage Direct Current
IPFC	Interline Power Flow Controller
LMI	Linear Matrix Inequality
LTI	Linear Time Invariant
MIMO	Multiple-Input and Multiple-Output
MISO	Multiple-Input and Single-Output
PMU	Phasor Measurement Unit
PSS	Power System Stabilizer
RTDS	Real-Time Digital Simulator
SISO	Sinlge-Input and Single-Output
SMIB	Single Machine Infinite Bus
SSSC	Static Synchronous Series Compensator
STATCOM	Static Synchronous Compensator
SVC	Static VAR Compensator
TCR	Thyristor Controlled Reactor
TCSC	Thyristor Controlled Series Compensator
TPSC	Thyristor Protected Series Compensator
TSC	Thyristor Switched Capacitor
TSR	Thyristor Switched Reactor
UPFC	Unified Power Flow Controller
VSC	Voltage Source Converter
WAMS	Wide-Area Measurement System

CHAPTER 1 INTRODUCTION

1.1. Research Background

1.1.1. Demand and Generation of Electric Power

With the rapid development of the social economy and science technology, the demand of the electric power is greater today than ever before. Because of the excessive exploitation and utilization of coal and natural gas, the shortage of the energy reserve has been widely recognized. For electric power industry, the depletion trend of primary energy resource is becoming a tremendous threat to sustainably maintain the increasing electric power demand of our highly-electrified human civilization. Besides, the concept of carbon emission reduction has drawn a lot attention during the last ten years, it is known that the burning of coal, fossil oil and natural gas in electric power generation is one of the major causes of the greenhouse gas emission [1].

The electric power industry is undergoing great challenges to deal with the energy shortage and carbon emission reduction problems. A lot of researches and developments have been conducted to improve the combustion ratio of the traditional fuels, however, this will not radically resolve the problems. Therefore, it is necessary to find an effective and sustainable way to address the energy problems in the long term. During the last few decades, the energy

resource structure of electric power generation was gradually changing, new types of energy resources such as nuclear energy and marine energy were applied in electric power generation, despite the fact that traditional energy resources such as coal and natural gas still dominate the market.

Among all the new energy resources, the nuclear energy is one of the most promising substitutions of the traditional energy resource; however, its potential risks are huge as well. On 11 March 2011, the Fukushima Daiichi nuclear plant was seriously damaged by an earthquake [2]. Three of the six nuclear reactors were melted down in the catastrophic incident resulting in large-area radiation exposure, and the contamination may affect several generations of people.

Compared with the nuclear energy, the renewable energy seems to be a better candidate for future electric power generation in terms of operation security. Renewable energies such as wind and solar energy are considered to be safe, clean and most importantly sustainable. Thanks to the technological developments in relevant areas, the benefits of the renewable energies are now widely recognized, and the utilization of renewable energies are now on a fast track. Take wind energy for example. The global installation capacity of wind energy is only 24.3GW in 2001 [3], and this value has been increased to 199.7GW by the end of 2010. By the end of 2013, the worldwide installation capacity of wind energy is approximately 318GW [4].

As compared with central European continent, the UK is rich in wind energy. The current installation capacity of all on-shore and off-shore wind farms in the UK is 10.7GW (by the first quarter of 2014) [5] and this number has doubled during the last three years; yet, it is still continuously increasing rapidly. According to [6], by 2020, the UK is expected to have approximately 30% of the electric power demand provided by renewable energy and the total

installation capacity of wind energy will be 25.7GW, in which, 16.6GW will be generated from off-shore wind farms.

An estimation of electric power generation in the UK to the year of 2050 is shown in Figure 1-1. It is clear that the nuclear and wind energy will become the major energy resources for future electric power generation in the UK and the utilization of coal and gas will be greatly reduced [7].

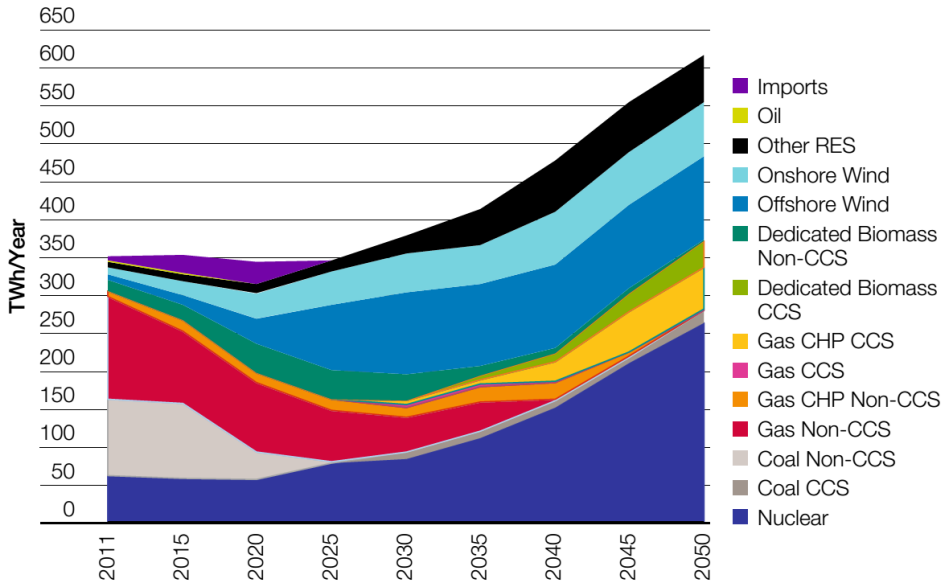

Figure 1-1 Electric power generation to 2050 in the UK [7]

1.1.2. Transmission System Reinforcement

The reinforcement of the existing electric power transmission system is naturally driven by the increasing electric power demand disregarding the changes of energy structures in power generation. The power transfer capability of each network in the existing transmission system is always finite and the incremental power flow will gradually push the transmission system towards its working limits.

In the UK, the backbone transmission grids were constructed in 1960s and many of the transmission lines are already working at their maximum capacity, such as the transmission corridors between England and Scotland. According to [6], the on-shore and off-shore wind generation will be tremendously increased by 2020, and most of the wind energy will be injecting into the main AC grid from northern Scotland. Correspondingly, the transferred power from Scotland to England will be significantly increased and this will apparently exceed the power transfer capability of the existing transmission system. Therefore, the reinforcement of the existing transmission system is vital in consideration of future power system operation.

The reinforcement of the existing transmission system can be realized in many ways. Building new transmission lines could obviously reduce the stress of the transmission system. However, the construction of new lines is restricted both economically and geographically. In some developed countries, the transmission system upgrade cannot be simply achieved by adding new lines due to high cost and environmental issues; while in some fast developing countries, China for instance, hundreds of newly constructed transmission lines with different voltage levels have been put into operation in the last decade, but the transmission system is still under great pressure because of the fast growing demand and the long distance of the transmission.

Thus, it is essential to find additional solutions to facilitate the upgrade and reinforcement of the existing transmission system with more flexibility and higher cost efficiency.

1.1.3. Flexible AC Transmission System

Flexible AC transmission system, also known as FACTS, is able to provide such new solutions to the upgrade and reinforcement of the existing transmission system. With the help of fast-switching power electronic components, FACTS is capable of controlling interrelated power

system parameters for different purposes. The major applications of FACTS are concluded as [8, 9]:

- Series compensation,
- Bus voltage regulation,
- Power flow control,
- Power quality improvement,
- System stability enhancement, etc.

Table 1-1 shows the classification of the existing FACTS devices. According to their connection styles to the power system, FACTS can be broadly divided into three categories: series-connected devices, shunt-connected devices and series-shunt-connected devices; while, according to their internal structures, FACTS can be classified as thyristor-valve based devices and VSC (voltage-source-converter) based devices.

Table 1-1 Classification of FACTS devices

FACTS devices		
	Thyristor-valve based	**VSC based**
Shunt	SVC	STATCOM
Series	TCSC/TPSC	SSSC
Series-shunt	DPFC	UPFC/IPFC

Series-connected FACTS devices are usually used for series compensation which could effectively reduce the impedance of the transmission line, and as a result, the power flow transferred through the line can be accordingly increased. The most widely used series-connected FACTS device is TCSC (thyristor controlled series compensator) and it has already been applied in many practical projects. According to [6], the first TCSC project in the UK will be commissioning by 2014; it is aimed to increase the capacity of the two backbone

transmission corridors between England and Scotland from 3.3GW to 4.4GW.

Shunt-connected FACTS devices are usually used for voltage regulation. With the control of certain fast-switching power electronic components, the susceptance of the shunt device can be continuously controlled, hence the bus voltage can be regulated. SVC (static var compensator) and STATCOM (static synchronous compensator) are two commonly used shunt-connected FACTS devices and they are usually installed on heavily loaded areas of the system to provide voltage support.

Series-shunt-connected FACTS devices are developed for the purpose of dynamic power flow control and typical devices include DPFC (distributed power flow controller) and UPFC (unified power flow controller). These devices are capable of balancing the power flows in power systems by shifting the power flows from heavily loaded areas to the areas with free transmission capacity [8].

1.1.4. Stability of the FACTS Integrated Power System

As mentioned above, FACTS offers a solution to the enhancement of power system transmission capability with great flexibility. Furthermore, it is also beneficial to make use of FACTS to improve power system stability.

Power system dynamic stability can be categorized as small-signal stability and transient stability [10]. Small-signal stability defines the ability of power systems to recover to its original steady state after small disturbances without losing synchronism. In normal power system operations, small disturbances caused by random fluctuations in certain system parameters may excite power system oscillations; these oscillations are also known as low frequency oscillations since the their frequencies (0.1Hz~2.0Hz) are relatively low comparing

to the fundamental frequency of AC system (60Hz) [11]. Insufficient damping of low frequency oscillations is one of the main causes of small-signal instability; and even for a stable system, it is also important to make sure that the system has enough damping so that the settling time of the decaying oscillations can be minimized based on certain system operating requirements. The following practices are normally suggested to increase system small-signal stability [10]:

- Improve power system network topologies
- Increase real and reactive power reserve
- Improve the AVR (automatic voltage regulator) on excitation systems
- Install PSS (power system stabilizer) and FACTS supplementary damping controllers

in which, the first three approaches improve the small-signal stability of power systems inherently by reducing the electric distance between the synchronous generator and the grid; while PSS and FACTS supplementary damping controller could increase the power system damping against low frequency oscillations by the dynamic control of interrelated system parameters such as bus voltage and line power flow.

Transient stability is the ability of power system to maintain synchronism subject to large disturbances such as system fault and transmission line outage. Different from small-signal stability, the transient stability of a particular system might be disparate with respect to different disturbances and the loss of synchronism caused by transient instability usually happens within 2 to 3 seconds after the disturbance, which is much faster than that caused by small-signal instability. To improve system transient stability, the following practices are suggested [10]:

- Fast fault clearance and auto-reclose
- Increase electromagnetic power output of the generator

- Decrease mechanical power output of the prime mover

Besides, reducing electric distance can also help enhancing transient stability in a certain degree.

Failing to address the dynamic stability issues may lead to serious consequences. Take low frequency oscillation for example, the loss of synchronism caused by low frequency oscillation can result in inter-connected system separation and even wide-area blackouts. Some of the noteworthy low frequency oscillation incidents in history are summarized in Table 1-2 [12].

Table 1-2 Noteworthy low frequency oscillation incidents in history

Low frequency oscillation incident	Oscillation frequency
UK (1980)	0.50Hz
Taiwan (1984, 1989, 1990, 1991, 1992)	0.78-1.05Hz
West USA/Canada system separation (1996)	0.22Hz
Scandinavia (1997)	0.50Hz
China blackout (2003)	0.40Hz
USA blackout (2003)	0.17Hz
Italian blackout (2003)	0.55Hz

Based on different causes, low frequency oscillations can be classified as local oscillatory mode and inter-area oscillatory mode. The local oscillatory mode describes the oscillations between a single generator or a group of generators in the same area and the rest of the system with the frequency of 1.0 to 2.0Hz; while the inter-area oscillatory mode is aroused by generators or generator groups from different areas oscillating against each other with the frequency of 0.1 to 1.0Hz [11]. From Table 1-2, it should be noticed that these incidents are actually inter-area oscillations. In wide-area interconnected power systems, local oscillations can be effectively suppressed by the proper designs of AVR and PSS. However, for inter-area oscillations involving multiple areas, the regulations from the generator side could be quite limited. Therefore, it is essential to design FACTS supplementary damping controllers to mitigate the inter-area oscillations.

On the other hand, the integration of FACTS also increases the complexity of the system with potential stability hazards. For instance, the series capacitors of FACTS may cause sub-synchronous oscillations [10]. If the frequency of the oscillation is close to the natural frequency of the generator shaft, it will excite large resonance which could severely damage the synchronous machine. Besides, the dynamic control of series compensation may also affect protection systems which could result in forward and reverse overreaching [6].Therefore, how to utilize the FACTS devices to address these potential problems is also important.

In this thesis of study, research investigations are carried out for the purpose of enhancing power system dynamic stability, particularly in the scope of improving system small-signal stability with supplementary FACTS damping controllers. A detailed literature review in the area of power system damping control is presented in the next section.

1.2. Literature Review

Over the years, the power system low frequency oscillation damping control is always regarded as one of the most essential topics in small-signal stability enhancement. Based on decades of theoretical research and practical experience, it is known that the damping control can be realized with the design of supplementary control devices such power system stabilizers and FACTS supplementary damping controllers.

1.2.1. Power System Stabilizer

The historical development of PSS can be traced back to the mid of 1960s, when the excitation system control schemes with supplementary feedback signals were proposed for the first time for the damping of synchronous generator rotor oscillations [13], [14]. With the advent of high-

speed excitation systems, the power system steady-state stability and transmission capability has been largely improved. However, these excitation systems with fast-responding voltage regulators also resulted in a reduction in damping torque to the synchronous generators [15]. In order to overcome the problem mentioned above, the feedback control of excitation systems with auxiliary signals were introduced. The corresponding feedback controllers were also known as PSS.

Figure 1-2 depicts the basic working mechanism of a PSS in a block diagram. By forming a feedback control loop with a suitable input signal, the PSS is able to generate an electrical damping torque to restore the diminished damping force on the rotor of the generator [10]. The most widely used feedback input signal for PSS is the measured rotor speed deviation $\Delta\omega$ as it is most logical in consideration of producing damping torque; besides, signals such as the deviation in power flow and frequency are also considered to be effective candidates of the feedback signals [16, 17].

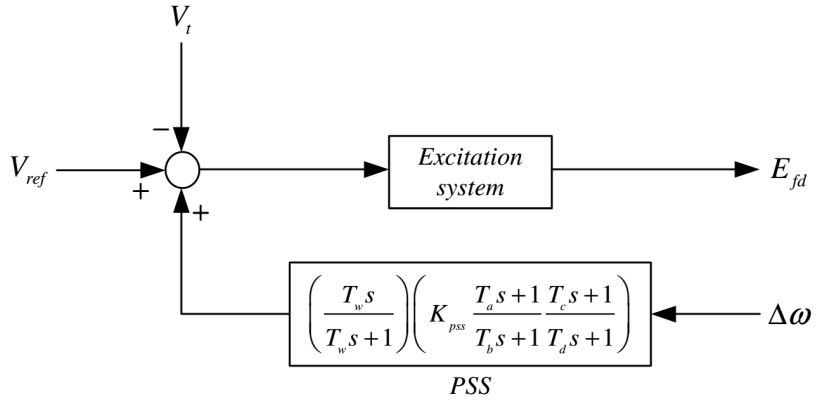

Figure 1-2 Working mechanism of PSS

The transfer function of PSS has a fixed structure which usually consists of a wash-out block and a lead-lag phase compensation block [18]. The role of the compensation block is to compensate the phase lag between the excitation system input and the produced electric torque

out; while the additional wash-out block can be considered as a band-pass filter for the purpose of removing d.c. signals so that PSS will not adjust the generator terminal voltage for very slow changes in rotor speed at off-nominal frequencies. The time constant of a wash-out block can be any value between 1 and 20s. It is suggested in [19] that a time constant of 1-2s is sufficient for the damping of local oscillatory modes and a time constant of 10s is usually selected for the damping of inter-area oscillatory modes.

PSS is originally developed for the damping of local oscillatory modes as it is locally installed on the exciter of the synchronous generator. Moreover, it could also contribute to the damping of inter-area oscillatory modes. However, the performance of PSS with regard to a local oscillatory mode and an inter-area oscillatory mode could be significantly different with respect to different load models and installation locations [20]. In order to improve the damping capability of PSS over the common low frequency band, many research studies were carried out on the design of PSS especially aimed at the damping of inter-area oscillatory modes [21-25]. Anyhow, PSS is still quite limited in terms of inter-area oscillation damping due to its local compensation mechanism.

1.2.2. Supplementary FACTS Damping Controller

The inter-area oscillatory modes are aroused by generators or generator groups oscillating against each other from different areas. From the controllability and observability point of view, the damping control of inter-area oscillations will be more effective when it is applied on certain transmission lines. Therefore, compared to the PSS units, the FACTS devices appear to be better candidates in damping inter-area oscillatory modes as they are installed on transmission lines and originally developed for the purpose of control and regulating transmission system parameters.

The damping mechanism provided by FACTS can be concluded as system parameter (active power, reactive power, voltage, etc.) modulation. The basis of active line power modulation is depicted in Figure 1-3 [26], while the modulation of other system parameters follows the same concept: When two generators SM_1 and SM_2 are oscillating at a relative angle $\Delta\varphi = \varphi_2 - \varphi_1$ and speed $\Delta\eta = \eta_2 - \eta_1$, the inter-area oscillation can be damped by the continuous control of incremental power ΔP_{mod} as the modulated line power could create a machine torque in the opposite sign to the rotor speed deviation.

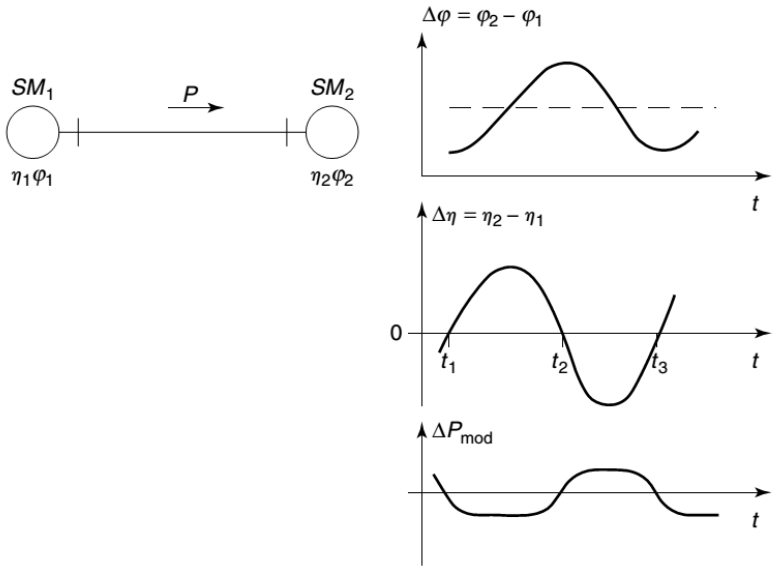

Figure 1-3 Power modulation for damping enhancement [26]

System parameter modulation can be attained by designing supplementary FACTS damping controllers. Figure 1-4 illustrates a block diagram of the FACTS internal control system with a supplementary damping controller. It can be seen that the damping control with FACTS is actually very similar to the excitation system control with PSS.

Although supplementary damping control is usually considered to be a secondary function of FACTS, its effectiveness in inter-area oscillation damping is still undeniable. With the

continuous development of FACTS techniques, more and more practical applications have included inter-area oscillation damping as an essential feature of their existing or new FACTS installations [27-31].

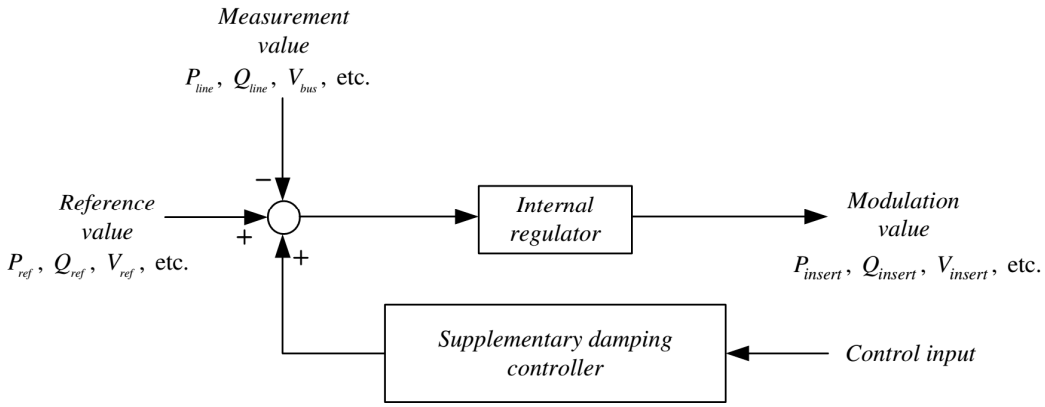

Figure 1-4 FACTS with supplementary damping controller

1.2.3. Damping Control Design Approaches

Convention Damping Control Approaches

Despite its relative simplicity, the damping torque approach is considered to be the most classic design approach for power system stability enhancement and has been presented in many textbooks of power system control and stability [10, 11]. The approach is initially proposed for the design of PSS to compensate the phase lag between the feedback signal $\Delta\omega$ and the excitation system input ΔV_t and it is fundamentally based on a Phillips-Heffron model [32, 33]. The Phillips-Heffron model is in fact a SMIB (single-machine infinite-bus) model; it only includes the dynamics of one particular generator where the PSS is installed, while the rest of the power system is represented by an infinite bus. The model very much simplifies the actual system so that classical control techniques such as root locus method can be easily applied for the design of PSS.

The SMIB system based damping torque approach could also be applied to the FACTS damping controller designs [34-36]. However, the approach is helpless to the damping of inter-area oscillations involving multiple generators, especially for complex systems with multiple dominant oscillatory modes. Because it is difficult to find the damping path and synchronizing torque for controller designs in multi-machine systems.

An approximate multi-modal decomposition method is proposed in [37]. The method is a generalization of the damping torque approach and applicable to multi-machine systems with multiple dominant oscillatory modes. But the method is only restricted to small systems and only one oscillatory mode can be taken account of in each design. Reference [38] presented a residue based damping control approach: lead-lag compensation block is designed for each weakly damped oscillatory mode to shift their eigenvalues away from the imaginary axis in order to increase system damping; a weighted summation of the residue for all dominant modes is employed so that multiple oscillatory modes could be simultaneously considered. However, the method may require multiple iterations to determine the controller parameters for the damping of multiple dominant modes.

Robust Damping Control Approaches

As most of the damping control approaches are developed on linear system models, it is vital that the designed FACTS damping controllers could actually work under a certain degree of system uncertainties. The power system low frequency oscillations are usually aroused by disturbances such as system load variations, excitation system action during off-nominal frequencies, line outage and reclosing, etc. In order to make sure that these unpredictable system activities won't compromise the controllers' damping performance, the impacts of disturbances to systems should be minimized in controller designs (i.e. disturbance rejection). Besides, it is

also required that the damping controllers should be able to function under various off-nominal operating points as the system might deviate from its original steady state after large disturbances. The study of uncertainties in mathematical model of a system is recognised as robustness [39].

The H_∞ approach was initially proposed in early 1980s to express the robustness problem regarding system uncertainties [40] which is considered to be the beginning of modern robust control. The approach deals with the minimization of the largest singular gain of certain close-loop system frequency responses so that the sensitivity between the disturbances and system outputs can be reduced, where the largest singular gain is also known as the H_∞ norm and the minimization is also considered to be the worst-case optimization [41]. The approach was then migrated to state-space models [42] and laid a solid foundation for further robustness control developments.

The H_∞ control approach has been introduced in many studies regarding robust FACTS damping controller designs. Reference [43] presented a robust TCSC damping controller design approach based on H_∞ performance; the problem is expressed as a mixed-sensitivity H_∞ optimization problem and conventionally solved via the Riccati approach [44]. However, as that has been mentioned in [45], the controller designed via the conventional Riccati approach could have problems in pole-zero cancellation due to unobservable modes.

In [46], an LMI-based H_∞ mixed-sensitivity approach was proposed for the robust design of UPFC damping controller. The LMI-based approach doesn't suffer from pole-zero cancellation and exhibits great complexity in problem formulation, by which, multiple robust control objectives including disturbance rejection and control effort optimization can be simultaneously

considered as the inequality constraints of a synthesis optimization problem. Afterwards, the LMI-based H_∞ mixed-sensitivity approach was extended to the damping controller designs involving multiple FACTS devices [47] and multiple feedback signals [48, 49] for the purpose of damping multiple oscillatory modes. In addition to the H_∞ norm, the mixed-sensitivity approach could also incorporate the H_2 norm [42]; the mixed H_2/H_∞ approach was used in [50, 51] for the coordination damping control between multiple FACTS devices (and HVDC systems). Moreover, the H_∞ norm based method is also compatible with the loop-shaping methodology [52]: A robust PSS design was proposed in [53] through a H_∞ loop shaping approach and a robust TCSC damping controller was proposed in [54] via a LMI-based H_∞ loop shaping approach. Generally, the norm bounded robust control approaches are able to guarantee robustness around a particular system operating point, but the robustness under off-nominal operating conditions is not directly dealt with.

Recently, the robust damping controller designs involving off-nominal or multiple system operating points drew significant attention. Reference [55] proposed a PSO (particle swarm optimization) [56] based robust damping control method so that multiple system operating conditions can be included in the design stage through parameter optimization. Similar concept was also adopted in [57], where the robustness problem was formulated as inter-area mode oriented pole-shifting and solved by sequential quadratic programming. Other optimization-based damping control approaches involving multiple operating points were also reported in [58-62]. A remarkable advantage of the optimization-based methods is that they are particularly useful for the coordination tuning between different FACTS devices or PSS units as the structure of the controllers to be designed can be fixed in advance. However, the formulation of the optimization problem is indeed more complicated.

Compared with the optimization-based damping control approaches mentioned above, the LMI-based approach is much more straightforward. To overcome its difficulties in extending to multi-model systems, [63] presented an LMI-based H_∞ approach with polytopic models. Another approach was proposed in [64], where the multi-model system is normally formulated but solved via a two-step NMI optimization approach. However, the control effort was not optimized in both studies; as a result, the controllers were over designed and the eigenvalues of the close-loop system poles were far away from the desired value.

The H_∞ approach is developed based on unstructured uncertainty models, where the system uncertainties are actually norm-bounded sensitivities. Based on different uncertainty modelling techniques, the robust control problem could also be in other forms [39]. Parametric uncertainty models was initially proposed in [65]. Instead of dealing with norm bounded sensitivities, the uncertainties are formulated into the system transfer function or state-space as real parameters. This creates an opportunity to carry out system robust stability studies on transfer function polynomials and the corresponding stability criterion is known as the Kharitonov theorem [66]. The polynomial based robust design method was adopted in [55, 67] for FACTS damping controller designs.

1.2.4. Wide-Area Coordination Control

Large multi-machine systems may exhibit multiple dominant oscillatory modes. A conventional local decentralised FACTS damping controller (in the form SISO) sometimes could be insufficient to damp out all the dominant modes due to low observability of the modes in feedback signal. The recent advent of PMU (phasor measurement unit) based wide-area measurement techniques now has provided new solutions to the enhancement of power system

stability [68, 69]. With the help of high-speed remote signals, the damping controller designs are no longer restricted to a local decentralized structure. In [48, 49, 55, 70], MISO (multiple-input and single-output) TCSC robust damping controllers were proposed in order to maximize the benefits of a single FACTS device in damping multiple inter-area oscillatory modes with remote signals. But the controllability of a single FACTS device to multiple oscillatory modes is still limited and the MISO controllers proposed in the above studies are only able to cover three of the four weakly damped inter-area oscillatory modes.

The coordinated damping control of multiple FACTS devices is an effective alternative in terms of damping multiple oscillatory modes. The coordination control can be broadly divided into two classes: centralized and decentralized control. Centralized controllers in a MIMO structure (so as the MISO controllers mentioned above) heavily rely on remote signals, so communication failure of any control inputs could easily compromise the control action as the design creates strong coupling between different inputs and outputs. Reference [71] presented a coordinated damping control scheme with multiple VSC converters; the control design was initially centralized, then the author employed a homotopy method to decentralize the MIMO controller so that a series of SISO controllers without cross-coupling can be obtained.

Consequently, direct decentralized designs are more preferable over centralized designs. As that has been mentioned in the literatures of robust damping control approaches, the optimization based robust control approaches [58-62] have great advantages in coordination control as the controllers are in fixed decentralized structures. However, if the parameters of multiple controllers are simultaneously tuned by performing optimization, the cross-coupling issue still exits. Instead of simultaneous tuning, the decentralized design could also be realized in a sequential approach [72], where multiple controllers are designed in a sequential manner

based on the close-loop systems with the previous designed controllers. Therefore, the sequentially designed controllers are independent and considerably more reliable.

1.3. Research Focuses and Contributions

The research study presented in this thesis focuses on the robust damping control of the FACTS integrated power systems against low frequency oscillations. The primary objective of this study is to improve the system damping ratio of the weakly damped oscillatory modes by designing robust FACTS supplementary damping controllers. The major focuses and contributions of this study can be summarized as follows.

1.3.1. Robust FACTS Damping Controller Design

How to effectively increase the damping ratio of the weakly damped oscillatory modes is the most essential part of the entire controller design. This usually relates to the system configuration and applied control methodologies. Besides, it is also important that the designed controllers are robust enough to work under multiple system operating conditions.

In this study, the linear system analyses and controller designs are conducted on state-space models. A BMI-based multi-objective multi-model system approach is developed for the design of robust FACTS damping controllers. The features of the approach are concluded as follows:

- Multiple control objectives including regional pole placement and control effort optimization (H_2 performance) are simultaneously considered to ensure the effectiveness of the design.
- Multiple system operating points (structured system uncertainties) are included in the

modelling stage to ensure the robustness of the design.

- The robust damping control problem is formulated as a BMI synthesis optimization problem and systematically solved via a two-step approach.
- Unstructured H_∞ norm bounded uncertainties can also be included if necessary.

The proposed robust damping control approach inherits the idea of polytopic system regional pole placement from [64], and in a further step, it addresses the problem of control effort optimization which significantly improves the convergence of the optimization problem and the controller reliability.

1.3.2. Coordinated Design of Multiple Robust FACTS Damping Controllers

In bulk power systems, it is common that the system may exhibit multiple dominant oscillatory modes. Another challenge in robust damping control is how to coordinate multiple FACTS devices to improve system damping of multiple weakly damped oscillatory modes.

In this study, a BMI-based sequential design approach is introduced for the coordinated design of multiple FACTS damping controllers as an extension of the multi-objective multi-model system approach mentioned above. The approach is inherently decentralized. To improve the effectiveness of the design, comprehensive studies in system mode shapes and modal residues are conducted and the remote feedback signals are accordingly selected for different FACTS controllers.

1.4. Thesis Outlines

This thesis is organized as follows:

Chapter 2: The small-signal modelling of power systems and different FACTS devices is presented along with a brief description of system linearization and multi-model system formulation.

Chapter 3: The formulation of the robust damping control problem involving multiple control objectives is presented, then a BMI-based two-step approach is proposed to solve the multi-objective damping control problem with respect to a multi-model system.

Chapter 4: The multi-objective multi-model system approach introduced in Chapter 3 is then applied to the damping controller designs of a TCSC and an SVC respectively. The designs are successively implemented on a two-area system and a five-area system to explore the generality and feasibility of the approach.

Chapter 5: The multi-objective multi-model system approach proposed in Chapter 3 is extended to the coordinated design of multiple FACTS damping controllers in this chapter. Robust controllers of SVC and TCSC are sequentially designed for a five-area system to improve its damping over multiple dominant inter-area oscillatory modes.

Chapter 6: A conclusion of the study is presented and discussions are made on possible future research topics.

CHAPTER 2 SMALL-SIGNAL MODELLING OF THE POWER SYSTEM WITH FACTS

Abbreviations

FACTS	Flexible AC Transmission System
PSS	Power System Stabilizer
SVC	Static VAR Compensator
TCR	Thyristor Controlled Reactor
TCSC	Thyristor Controlled Series Compensator
TSC	Thyristor Switched Capacitor
TCR	Thyristor Controlled Reactor

2.1. Introduction

The damping of low frequency oscillations caused by small disturbances falls under the small-signal stability problem. By designing appropriate supplementary FACTS damping controllers, the close-loop system small-signal stability could be effectively enhanced. From the small-

signal point of view, system modelling should be conducted on an electromechanical transient level including both statics and dynamics of the entire power system as well as other individual components such as FACTS devices in order to make further assessments of system damping performance.

In this chapter, the small-signal modelling of FACTS integrated power systems is presented. The static and dynamic behaviours of the systems are initially described by a set of algebraic and differential equations. Then linearization and further arrangements are carried out for these equations to transform the mathematical expressions into state-space representations so that small-signal analysis and linear modal control theories can be applied in the following studies. Finally, a multi-model system which includes the information of multiple linear system models under different system operating points is formed for the robustness design.

2.2. Power System Modelling

The power system statics and dynamics are consisting of two major parts: the generator (including excitation system and PSS) and the power network and loads.

2.2.1. Generator

The generators to be used in this study are synchronous machines. The synchronous machine dynamics depends on the simplification level of the machine; a machine can be represented by either a classic swing model in the order of two or a detailed model in the order of up to eight. In the following designs, a 6^{th} order generator model with the dynamics up to the subtransient level is selected; thus, the modelling of the generator is considered to be sufficient but also not over complicated. The generator dynamic equations are given as follows [73]:

$$\dot{\delta}_i = \omega_i - \omega_s \tag{2.1}$$

$$\dot{\omega}_i = \frac{\omega_s}{2H_i}\left(T_{Mi} - D_i(\omega_i - \omega_s) - \frac{X''_{di} - X_L}{X'_{di} - X_L} E'_{qi} I_{qi} - \frac{X''_{qi} - X_L}{X'_{qi} - X_L} E'_{di} I_{di} - \frac{X'_{di} - X''_{di}}{X'_{di} - X_L} \varphi_{1di} I_{qi} \cdots \right. \\ \left. \cdots + \frac{X'_{qi} - X''_{qi}}{X'_{qi} - X_L} \varphi_{2qi} I_{qi} + (X''_{qi} - X''_{di}) I_{di} I_{qi} \right) \tag{2.2}$$

$$\dot{E}'_{qi} = \frac{1}{T'_{doi}}\left(-E'_{qi} - \left(X_{di} - X'_{di} \right)\left(-I_{di} - \frac{X'_{di} - X''_{di}}{(X'_{di} - X_L)^2}\left(\varphi_{1di} - \left(X_{di} - X_L \right) I_{di} - E'_{qi} \right) \right) + E_{fdi} \right) \tag{2.3}$$

$$\dot{E}'_{di} = \frac{1}{T'_{qoi}}\left(-E'_{di} - \left(X_{qi} - X'_{qi} \right)\left(I_{qi} - \frac{X'_{qi} - X''_{qi}}{(X'_{qi} - X_L)^2}\left(-\varphi_{2qi} + \left(X_{qi} - X_L \right) I_{qi} - E'_{di} \right) \right) \right) \tag{2.4}$$

$$\dot{\varphi}_{1di} = \frac{1}{T''_{doi}}\left(-\varphi_{1di} + E_{qi} + (X'_{di} - X_L) I_{di} \right) \tag{2.5}$$

$$\dot{\varphi}_{2qi} = \frac{1}{T''_{qoi}}\left(\varphi_{2qi} + E_{di} + (X'_{qi} - X_L) I_{qi} \right) \tag{2.6}$$

$i = 1, 2, \cdots, m,$ where i is the generator index number, m is the total number of generators and the rest of the notations are listed as follows:

ω_i	generator rotor speed
δ_i	generator rotor angle
E'_{di}, E'_{qi}	induced transient electromagnetic force (emf)
$\varphi_{1di}, \varphi_{2di}$	subtransient induced emf
I_{di}, I_{qi}	generator stator current (d-q axis)
$X_{di}, X'_{di}, X''_{di}$	synchronous, transient , subtransient reactance (direct axis)
$X_{qi}, X'_{qi}, X''_{qi}$	synchronous, transient , subtransient reactance (quadrature axis)
T'_{doi}, T''_{doi}	transient and subtransient time constant (direct axis)

T'_{qoi}, T''_{qoi} transient and subtransient time constant (quadrature axis)

X_{Li} armature leakage reactance

E_{fdi} field voltage

T_{Mi} mechanical torque input

H_i inertial constant

ω_s rated rotor speed

Besides, there are two stator algebraic equations describing the generator terminal output voltage [73]:

$$0 = V_i \sin(\delta_i - \theta_i) - \frac{X''_{qi} - X_L}{X'_{qi} - X_L} E'_{di} + \frac{X'_{qi} - X''_{qi}}{X'_{qi} - X_L} \varphi_{2qi} + R_{si} I_{di} - X''_{qi} I_{qi} \tag{2.7}$$

$$0 = V_i \cos(\delta_i - \theta_i) - \frac{X''_{di} - X_L}{X'_{di} - X_L} E'_{qi} - \frac{X'_{di} - X''_{di}}{X'_{di} - X_L} \varphi_{1di} + R_{si} I_{qi} + X''_{di} I_{di} \tag{2.8}$$

where

R_{si} armature resistance

V_i magnitude of the generator terminal voltage

θ_i phase angle of the generator terminal voltage

It should be noticed that the generator terminal voltage $V_i \angle \theta_i$ is also the internal bus voltage of the generator, and the bus voltages of the non-generator buses follow the same notations of the generator buses with $i = m+1, m+2, \cdots, n$, where n is the total number of buses of the system network.

2.2.2. Excitation System

The dynamics of excitation systems should always be considered along with the synchronous generator dynamics. The influence of different excitation systems to the small-signal characteristics of the entire system can be very different. For the simplicity of the design, static AC excitation systems are used in this study. The voltage regulation behaviour of the static AC excitation systems is depicted by the block diagram in Figure 2-1 [11], and the dynamics of the excitation system is described by the differential equation presented in (2.9).

$$\dot{E}_{fdi} = -\frac{E_{fdi}}{T_{Ai}} + \frac{K_{Ai}}{T_{Ai}}(V_{refi} - V_i) \tag{2.9}$$

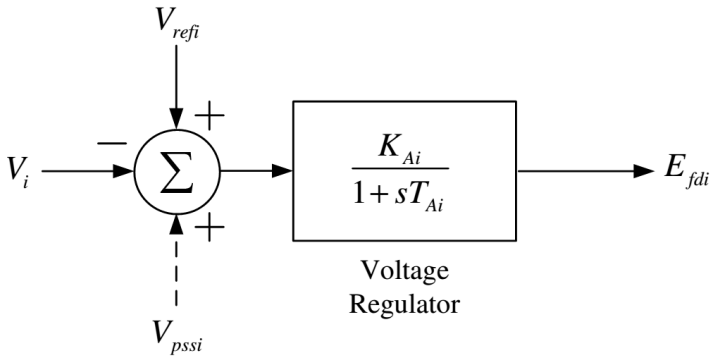

Figure 2-1 Static AC excitation system

where

V_{refi}	voltage reference of the excitation system
T_{Ai}	time constant of the voltage regulator
K_{Ai}	transient gain of the voltage regulator
V_{pssi}	input of PSS if it is installed

2.2.3. System Power Flow

The network power flow equations can be expressed in either the power-balance form or the current-balance form. The power-balance form is adopted in this study. For generator buses (*PV* buses), the network power flow equations are described by the following algebraic equations of active and reactive power flow balancing [73]:

$$\begin{aligned} &V_i\left(I_{qi}\cos(\delta_i-\theta_i)+I_{di}\sin(\delta_i-\theta_i)\right)+P_{Li}=\sum_{k=1}^{n}V_iV_k\left(G_{ik}\cos(\theta_i-\theta_k)+B_{ik}\sin(\theta_i-\theta_k)\right)\\ &V_i\left(I_{di}\cos(\delta_i-\theta_i)-I_{qi}\sin(\delta_i-\theta_i)\right)+Q_{Li}=\sum_{k=1}^{n}V_iV_k\left(G_{ik}\sin(\theta_i-\theta_k)-B_{ik}\cos(\theta_i-\theta_k)\right)\\ &i=1,2,\cdots,m \end{aligned} \tag{2.10}$$

where m is the total number of generator buses, n is the total number of buses of the entire system, G_{ik} and B_{ik} are the conductance and susceptance between bus i and k from the node admittance matrix. For non-generator buses (*PQ* buses), the algebraic equations of active and reactive power balancing are [73]:

$$\begin{aligned} &P_{Li}=\sum_{k=1}^{n}V_iV_k\left(G_{ik}\cos(\theta_i-\theta_k)+B_{ik}\sin(\theta_i-\theta_k)\right)\\ &Q_{Li}=\sum_{k=1}^{n}V_iV_k\left(G_{ik}\sin(\theta_i-\theta_k)-B_{ik}\cos(\theta_i-\theta_k)\right)\\ &i=m+1,m+2,\cdots,n \end{aligned} \tag{2.11}$$

Note that, P_{Li} and Q_{Li} are the active and reactive loads on bus i. In the system modelling, the loads can be classified as static loads and dynamic loads. Static loads with constant impedance (CI), constant current (CC) and constant power (CP) are used here; the load models are described by the following algebraic equations [74]:

$$P_{Li} = P_{Li0}\left(p_1\left(\frac{V_i}{V_{i0}}\right)^2 + p_2\left(\frac{V_i}{V_{i0}}\right) + p_3 \right)$$

$$Q_{Li} = Q_{Li0}\left(q_1\left(\frac{V_i}{V_{i0}}\right)^2 + q_2\left(\frac{V_i}{V_{i0}}\right) + q_3 \right) \tag{2.12}$$

$$i = 1, 2, \cdots, n$$

where P_{Li0} and Q_{Li0} are the steady state values of the active and reactive loads on bus i, V_{i0} is the steady state value of the corresponding bus voltage, $p_1 \sim p_3$ and $q_1 \sim q_3$ are the relative weights of the CI, CC and CP components.

2.3. FACTS Modelling

There are various types of FACTS devices which have been developed over the years. In this thesis, two different FACTS devices are studied: TCSC and SVC. Similar to the power system modelling, the modelling of FACTS also consists of two major parts: the small-signal dynamics of the FACTS devices themselves and their influence on the system power flows.

2.3.1. TCSC

A typical model of TCSC, as depicted in Figure 2-2, consists of a TCR in parallel with a fixed series capacitor [8]. By controlling the firing angle of the thyristors in the TCR, the device can be deemed a controllable reactance. In practical application, TCSC is mostly configured to be a capacitive reactance to compensate the total reactance of the adjacent transmission line so that the power transfer capability of the line can be increased.

There are different types of internal control strategies for TCSC, such as current regulation,

voltage regulation, reactance control, etc. In this study, the reactance control mode is used and the dynamics of the TCSC can be simply considered as a delay unit with the desired TCSC reactance reference as the input and the actual TCSC reactance as the output.

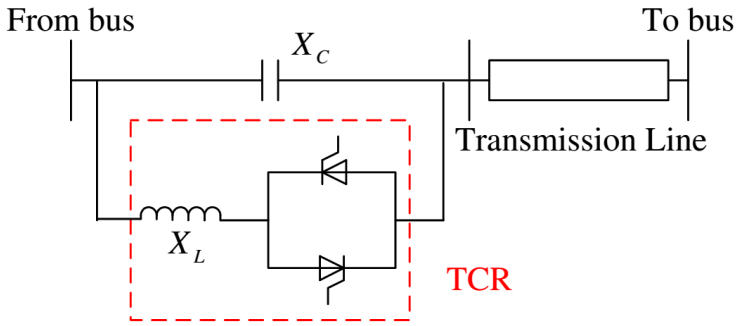

Figure 2-2 A typical model of TCSC

A block diagram of the TCSC dynamics is illustrated in Figure 2-3 [72], in which, the firing and synchronizing control are neglected (replaced by a delay block) since they have little impact on the system small-signal dynamics. Damping control signal is added on the TCSC reactance reference so that the actual reactance of the TCSC could be continuously controlled by the feedback damping controller to modulate the line power flow in order to damp out the low-frequency oscillations.

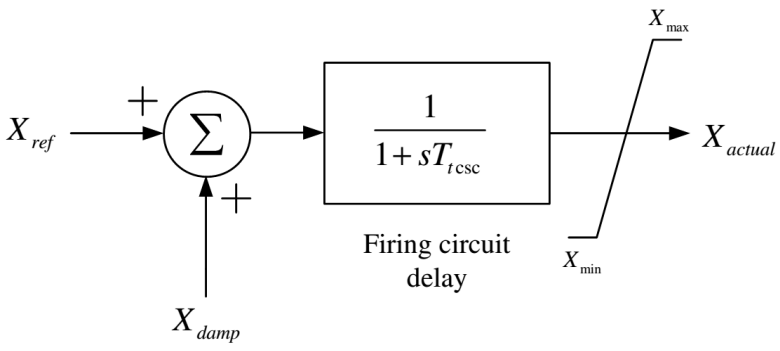

Figure 2-3 Small-signal dynamics of a TCSC

The small-signal dynamics of the TCSC can be expressed in the following differential equation:

$$\dot{X}_{actual} = -\frac{1}{T_{t\mathrm{csc}}}(-X_{actual} + X_{ref} + X_{damp}) \tag{2.13}$$

where

X_{actual}	actual reactance of the TCSC
X_{ref}	reference reactance of the TCSC
X_{damp}	supplementary damping control input
$T_{t\mathrm{csc}}$	time constant of the delay unit block

As TCSC is a series connected FACTS device which could continuously alter the transmission line impedance, its power flow modulation behaviour should be equivalently represented by power injection models, otherwise the system admittance matrix will be not be fixed during the power flow iterations. The power injection model is depicted in Figure 2-4, and the corresponding power injections are expressed in the following algebraic equations [75]:

$$P_k = \frac{K_c}{1-K_c} V_k V_m B_{km} \sin(\theta_k - \theta_m) \tag{2.14}$$

$$Q_k = \frac{K_c}{1-K_c} B_{km}[V_k^2 - V_k V_m \cos(\theta_k - \theta_m)] \tag{2.15}$$

$$P_m = \frac{K_c}{1-K_c} V_m V_k B_{km} \sin(\theta_m - \theta_k) \tag{2.16}$$

$$Q_m = \frac{K_c}{1-K_c} V_m V_k B_{km} \sin(\theta_m - \theta_k) \tag{2.17}$$

in which, B_{km} is the susceptance between bus *k* and *m*, K_c is the actual compensation level of the transmission line reactance X_{km}, defined by $K_c = X_{actual} / X_{km} \times 100\%$.

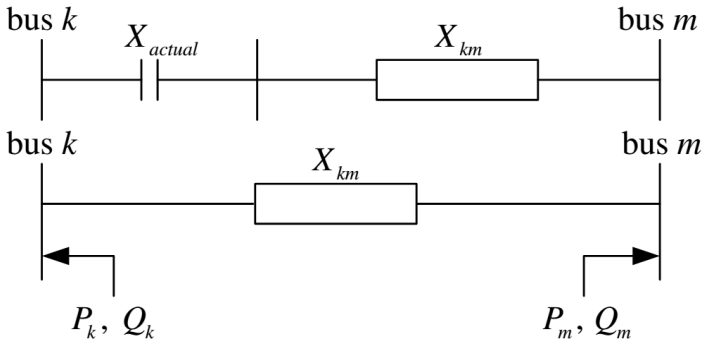

Figure 2-4 Power injection model of a TCSC

2.3.2. SVC

There are different types of SVC models which can be constructed by TSC, TSR and TCR. In the following study, the SVC model consisting of a TCR in parallel with a TSC is adopted [8]. A schematic diagram of the model is illustrated in Figure 2-5, where the TSC in the SVC can be deemed a fixed capacitor and the TCR can be considered as a controllable reactance. With the control of the TCR, the SVC should be able generate or absorb reactive power to regulate the bus voltage. The actual susceptance value of the SVC is given by:

$$B_{SVC} = B_{TSC} + B_{TCR} \tag{2.18}$$

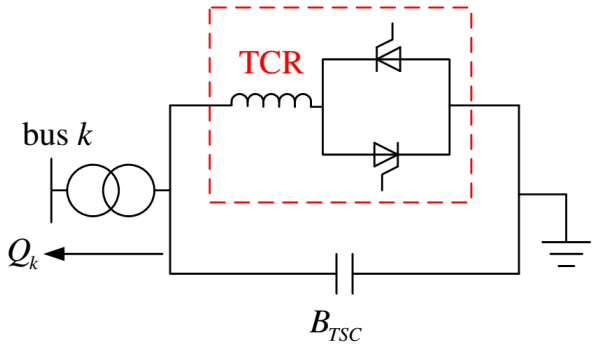

Figure 2-5 A typical model of SVC

The internal control of the SVC is voltage regulation; the reference voltage and the measured

voltage are compared and feed into a regulator block whose output is the actual reactance of the SVC; the firing and synchronizing are neglected (replaced by a delay unit) since they have little effect on the system small-signal dynamics. The block diagram in Figure 2-6 shows the small-signal dynamics of an SVC.

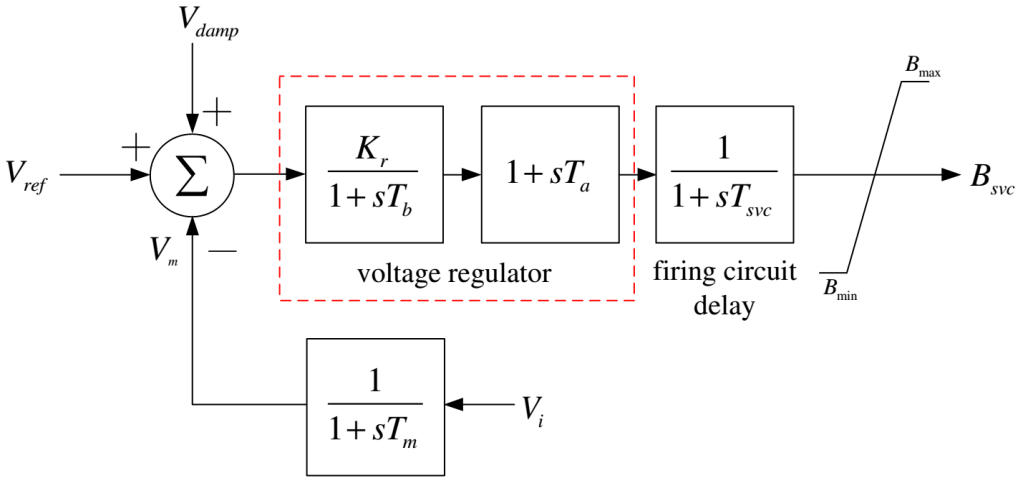

Figure 2-6 Small-signal dynamics of an SVC

According to Figure 2-6, the differential equations of the SVC dynamics can be easily derived:

$$\dot{B}_{svc} = \frac{1}{T_{svc}}\left(-B_{svc} + \left(1-\frac{T_a}{T_b}\right)V_1 - \left(\frac{K_r T_a}{T_b}\right)V_m\right) + \frac{K_r T_a}{T_{svc} T_b}\left(V_{damp} + V_{ref}\right) \tag{2.19}$$

$$\dot{V}_1 = \frac{1}{T_b}\left(-V_1 - K_r V_m + K_r V_{ref} + K_r V_{damp}\right) \tag{2.20}$$

$$\dot{V}_m = \frac{1}{T_m}\left(V_i - V_m\right) \tag{2.21}$$

where:

V_{ref} voltage reference of SVC

V_m measured voltage of SVC

V_{damp}	supplementary damping control input
V_1	intermediate modelling signal
V_i	instantaneous bus voltage of SVC
T_{svc}	time constant of the delay unit block (firing circuit)
T_m	time constant of the delay unit block (voltage measurement)
T_a, T_b	time constants of the voltage regulation block
K_r	voltage regulation block gain

Since the SVC is shunt-connected in the power system and it alters the bus voltage by generating or absorbing reactive power, its impact on the system power flows is relatively simple. The power injection equation of the SVC is given by:

$$Q_k = V_i^2 B_{svc} \tag{2.22}$$

2.4. System Linearization and Multi-model System Formulation

2.4.1. System Linearization without FACTS

To examine the system small-signal stability, it is required that the system models should be linearized and reformed into state-space representations. The linearization of the generator dynamics (2.1)-(2.6) and the excitation system dynamics (2.9) can be expressed as:

$$\Delta \dot{x}_i = A_{1i}\Delta x_i + B_{1i}\Delta I_{gi} + B_{2i}\Delta V_{gi} + E_{1i}\Delta u_{gi} \tag{2.23}$$

where $\Delta x_i = \begin{bmatrix} \Delta\delta_i & \Delta\omega_i & \Delta E'_{qi} & \Delta E'_{di} & \Delta\varphi_{1di} & \Delta\varphi_{2qi} & \Delta E_{fdi} \end{bmatrix}^T$, $\Delta I_{gi} = \begin{bmatrix} \Delta I_{di} & \Delta I_{qi} \end{bmatrix}^T$,

$\Delta V_{gi} = \begin{bmatrix} \Delta\theta_i & \Delta V_i \end{bmatrix}^T$, $\Delta u_{gi} = \begin{bmatrix} \Delta T_{Mi} & \Delta V_{refi} \end{bmatrix}^T$.

Subsequently, the dynamics of multiple generators can be expressed in a compact matrix form:

$$\Delta\dot{x} = A_1\Delta x + B_1\Delta I_g + B_2\Delta V_g + E_1\Delta u_g \tag{2.24}$$

where $\Delta x = \begin{bmatrix} \Delta x_1^T & \cdots & \Delta x_m^T \end{bmatrix}^T$, $\Delta I_g = \begin{bmatrix} \Delta I_{g1}^T & \cdots & \Delta I_{gm}^T \end{bmatrix}^T$, $\Delta V_g = \begin{bmatrix} \Delta V_{g1}^T & \cdots & \Delta V_{gm}^T \end{bmatrix}^T$ and $\Delta u_g = \begin{bmatrix} \Delta u_{g1}^T & \cdots & \Delta u_{gm}^T \end{bmatrix}^T$; here, A_1, B_1, B_2, E_1 are block diagonal matrices.

The linearization of the generator stator algebraic equations (2.7)-(2.8) can be expressed as:

$$0 = C_{1i}\Delta x_i + D_{1i}\Delta I_{gi} + D_{2i}\Delta V_{gi} \tag{2.25}$$

Similar to the generator dynamic equations, the stator algebraic equations of multiple generators can be formed with block diagonal matrices C_1, D_1, D_2 in a compact matrix form:

$$0 = C_1\Delta x + D_1\Delta I_g + D_2\Delta V_g \tag{2.26}$$

The linearization of the system power flow balancing equations (2.10)-(2.11) is given as follows:

$$0 = C_2\Delta x + D_3\Delta I_g + D_4\Delta V_g + D_5\Delta V_l \tag{2.27}$$

$$0 = D_6\Delta V_g + D_7\Delta V_l \tag{2.28}$$

where $\Delta V_l = \begin{bmatrix} \Delta V_{l,m+1}^T & \Delta V_{l,m+2}^T & \cdots & \Delta V_{l,n}^T \end{bmatrix}^T$ and $\Delta V_{l,j} = \begin{bmatrix} \Delta\theta_j & \Delta V_j \end{bmatrix}^T$.

To sum up, the linearized system models without FACTS can be represented by (2.24), (2.26)-(2.28).

2.4.2. System Linearization with FACTS

The linearized FACTS dynamic equations can be expressed by the following state-space representation:

$$\Delta \dot{x}_{FACTS} = A_{FACTS}\Delta x_{FACTS} + B_{FACTS}\Delta u_{FACTS} \tag{2.29}$$

For TCSC, $\Delta x_{FACTS} = \Delta X_{actual}$ and $\Delta u_{FACTS} = \Delta X_{damp}$; while, for SVC, $\Delta u_{FACTS} = \Delta V_{damp}$ and $\Delta x_{FACTS} = \begin{bmatrix} \Delta B_{svc} & \Delta V_1 & \Delta V_m \end{bmatrix}^T$.

The linearization of the TCSC power flow injection equations (2.14)-(2.17) yields:

$$\Delta P_k = K_{11}\Delta X_{actual} + K_{12}\Delta V_l \tag{2.30}$$

$$\Delta Q_k = K_{21}\Delta X_{actual} + K_{22}\Delta V_l \tag{2.31}$$

$$\Delta P_m = M_{11}\Delta X_{actual} + M_{12}\Delta V_l \tag{2.32}$$

$$\Delta Q_m = M_{21}\Delta X_{actual} + M_{22}\Delta V_l \tag{2.33}$$

The linearization of the SVC power flow injection equation (2.22) yields:

$$\Delta Q_k = K_1\Delta B_{svc} + K_2\Delta V_l \tag{2.34}$$

It is assumed that all the FACTS devices are installed on or between non-generator buses, hence all voltage-related terms in the linearized power injection models (terms in the form $*\Delta\theta_k$ and $*\Delta V_k$) can be reformed into $*\Delta V_l$. For FACTS devices that are installed on or between generator buses, the voltage-related terms should be reformed into $*\Delta V_g$ (or a combination of $*\Delta V_g$ and $*\Delta V_l$). With the linearized FACTS power injection equations, the non-generator bus

power flow equation (2.28) can be updated:

$$0 = D_6 \Delta V_g + \tilde{D}_7 \Delta V_l + D_8 \Delta x_{FACTS} \tag{2.35}$$

Now substituting algebraic equations (2.26), (2.27) and (2.35) into differential equation (2.24), the generator and excitation system dynamics can be expressed as:

$$\Delta \dot{x} = A_{sys1} \Delta x + A_{sys2} \Delta x_{FACTS} + B_{sys1} \Delta u_{FACTS} \tag{2.36}$$

Combining differential equation (2.36) and (2.29), the complete system small-signal dynamics with FACTS can be expressed by the following state-space representation:

$$\Delta \dot{\overline{x}} = A_{sys} \Delta \overline{x} + B_{sys} \Delta u_{FACTS} \tag{2.37}$$

where $\Delta \overline{x} = \begin{bmatrix} \Delta x \\ \Delta x_{FACTS} \end{bmatrix}$, $A_{sys} = \begin{bmatrix} A_{sys1} & A_{sys2} \\ 0 & A_{FACTS} \end{bmatrix}$ and $B_{sys} = \begin{bmatrix} B_{sys1} \\ B_{FACTS} \end{bmatrix}$.

2.4.3. Forming the Multi-model System

To increase the robustness of damping control designs, multiple system operating points are included in the system modelling stage by forming a multi-model system. The multi-model system contains a series of linearized system models:

$$\begin{aligned} \Delta \dot{\overline{x}} &= A_{sys,i} \Delta \overline{x} + B_{sys,i} \Delta u_{FACTS} \\ \Delta y &= C_{sys,i} \Delta \overline{x} + D_{sys,i} \Delta u_{FACTS} \\ i &= 1, 2, \cdots, L \end{aligned} \tag{2.38}$$

where i is the operating point index number; L is the total number of operating points and Δy is the system output which will be used as the feedback signal for the damping controller. If a

common output-feedback controller can be found for all these system models, the design is then robust within the set range.

2.5. Summary

This chapter presented the small-signal modelling of power systems with FACTS where system statics and dynamics were comprehensively considered at the electromechanical transient level. For a system without FACTS, its dynamic behaviour was represented by the differential equations of synchronous generators' dynamics (including excitation system and PSS), while the static behaviour was described by the algebraic equations of stator output voltages and system network power flows.

FACTS devices were installed for the purpose of maintaining or controlling specific system parameters such as line power flow and bus voltage. Hence, the small-signal modelling of FACTS should not only include the internal dynamics of FACTS devices but also their impacts on system power flows. To this end, the internal dynamics of FACTS devices were expressed in differential equations and power injection models in algebraic equations were adopted to describe the power or voltage modulation behaviours.

Linearization was applied to all the differential and algebraic equations. By substituting the linearized algebraic equations into the differential equations, redundant variables were eliminated and the system small-signal dynamics was finally expressed in a state-space form which could be used in stability studies and control designs. In the end, a multi-model system was formed by a series of LTI state-space equations so that multiple system operating points can be included in the modelling stage for robustness design.

CHAPTER 3 BMI-BASED MULTI-OBJECTIVE DAMPING CONTROL APPROACH WITH MULTI-MODEL SYSTEM

Abbreviations

BMI	Bilinear Matrix Inequality
FACTS	Flexible AC Transmission System
LMI	Linear Matrix Inequality
PSS	Power System Stabilizer

3.1. Introduction

The damping control of power system can be attained by designing feedback controllers with suitable power system components. With an appropriate damping controller, power system parameters, such as power flow and current, can be effectively regulated during oscillations; and as a result, the close-loop system damping performance can be accordingly improved.

Low frequency oscillations can be classified as local oscillatory mode and inter-area oscillatory

mode according to their causes. The installation of PSS is a good solution to mitigate local oscillations as PSS is able to provide supplementary damping through the control of generator excitation system. For a similar reason, supplementary damping controllers can be developed for FACTS to mitigate inter-area oscillations. In the following study, it is assumed that the local oscillatory modes are adequately damped by PSSs; hence, the damping control will mainly focus on inter-area oscillatory modes.

In this chapter, a BMI-based control approach is proposed for the designs of robust FACTS supplementary damping controllers. In pursuit of robustness, the controller design is implemented on a multi-model system, so that multiple system operating points can be included in the design stage. To assure the effectiveness of the design, multiple control objectives are considered in the form of matrix inequalities. Subsequently, the damping control problem is formulated as a synthesis BMI optimization problem.

Solving the synthesis BMI optimization problem can be complicated as the problem is non-convex. Incorporating multi-model system makes the problem even harder to solve because of the changing system matrix variables. A two-step method is introduced to find the optimal solutions for the synthesis BMI optimization problem. Following the two-step method, the BMI constraints can be linearized and the optimization problem can be solved systematically by convex LMI solvers.

3.2. Multi-Objective Damping Control Problem Formulation in BMI

The control objectives to be included in the robust damping control problem comprises the regional pole placement, control effort optimization and disturbance rejection. These control objectives under different system operating points will be initially formulated as multiple sets

of matrix inequalities and then combined and treated as a unified set of BMI constraints of a synthesis optimization problem.

3.2.1. Regional Pole Placement

Suppose an LTI system is given in the state-space representation as shown in (3.1), the system damping characteristics are normally decided by the eigenvalues of matrix A.

$$\begin{aligned} \dot{x} &= Ax + Bu \\ y &= Cx + Du \end{aligned} \tag{3.1}$$

From the small-signal stability point of view, the system is considered to be asymptotically stable if all the eigenvalues are on the left hand side of the complex plane (with negative real part) [76]. A real eigenvalue indicates that the mode is non-oscillatory, while the complex eigenvalues in a conjugate pair indicate that the mode is oscillatory.

The damping ratio and frequency of a particular oscillatory mode can be directly determined from its corresponding eigenvalues. If the eigenvalues of an oscillatory mode are given by:

$$\lambda = \sigma \pm j\omega \tag{3.2}$$

the oscillatory frequency of the mode will be ω rad/s, and the damping ratio of the mode can be determined by [10]:

$$\zeta = \frac{-\sigma}{\sqrt{\sigma^2 + \omega^2}} \tag{3.3}$$

A larger damping ratio will result in a faster decay of the oscillation and shorter period of settling time. According to (3.3), it is also known that the damping ratio is closely related to the

positions of the eigenvalues. If the oscillatory frequency of a mode is fixed at ω, the damping ratio ζ can be effectively increased by moving the eigenvalues away from the imaginary axis (i.e. reducing the value of σ). This idea is also known as pole-shifting and can be realized by regional pole placement [77].

LMI Pole Placement Region

A subset *D* of the left complex plane can be expressed as a convex LMI region if there exists symmetric matrices α and β such that [77]:

$$D = \left\{ z \in C : f_D(\mathrm{z}) = \alpha + \mathrm{z}\,\beta + \bar{\mathrm{z}}\,\beta^T < 0 \right\} \tag{3.4}$$

Equation (3.4) is also known as the characteristic equation of the LMI region, where $\bar{z}$ is the conjugate of z and the "<" indicates that the left side of the matrix inequality is negative definite.

Suppose a conic sector D_p, as illustrated in Figure 3-1, is assigned as the pole placement region for the damping control design; the exact LMI expression of this region is given by:

$$\begin{aligned} D_p &= \left\{ z \in C : f_{D_p}(\mathrm{z}) = \alpha + \mathrm{z}\,\beta + \bar{\mathrm{z}}\,\beta^T < 0 \right\} \\ \alpha = 0 \;\;\&\;\; \beta &= \begin{bmatrix} \sin\theta & -\cos\theta \\ \cos\theta & \sin\theta \end{bmatrix} \end{aligned} \tag{3.5}$$

Generalized Lyapunov Theory with Regional Pole Placement

The classic Lyapunov theory is widely recognized as the stability criterion of control systems [78]: the close-loop system with state matrix A_{cl} is stable if and only if there exists a symmetric positive definite matrix *P* such that:

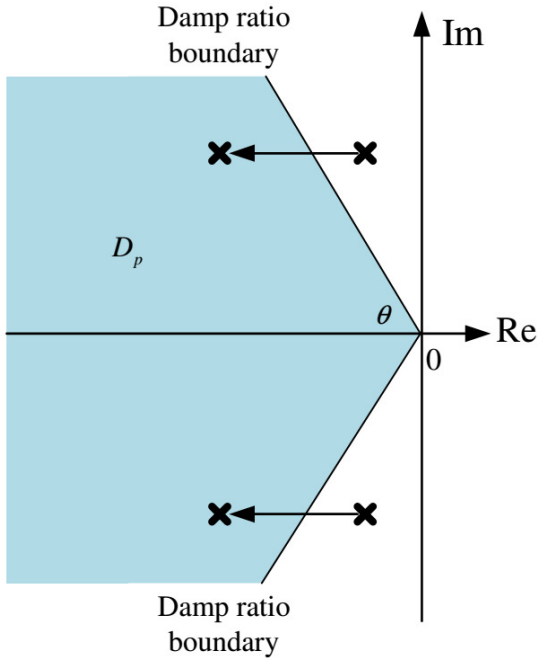

Figure 3-1 The pole placement region with a minimum damping ratio

$$A_{cl}^T P + P A_{cl} < 0 \tag{3.6}$$

As a result of the regional pole placement design, it is required that the close-loop system is stable and also has all the eigenvalues in the specified LMI region D_p; thus a generalized Lyapunov theory with regional pole placement is proposed in [77]: the close-loop system with state matrix A_{cl} is D_p- stable if and only if there exists a symmetric matrix P such that:

$$\begin{aligned} &\alpha \otimes P + \beta \otimes (P A_{cl}) + \beta^T \otimes (A_{cl}^T P) < 0 \\ &P > 0 \end{aligned} \tag{3.7}$$

where "$\otimes$" denotes the Kronecker product of two matrices.

Therefore, the control objective of regional pole placement can be described by the two matrix inequalities given in (3.7). It should be noticed that the first matrix inequality is actually bilinear, and the details of linearization will be discussed in Section 3.3.

3.2.2. Control Effort Optimization and Disturbance Rejection

Low frequency oscillations are usually excited by system disturbances. It is required that the damping controller to be designed could effectively reduce the impact of the disturbances on the system (i.e. disturbance rejection); besides, it is also expected that the controller output effort could be optimized.

The H_2 and H_∞ performance will be considered here to quantify the disturbance rejection and control effort optimization [79, 80]. A typical configuration of the disturbance rejection and control effort optimization [72] is illustrated in Figure 3-2. The sensitivity between the disturbance signal $w(s)$ and the system measured output signal $y(s)$ is defined by transfer function $G_{wzy}(s)$; the sensitivity between the disturbance signal $w(s)$ and the controller output signal $u(s)$ is defined by transfer function $G_{wzu}(s)$.

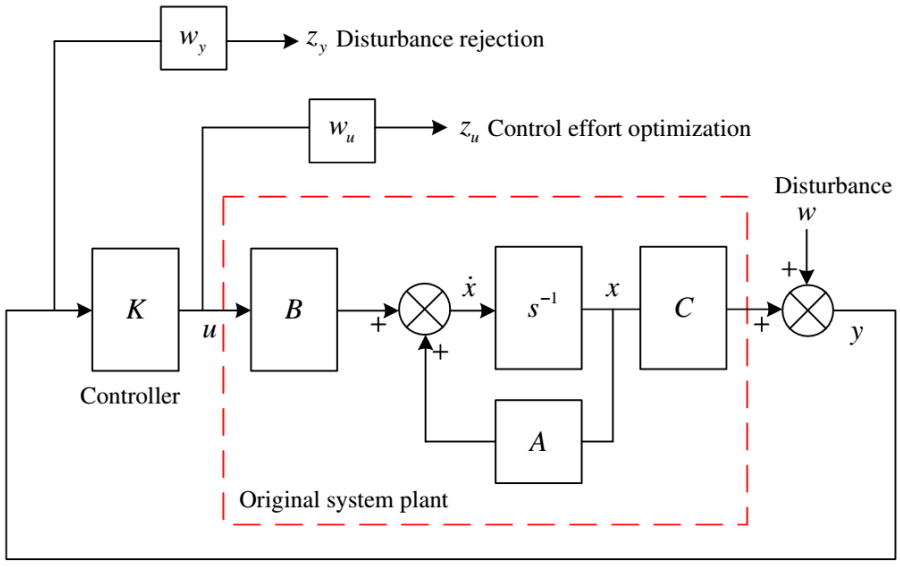

Figure 3-2 Synthesis system with augemented outputs

According to Figure 3-2, the state-space realization of the open-loop system is expressed as:

$$\begin{aligned} \dot{x} &= Ax + Bu \\ z_y &= Cx + w \\ z_u &= u \\ y &= Cx + w \end{aligned} \tag{3.8}$$

And the corresponding close-loop system with controller K is given by:

$$\begin{aligned} \dot{x}_{cl} &= A_{cl}x_{cl} + B_{cl}w \\ z_y &= C_{cl1}x_{cl} + D_{cl1}w \\ z_u &= C_{cl2}x_{cl} + D_{cl2}w \end{aligned} \tag{3.9}$$

where x_{cl} is the close-loop system state. It is noticed that band-pass filters w_u and w_y are added in front of the augmented outputs z_u and z_y as it is impossible and also unnecessary to optimize both performances across all frequencies [72].

H_2 Performance

In consideration of control effort optimization, the H_2 norm of the transfer function $G_{wzu}(s)$, as shown in (3.10) [81], should be minimized.

$$\left\|G_{wzu}(s)\right\|_2 = \sqrt{\frac{1}{2\pi}\int_{-\infty}^{+\infty}\left\{Trace\left[G_{wzu}(j\omega)^H G_{wzu}(j\omega)\right]\right\}d\omega} \tag{3.10}$$

The H_2 norm in (3.10) measures the overall energy relating *w* to z_u, and it can be numerically computed as [72]:

$$\left\|G_{wzu}(s)\right\|_2 = \sqrt{Trace\left(C_{cl2}PC_{cl2}^T\right)} \tag{3.11}$$

where "*Trace*" denotes the sum of the diagonal elements of the matrix, and *P* is the Lyapunov

matrix which satisfies:

$$A_{cl}P + PA_{cl}^T + B_{cl}B_{cl}^T < 0 \tag{3.12}$$

Therefore, the objective of control effort optimization can be considered as finding a symmetric positive definite matrix P which minimizes the object function $\sqrt{Trace(C_{cl2}PC_{cl2}^T)}$ subject to the following two inequalities

$$Trace(C_{cl2}PC_{cl2}^T) < \nu \tag{3.13}$$

$$A_{cl}P + PA_{cl}^T + B_{cl}B_{cl}^T < 0 \tag{3.14}$$

where ν is the upper limit of the control output energy. Subsequently, inequalities (3.13) and (3.14) can be rewritten into the following matrix inequalities:

$$\begin{bmatrix} PA_{cl} + A_{cl}^T P & PB_{cl} \\ B_{cl}^T P & -I \end{bmatrix} < 0 \tag{3.15}$$

$$\begin{bmatrix} Q & C_{cl2} \\ C_{cl2}^T & P \end{bmatrix} > 0 \tag{3.16}$$

$$Trace(Q) < \nu \tag{3.17}$$

where Q is an auxiliary matrix.

H_∞ Performance

The H_∞ norm measures the largest magnitude of the frequency response across all frequencies. It is also the highest spike value on the bode diagram. For the purpose of disturbance rejection, the H_∞ norm of the transfer function $G_{wzy}(s)$, defined by (3.18) [72], should be minimized.

$$\left\|G_{wzy}(s)\right\|_{\infty} = \max_{\omega}\left|G_{wzy}(j\omega)\right| \tag{3.18}$$

According to the bounded real lemma [44, 82], it is known that the inequality $\left\|G_{wzy}(s)\right\|_{\infty} < \gamma$ holds if and only if there exists a symmetric Lyapunov matrix P such that:

$$\begin{bmatrix} PA_{cl} + A_{cl}^T P & PB_{cl} & C_{cl1}^T \\ B_{cl}^T P & -\gamma I & D_{cl}^T \\ C_{cl1} & D_{cl1} & -\gamma I \end{bmatrix} < 0 \tag{3.19}$$

Therefore, the control objective of disturbance rejection can be considered as finding a symmetric positive definite matrix P which minimizes the value of γ subject to matrix inequalities as presented in (3.19).

3.2.3. Forming the Synthesis BMI Optimization Problem

A synthesis BMI optimization problem of regional pole placement, control effort optimization and disturbance rejection can be formulated as follows:

$$\min\left[\alpha_1 Trace(Q) + \alpha_2 \gamma\right]$$

$$s.t. \quad \begin{cases} \alpha \otimes P + \beta \otimes (PA_{cl}) + \beta^T \otimes (A_{cl}^T P) < 0 \\ \begin{bmatrix} PA_{cl} + A_{cl}^T P & PB_{cl} & C_{cl1}^T \\ * & -\gamma I & D_{cl1}^T \\ * & * & -\gamma I \end{bmatrix} < 0 \\ \begin{bmatrix} Q & C_{cl2} \\ * & P \end{bmatrix} > 0 \\ Trace(Q) < \nu \end{cases} \tag{3.20}$$

where α_1 and α_2 are the relative weightings of the H_2 and H_∞ performance, "$*$" indicates

that the entry follows the transpose of its symmetry. It should be emphasized that when multiple objectives are included in a synthesis problem, it is mandatory that the Lyapunov matrix P of different objectives should be solved as the same one [77]. Otherwise, the solution won't be feasible for a joint convex.

3.3. Solving the Synthesis BMI Optimization Problem

As that has been described in section 3.2, the robust damping control problem can be formulated as a synthesis BMI optimization problem. Thus, finding an optimal solution for the optimization problem is the crucial part of the controller design. The traditional damping control design approaches involving multiple control objectives are mostly nominal model based. The robustness of the controller is only guaranteed around a particular operating point by H_2 or H_∞ performance. It is of great interest to consider multiple operating points in the controller design stage so that the robustness of the controller can be further improved. Solving the BMI optimization problem with respect to a nominal model system is quite straightforward, and it has already been brought up in many existing literatures [47, 72]. It is also included here to demonstrate the completeness of the BMI-based design approach.

3.3.1. Nominal Model System Approach

The state-space realization of a nominal model system with augmented H_2 and H_∞ outputs is given by:

$$\begin{aligned} \dot{x} &= Ax + Bu \\ z_\infty &= Cx + w \\ z_2 &= u \\ y &= Cx + w \end{aligned} \tag{3.21}$$

The damping controller is designed as an SISO output-feedback controller in the following state-space form:

$$\begin{aligned} \dot{x}_c &= A_c x_c + B_c y \\ u &= C_c x_c \end{aligned} \tag{3.22}$$

By substituting (3.22) into (3.21), the close-loop system can expressed as:

$$\begin{aligned} \dot{x}_{cl} &= A_{cl} x_{cl} + B_{cl} w \\ z_\infty &= C_{cl1} x_{cl} + D_{cl1} w \\ z_2 &= C_{cl2} x_{cl} + D_{cl2} w \end{aligned} \tag{3.23}$$

where $x_{cl} = \begin{bmatrix} x \\ x_c \end{bmatrix}$, $A_{cl} = \begin{bmatrix} A & BC_c \\ B_c C & A_c \end{bmatrix}$ $B_{cl} = \begin{bmatrix} 0 \\ B_c \end{bmatrix}$, $C_{cl1} = \begin{bmatrix} C & 0 \end{bmatrix}$, $C_{cl2} = \begin{bmatrix} 0 & C_c \end{bmatrix}$, $D_{cl1} = I$ and $D_{cl2} = 0.$

It should be pointed out that strictly proper system and controller structures (i.e. $D = D_c = 0$) are used here to simplify the derivations as they are sufficient for the damping controller designs.

The synthesis BMI optimization problem described by (3.20) can be expressed as:

$$\min \left[\alpha_1 Trace(Q) + \alpha_2 \gamma \right]$$

$$s.t. \quad \begin{Bmatrix} \begin{bmatrix} P\begin{bmatrix} A & BC_c \\ B_c C & A_c \end{bmatrix} + \left(P\begin{bmatrix} A & BC_c \\ B_c C & A_c \end{bmatrix} \right)^T & P\begin{bmatrix} 0 \\ B_c \end{bmatrix} & \begin{bmatrix} C^T \\ 0 \end{bmatrix} \\ * & -\gamma I & I \\ * & * & -\gamma I \end{bmatrix} < 0 \\ \vdots \end{Bmatrix} \tag{3.24}$$

$$
s.t. \quad \begin{cases} \vdots \\ \begin{bmatrix} Q & [0 \quad C_c] \\ * & P \end{bmatrix} > 0 \\ Trace(Q) < \nu \\ \alpha \otimes P + \beta \otimes \left(P \begin{bmatrix} A & BC_c \\ B_c C & A_c \end{bmatrix} \right) + \beta^T \otimes \left(\begin{bmatrix} A & BC_c \\ B_c C & A_c \end{bmatrix}^T P \right) < 0 \end{cases}
$$

It is easy to see that the inequality constraints of optimization problem in (3.24) are bilinear due to unknown controller variables A_c, B_c, C_c and Lyapunov matrix P. Therefore, it is impossible to utilize convex optimization techniques to solve such problem directly. However, with Lyapunov matrix parameterization and appropriate system matrix variable transformation [77], these BMI constraints can be converted into LMI constraints.

Partition the Lyapunov matrix P and its inverse P^{-1} as:

$$
P = \begin{bmatrix} S & N \\ N^T & U \end{bmatrix}, \quad P^{-1} = \begin{bmatrix} R & M \\ M^T & V \end{bmatrix} \tag{3.25}
$$

where R and S are symmetric matrices. From $PP^{-1} = I$, it can be derived that:

$$
\begin{aligned} SR + NM^T &= N^T M + UV = I \\ SM + NV &= N^T R + UM^T = 0 \end{aligned} \tag{3.26}
$$

Let $\prod_1 = \begin{bmatrix} R & I \\ M^T & 0 \end{bmatrix}$ and $\prod_2 = \begin{bmatrix} I & S \\ 0 & N^T \end{bmatrix}$, we have:

$$
P\prod_1 = \begin{bmatrix} SR + NM^T & S \\ N^T R + UM^T & N^T \end{bmatrix} = \begin{bmatrix} I & S \\ 0 & N^T \end{bmatrix} = \prod_2 \tag{3.27}
$$

As P is a symmetric matrix, (3.27) can be rewritten as:

$$\prod_1^T P = \prod_2^T \tag{3.28}$$

By pre-multiplying $\prod_1^T$ and post-multiplying $\prod_1$, the Lyapunov matrix P is transformed as:

$$\prod_1^T P \prod_1 = \prod_1^T \prod_2 = \begin{bmatrix} R & RS + MN^T \\ I & S \end{bmatrix} = \begin{bmatrix} R & I \\ I & S \end{bmatrix} \tag{3.29}$$

Similarly, the nonlinear term $P\begin{bmatrix} A & BC_c \\ B_c C & A_c \end{bmatrix}$ and its transpose in the first matrix inequality of (3.24) can be transformed as:

$$\prod_1^T \left(P \begin{bmatrix} A & BC_c \\ B_c C & A_c \end{bmatrix} \right) \prod_1 = \begin{bmatrix} AR + BC_c M^T & A \\ (SA + NB_c C)R + (SBC_c + NA_c)M^T & SA + NB_c C \end{bmatrix} \tag{3.30}$$

$$\prod_1^T \left(\begin{bmatrix} A & BC_c \\ B_c C & A_c \end{bmatrix}^T P \right) \prod_1 = \begin{bmatrix} AR + BC_c M^T & A \\ (SA + NB_c C)R + (SBC_c + NA_c)M^T & SA + NB_c C \end{bmatrix}^T \tag{3.31}$$

The second and third matrix inequalities in (3.24) should also be applied with the same transformation. By pre-multiplying $diag\left(\prod_1^T, I, I\right)$, $diag\left(I, \prod_1^T\right)$ and post-multiplying $diag\left(\prod_1, I, I\right)$, $diag\left(I, \prod_1\right)$, the second and third matrix inequalities are transformed as:

$$\begin{Bmatrix} \begin{bmatrix} \prod_2^T \begin{bmatrix} A & BC_c \\ B_c C & A_c \end{bmatrix} \prod_1 + \left(\prod_2^T \begin{bmatrix} A & BC_c \\ B_c C & A_c \end{bmatrix} \prod_1 \right)^T & \prod_2^T \begin{bmatrix} 0 \\ B_c \end{bmatrix} & \prod_1^T \begin{bmatrix} C^T \\ 0 \end{bmatrix} \\ * & -\gamma I & I \\ * & * & -\gamma I \end{bmatrix} < 0 \\ \begin{bmatrix} Q & [0 \quad C_c] \prod_1 \\ * & \begin{bmatrix} R & I \\ I & S \end{bmatrix} \end{bmatrix} > 0 \end{Bmatrix} \tag{3.32}$$

Now, define the new controller variables as:

$$\tilde{A}_c = (SA + NB_cC)R + (SBC_c + NA_c)M^T \tag{3.33}$$

$$\tilde{B}_c = NB_c \tag{3.34}$$

$$\tilde{C}_c = C_cM^T \tag{3.35}$$

The BMI optimization problem in (3.24) can be converted into an LMI optimization problem as follows:

$$\min\left[\alpha_1 Trace(Q) + \alpha_2\gamma\right] \tag{3.36}$$

$$s.t. \quad \begin{cases} \alpha \otimes \begin{bmatrix} R & I \\ I & S \end{bmatrix} + \beta \otimes \begin{bmatrix} AR + B\tilde{C}_c & A \\ \tilde{A}_c & SA + \tilde{B}_cC \end{bmatrix} + \beta^T \otimes \begin{bmatrix} AR + B\tilde{C}_c & A \\ \tilde{A}_c & SA + \tilde{B}_cC \end{bmatrix}^T < 0 \\ \begin{bmatrix} \begin{bmatrix} AR + RA^T + B\tilde{C}_c + \tilde{C}_c^TB^T & A + A^T \\ \tilde{A}_c + \tilde{A}_c^T & SA + A^TS + \tilde{B}_cC + C^T\tilde{B}_c^T \end{bmatrix} & \begin{bmatrix} 0 \\ \tilde{B}_c \end{bmatrix} & \begin{bmatrix} RC^T \\ C^T \end{bmatrix} \\ * & -\gamma I & I \\ * & * & -\gamma I \end{bmatrix} < 0 \\ \begin{bmatrix} Q & \begin{bmatrix} \tilde{C}_c & 0 \end{bmatrix} \\ * & \begin{bmatrix} R & I \\ I & S \end{bmatrix} \end{bmatrix} > 0 \\ Trace(Q) < \nu \end{cases} \tag{3.37}$$

Solving the above LMI optimization problem with a convex LMI solver gives the optimal solutions of $\tilde{A}_c$, $\tilde{B}_c$, $\tilde{C}_c$, R and S. From (3.26) it is known that $NM^T = I - SR$, hence N and M^T can be determined by matrix decomposition. And the actual controller variables are determined as:

$$B_c = N^{-1}\tilde{B}_c \tag{3.38}$$

$$C_c = \tilde{C}_c (M^T)^{-1} \tag{3.39}$$

$$A_c = N^{-1}\left(\tilde{A}_c - (SA + NB_cC)R - SBC_cM^T\right)(M^T)^{-1} \tag{3.40}$$

To sum up, solving the BMI optimization problem with respect to a nominal model system mainly relies on Lyapunov matrix parameterization and system matrix variable transformation, by which, the BMI optimization problem can be linearized and subsequently solved by convex LMI optimization solvers. The controller variables to be designed can finally be determined from the optimal solutions.

3.3.2. Multi-Model System Approach

The state-space realizations of a multi-model system with augmented H_2 and H_∞ outputs are given by:

$$\begin{aligned} \dot{x} &= A_i x + B_i u \\ z_\infty &= C_i x + w \\ z_2 &= u \\ y &= C_i x + w \\ i &= 1, 2, \cdots, L \end{aligned} \tag{3.41}$$

where A_i, B_i, C_i are the state-space matrices of the open-loop system plant at the i^{th} operating point and *L* is the total number of operating points included in the multi-model system.

Suppose a common output-feedback controller in the form of (3.22) will be designed for the multi-model system, the corresponding close-loop systems with the output-feedback controller can be represented by:

$$
\begin{aligned}
&\dot{x}_{cl} = A_{cl,i}x_{cl} + B_{cl,i}w \\
&z_{\infty} = C_{cl1,i}x_{cl} + D_{cl1,i}w \\
&z_2 = C_{cl2,i}x_{cl} + D_{cl2,i}w \\
&i = 1, 2, \cdots, L
\end{aligned}
\tag{3.42}
$$

where $x_{cl} = \begin{bmatrix} x \\ x_c \end{bmatrix}$, $A_{cl,i} = \begin{bmatrix} A_i & B_iC_c \\ B_cC_i & A_c \end{bmatrix}$, $B_{cl,i} = \begin{bmatrix} 0 \\ B_c \end{bmatrix}$, $C_{cl1,i} = \begin{bmatrix} C_i & 0 \end{bmatrix}$, $C_{cl2,i} = \begin{bmatrix} 0 & C_c \end{bmatrix}$,

$D_{cl1,i} = I$ and $D_{cl2,i} = 0$.

Thus, the synthesis BMI optimization problem for the multi-model system can be expressed as:

$$
\min \left[\alpha_1 Trace(Q) + \alpha_2 \gamma \right]
$$

$$
s.t. \quad \begin{cases}
\alpha \otimes P + \beta \otimes \left(P \begin{bmatrix} A_i & B_iC_c \\ B_cC_i & A_c \end{bmatrix} \right) + \beta^T \otimes \left(\begin{bmatrix} A_i & B_iC_c \\ B_cC_i & A_c \end{bmatrix}^T P \right) < 0 \\
\begin{bmatrix}
P \begin{bmatrix} A_i & B_iC_c \\ B_cC_i & A_c \end{bmatrix} + \left(P \begin{bmatrix} A_i & B_iC_c \\ B_cC_i & A_c \end{bmatrix} \right)^T & P \begin{bmatrix} 0 \\ B_c \end{bmatrix} & \begin{bmatrix} C_i^T \\ 0 \end{bmatrix} \\
* & -\gamma I & I \\
* & * & -\gamma I
\end{bmatrix} < 0 \\
\begin{bmatrix} Q & \begin{bmatrix} 0 & C_c \end{bmatrix} \\ * & P \end{bmatrix} > 0 \\
Trace(Q) < \nu
\end{cases}
\tag{3.43}
$$

$$
i = 1, 2, \cdots, L
$$

The optimization problem can be interpreted as finding a common set of controller variables $(A_c,\ B_c,\ C_c)$ subject to multiple sets of BMI constraints. In addition, the Lyapunov matrix *P* of all constraints should be solved as the unified one.

The optimization problem in (3.43) is bilinear and impossible to be solved via the same method as that has been used for the nominal model system. Because the system matrices A_i, B_i, C_i are varying with respect to their operating points and the matrix inequalities with nonlinear terms cannot be linearized by Lyapunov matrix parameterization and system matrix variable transformation. To overcome the difficulties mentioned above, a two-step approach is introduced here to solve the BMI optimization problem in a circuitous way [83]:

Step 1: Find a state-feedback controller in the form of $u = Kx$ such that the close-loop systems satisfy the control objectives under all considered operating points.

Step 2: Find an output-feedback controller in the form of (3.22) with the controller variable C_c equal to the state-feedback controller gain K (i.e. $C_c = K$) such that the close-loop systems satisfy the control objectives under all considered operating points.

Step 1: State-Feedback Controller Design

Suppose a state-feedback controller in the form of $u = Kx$ is to be designed, the corresponding close-loop systems with such controller can be represented by:

$$\begin{aligned} \dot{x} &= (A_i + B_i K)x \\ z_\infty &= C_i x + w \\ z_2 &= Kx \\ i &= 1, 2, \cdots, L \end{aligned} \tag{3.44}$$

Based on (3.44), the synthesis BMI optimization problem can be expressed as:

$$\min\left[\alpha_1 Trace(Q)+\alpha_2\gamma\right]$$

$$s.t.\quad \begin{cases} \alpha\otimes P+\beta\otimes\left((A_i+B_iK)P\right)+\beta^T\otimes\left((A_i+B_iK)P\right)^T<0 \\ \begin{bmatrix} (A_i+B_iK)P+\left((A_i+B_iK)P\right)^T & 0 & PC_i^T \\ * & -\gamma I & I \\ * & * & -\gamma I \end{bmatrix}<0 \\ \begin{bmatrix} Q & KP \\ * & P \end{bmatrix}>0 \\ Trace(Q)<\nu \end{cases} \tag{3.45}$$

$$i=1,2,\cdots,L$$

Let $X=P$ and $Y=KP$, the BMI optimization problem in (3.45) can be easily converted into the following LMI optimization problem:

$$\min\left[\alpha_1 Trace(Q)+\alpha_2\gamma\right]$$

$$s.t.\quad \begin{cases} \alpha\otimes P+\beta\otimes\left(A_iX+B_iY\right)+\beta^T\otimes\left(A_iX+B_iY\right)^T<0 \\ \begin{bmatrix} A_iX+B_iY+\left(A_iX+B_iY\right)^T & 0 & XC_i^T \\ * & -\gamma I & I \\ * & * & -\gamma I \end{bmatrix}<0 \\ \begin{bmatrix} Q & Y \\ * & X \end{bmatrix}>0 \\ Trace(Q)<\nu \end{cases} \tag{3.46}$$

$$i=1,2,\cdots,L$$

Consequently, the problem can be solved by convex LMI solvers and the state-feedback controller can be determined as :

$$K=Y^*(X^*)^{-1} \tag{3.47}$$

where X^* and Y^* are the optimal solutions of (3.46).

Step 2: Output-Feedback Controller Design

The controller gain K is then plugged into the output-feedback controller, and we have:

$$\begin{aligned} \dot{x}_c &= A_c x_c + B_c y \\ u &= K x_c \end{aligned} \tag{3.48}$$

The close-loop systems with the above controller and the corresponding synthesis BMI optimization problem will be the same as that has been presented in (3.42) and (3.43) despite the fact that controller variable C_c in this step is already known ($C_c = K$). Therefore, we only have to find the controller variable A_c and B_c such that the close-loop systems with the controller $(A_c,\ B_c,\ K)$ satisfy all the control objectives.

To linearize the BMI constraints, it is firstly assumed that the Lyapunov matrix P is in the following structure:

$$P = \begin{bmatrix} X & 0 \\ 0 & Y \end{bmatrix} \tag{3.49}$$

where $X > 0$ and $Y > 0$.

According to [83], the necessity condition for (3.49) to hold is that the first block entry A_i of the close-loop state matrix $A_{cl,i} = \begin{bmatrix} A_i & B_i K \\ B_c C_i & A_c \end{bmatrix}$ is stable for $i = 1, 2, \cdots, L$. To remove this restriction, the following transformation of basis is introduced:

$$T = T^{-1} = \begin{bmatrix} I & 0 \\ I & -I \end{bmatrix} \tag{3.50}$$

By pre-multiplying T to the close-loop system state vector x_{cl} in (3.42), the close-loop systems can be transformed as:

$$\begin{aligned} \dot{\bar{x}}_{cl} &= \bar{A}_{cl,i}\bar{x}_{cl} + \bar{B}_{cl,i}w \\ z_\infty &= \bar{C}_{cl1,i}\bar{x}_{cl} + D_{cl1,i}w \\ z_2 &= \bar{C}_{cl2,i}\bar{x}_{cl} + D_{cl2,i}w \\ i &= 1,2,\cdots,L \end{aligned} \tag{3.51}$$

where

$$\begin{aligned} \bar{x}_{cl} &= Tx_{cl} = \begin{bmatrix} x \\ x - x_{cl} \end{bmatrix} \\ \bar{A}_{cl,i} &= TA_{cl,i}T^{-1} = \begin{bmatrix} A_i + B_iK & -B_iK \\ A_i + B_iK - (B_cC_i + A_c) & -B_iK + A_c \end{bmatrix} \\ \bar{B}_{cl,i} &= TB_{cl,i} = \begin{bmatrix} 0 \\ -B_c \end{bmatrix} \\ \bar{C}_{cl1,i} &= C_{cl1,i}T^{-1} = \begin{bmatrix} C_i & 0 \end{bmatrix}\begin{bmatrix} I & 0 \\ I & -I \end{bmatrix} = \begin{bmatrix} C_i & 0 \end{bmatrix} \\ \bar{C}_{cl2,i} &= C_{cl2,i}T^{-1} = \begin{bmatrix} 0 & K \end{bmatrix}\begin{bmatrix} I & 0 \\ I & -I \end{bmatrix} = \begin{bmatrix} K & -K \end{bmatrix} \end{aligned} \tag{3.52}$$

It can be seen that the first block entry of the close-loop system state matrix $\bar{A}_{cl,i}$ is $(A_i + B_iK)$ whose stability is already guaranteed by the state-feedback controller design in the previous step. Therefore, for the close-loop systems presented in (3.51), it is safe to apply variable transformations with the Lyapunov matrix P in the form of (3.49).

The BMI optimization problem with the close-loop systems in (3.51) can be expressed as:

$$\min\left[\alpha_1 Trace(Q)+\alpha_2\gamma\right]$$

$$s.t.\quad \begin{cases} \alpha\otimes P+\beta\otimes(P\overline{A}_{cl,i})+\beta^T\otimes(\overline{A}_{cl,i}^T P)<0 \\ \begin{bmatrix} P\overline{A}_{cl,i}+\overline{A}_{cl,i}^T P & P\overline{B}_{cl,i} & \overline{C}_{cl1,i}^T \\ * & -\gamma I & D_{cl1,i}^T \\ * & * & -\gamma I \end{bmatrix}<0 \\ \begin{bmatrix} Q & \overline{C}_{cl2,i} \\ * & P \end{bmatrix}>0, \\ Trace(Q)<\nu \end{cases} \tag{3.53}$$

$$i=1,2,\cdots,L$$

Substituting (3.48) and (3.49) into (3.53):

$$\min\left[\alpha_1 Trace(Q)+\alpha_2\gamma\right]$$

$$s.t.\quad \begin{cases} \alpha\otimes\begin{bmatrix} X & 0 \\ 0 & Y \end{bmatrix}+sym\left(\beta\otimes\begin{bmatrix} X(A_i+B_iK) & -XB_iK \\ Y(A_i+B_iK)-GC_i-Z & -YB_iK+Z \end{bmatrix}\right)<0 \\ \begin{bmatrix} sym\left(\begin{bmatrix} X(A_i+B_iK) & -XB_iK \\ Y(A_i+B_iK)-GC_i-Z & -YB_iK+Z \end{bmatrix}\right) & \begin{bmatrix} 0 \\ -G \end{bmatrix} & \begin{bmatrix} C_i^T \\ 0 \end{bmatrix} \\ * & -\gamma I & I \\ * & * & -\gamma I \end{bmatrix}<0 \\ \begin{bmatrix} Q & [K & -K] \\ * & \begin{bmatrix} X & 0 \\ 0 & Y \end{bmatrix} \end{bmatrix}>0 \\ Trace(Q)<\nu \end{cases} \tag{3.54}$$

$$i=1,2,\cdots,L$$

where $Z = YA_c$, $G = YB_c$ and $sym(M) = M + M^T$.

Now, the optimization problem in (3.54) is linearized. Solving the LMI optimization problem gives the optimal solutions X^*, Y^*, Z^*, G^*. Consequently, the output-feedback controller variables A_c and B_c can be determined as:

$$A_c = (Y^*)^{-1} Z^*, \quad B_c = (Y^*)^{-1} G^* \tag{3.55}$$

To sum up, solving the BMI optimization problem with a multi-model system is much more complex than that with a nominal model system as the direct system variable transformation is not applicable. However, the linearization of the BMI constraints can still be accomplished through a circuitous two-step approach. By plugging a predetermined state-feedback controller gain *K* into the output-feedback controller variable C_c, the transformation of basis can be safely applied to convert the BMI optimization problem into an LMI optimization problem.

3.4. Summary

In this chapter, a BMI-based robust damping control approach was proposed for FACTS damping controller designs. Multiple control objectives including regional pole placement, control effort optimization and disturbance rejection could be simultaneously considered to ensure the effectiveness and robustness of the design. Formulations of these control objectives were based on matrix inequalities and the robust damping control problem was mathematically expressed as an optimization problem with a set of BMI constraints. To emphasise the concept of multi-model system design, the optimization problem was expanded with multiple sets of BMI constraints regarding control objectives under different system operating conditions.

To solve the BMI optimization problem with the existing convex LMI solvers, linearization of the BMI constraints was necessary. However, the linearization procedures were different in terms of a nominal model system and a multi-model system. For a nominal model system, Lyapunov matrix parameterization and system matrix variable transformation could be directly applied to linearize the BMI constraints. But for a multi-model system, the same method was not applicable as the system matrices were varying with respect to different system operating points. To this end, a two-step method was introduced to convert the BMI optimization problem into two LMI optimization problems for a multi-model system. Following the two-step method, the output-feedback controller variables could be systematically determined.

CHAPTER 4 ROBUST FACTS DAMPING CONTROLLER DESIGNS VIA BMI-BASED MULTI-OBJECTIVE MULTI-MODEL SYSTEM APPROACH

Abbreviations

BMI	Bilinear Matrix Inequality
FACTS	Flexible AC Transmission System
LMI	Linear Matrix Inequality
LTI	Linear Time Invariant
PSS	Power System Stabilizer
RTDS	Real-Time Digital Simulator
SVC	Static VAR Compensator
TCSC	Thyristor Controlled Series Compensator

4.1. Introduction

The mathematical formulation of the robust damping control problem was presented in Chapter 3 with corresponding analytical solutions. In practical designs, it is essential that the damping

control problem to be formulated is actually feasible in terms of finding a reliable optimal solution.

This chapter presents the complete procedures of robust FACTS damping controller designs. The controller designs are fundamentally based on the approach proposed in Chapter 3, where control objectives under multiple operating conditions are considered via synthesis BMI optimization. Furthermore, discussions are also conducted on the choice of feedback signals and system model reductions in consideration of controller designs in real practice.

The robust FACTS damping controller designs are successively implemented on a two-area system and a five-area system. For each test system, a TCSC damping controller and an SVC damping controller are individually designed to validate the generality of the proposed method. The damping performance of the obtained controllers is evaluated through both linear eigenvalue analysis and real-time simulations on RTDS. Based on the numerical results, the benefits of the proposed design approach are discussed.

4.2. Controller Design Procedures

The complete design procedures of robust FACTS damping controllers are presented as follows:

Step 1. Formulate the multi-model system with a set of LTI state-space representations according to different system operating points.

Step 2. Identify the weakly damped oscillatory modes of the open-loop systems through eigenvalue analysis.

Step 3. Define the LMI pole placement region on the complex plane according to the system damping requirements.

Step 4. Select the feedback signal for the controller based on participation factors or system modal residues of the weakly damped oscillatory modes.

Step 5. Apply system order reduction to the open-loop system such that the reduced system is comparable to the original system.

Step 6. Define the H_2 augmented output for control effort optimization (disturbance rejection is not considered here as it may lead to controller over design under multiple system operating points).

Step 7. Formulate the robust damping control problem as a synthesis BMI optimization problem.

Step 8. Solve the synthesis BMI optimization problem via the two-step method and determine the controller transfer function.

Step 9. Validate the performance of the obtained FACTS damping controller through eigenvalue analysis of the full-order linear close-loop system.

Step 10. Validate the performance of the obtained FACTS damping controller by real-time simulations on RTDS.

4.3. Choice of Feedback Signal

The relationship between and the system oscillatory modes and their eigenvalues has already been explained in Chapter 3. Eigenvalue analysis should be performed for each open-loop system that has been included in the multi-model system to investigate the weakly damped oscillatory modes and their damping characteristics. Besides, the system eigenproperties also contain useful information about system mode shape, modal controllability and observability [10]. In this section, the choice of feedback signal will be discussed based on the eigenproperties of systems.

4.3.1. Participation Factor

System mode shapes are defined by the participation factors. Participation factor shows how much a generator is participated in a particular oscillatory mode [10]; be more specific, it shows the sensitivity of a generator state to a particular oscillatory mode.

The participation factor can be used for finding the optimal PSS installation location in a multi-machine system [20, 84]. Using the generator state with the highest participation factor to a particular local oscillatory mode as the feedback signal for PSS can effectively reduce the control effort; as a result, the damping performance can be improved.

The above rule can also be applied to the FACTS damping controller designs to a certain extent. However, a single generator state, even with the highest participation factor, is still a rough candidate feedback signal for the damping of inter-area oscillatory modes involving multiple generators from different areas, since its observability of the inter-area oscillatory modes is considerably low. Besides, some of the highly participated generator states such as machine rotor angles, are not directly measurable, which also makes the generator states useless in the damping of inter-area oscillations.

Nevertheless, we still can study the mode shape of an inter-area oscillatory mode through its participation factors (i.e. how the generator or the generator groups are involved in the inter-area oscillatory mode). But for FACTS damping controller designs, the feedback signals should be cautiously selected from signals with higher observability.

4.3.2. Modal Residue

The system modal controllability and observability should be comprehensively investigated in

advance to make sure that the system input and output are properly selected, otherwise, forcing the pole placement with inappropriate system input and output may result in infeasible solution or numerical instability.

Suppose a strictly proper open-loop system ($D=0$) is represented by the following transfer function:

$$G(s) = C(sI - A)^{-1}B \tag{4.1}$$

The system modal controllability to a certain oscillatory mode λ_i is decided by the eigenvectors of matrix *A* and the system input matrix *B*; and the system modal observability to oscillatory mode λ_i is decided by the eigenvectors of matrix *A* and the system output matrix *C*.

It is known that with different system inputs and outputs, the system modal controllability and observability to a certain oscillatory mode can be quite different. In order to numerically evaluate the modal controllability and observability, the concept of system modal residue is introduced [10, 72]. The transfer function in (4.1) can be rewritten in the following partial fraction expression:

$$G(s) = \sum_{i=1}^{n} \frac{Cv_i w_i B}{s - \lambda_i} = \sum_{i=1}^{n} \frac{R_i}{s - \lambda_i} \tag{4.2}$$

where v_i, w_i denote the i^{th} right and left eigenvectors of matrix A respectively, λ_i is the i^{th} eigenvalue of matrix A. R_i is called modal residue which contains system information about controllability $(w_i B)$ and observability (Cv_i) to the oscillatory mode λ_i.

From (4.2), it is known that the magnitude of the system transfer function $|G(s)|$ is very much

related to the value of modal residue R_i. For a particular oscillatory mode, a larger value of modal residue usually indicates that the choice of system input and output is better and less control effort will be needed in the feedback loop.

In the following designs, the installation locations of the FACTS devices are preselected which means the modal controllability to the oscillatory modes has already been fixed. However, the modal observability can still be modified with different choices of feedback signals.

The feedback signals are normally selected from system line currents and power flows with invaluable information of the objective oscillatory modes (with high modal observability of the oscillatory modes). In addition, the feedback signals should also be locally measurable so that the controller design is decentralized and easier to be realized in real practice.

4.4. System Order Reduction

The order of the linear open-loop systems depends on the scale of the test system, in other words, it depends on the number of generators and FACTS devices in the power system. Therefore, the system dynamics of a large system with multiple generators and FACTS devices could be in a high order. With the output-feedback controller, the order of the close-loop system is even higher.

It is hardly possible to implement the BMI optimization directly on a full-order system as the computational effort is tremendous. From the damping control point of view, it is also unnecessary to perform regional pole placement over all frequencies since the problem only focuses on a particular frequency band (0.1~2.0 Hz).

To simplify the optimization problem, balanced truncation model reduction [85, 86] will be

used to reduce the order of the original system. The system order reduction is considered to be valid if the system is reduced to an acceptable level without losing much information within the frequency range of our interests. The order-reduced system will be used as a substitution of the original system in the BMI optimization; when the damping controller is obtained, further reductions for the controller should be applied if it is necessary.

It should be pointed out that the state variable sequences $\Delta x = [\Delta\delta_1 \quad \Delta\omega_1 \quad \cdots]$ of all full-order systems that have been included in a multi-model system are in fact identical. However, after system order reduction, the state variables of different system models are no longer in the same sequence. This will cause a failure of finding a common state-feedback controller $u = Kx$ in the two-step approach. To keep the state variables of different system models in the same sequence, all reduced systems are represented in a controllable canonical form [76].

4.5. Real-time Simulations on RTDS

Real-time simulations will be carried on RTDS to evaluate the controller designs. The RTDS is a simulator well-known for its "hard real-time" feature; the virtual simulations on the RTDS can be interfaced with the hardware-based power system equipment such as commercial relay and external controller in real-time [87, 88]. Comparing with the conventional off-line simulation packages such as MATLAB and PSCAD/EMTDC, the RTDS has great dominance in both computational speed and simulation accuracy.

4.6. Applications on a Two-area System

The FACTS damping controller designs are firstly implemented on a classic two-area system

[10] as illustrated in Figure 4-1.

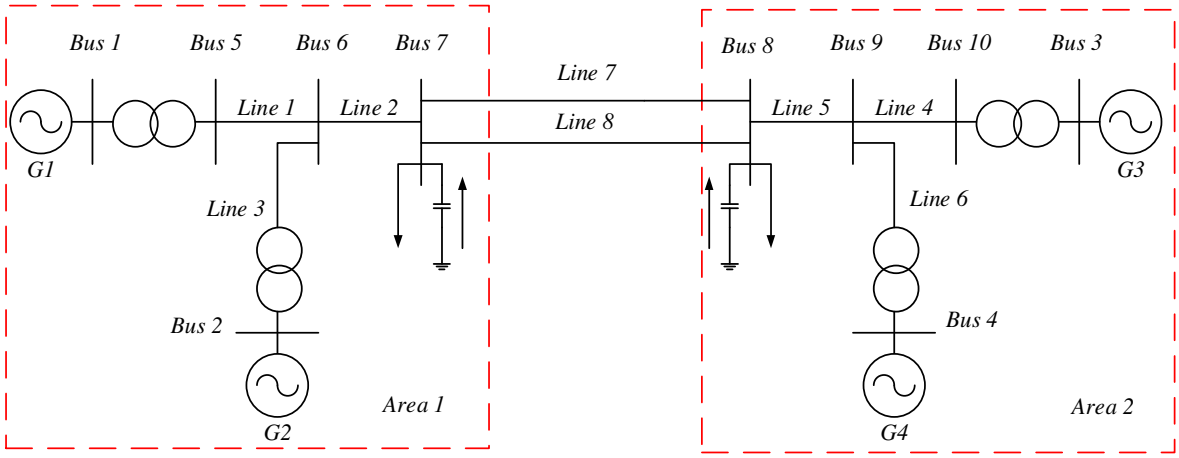

Figure 4-1 Two-area four-generator system

The system is consisting of four synchronous generators and ten buses. It can be seen that the system network topologies of Area 1 and 2 are in fact symmetrical and the two areas are connected by two transmission corridors Line 7 and 8. Each generator injects the same amount of power into the network, while the loads are installed on Bus 7 and 8 to consume the power.

If the loads are unevenly distributed on Bus 7 and 8, the difference value will be transferred between the two areas through Line 7 and 8 to balance the power flow. Multiple operating points can be generated by changing the power flow patterns with different load configuration as shown in Table 4-1. The multi-model system is formed based on these operating points.

Table 4-1 Multiple operating points for the two-area system

Operating points	Active power transferred in MW (Area 1 → Area 2)	Load at Bus 7 in MW	Load at Bus 8 in MW
1	250	1100	1600
2	300	1067	1667
3	350	1000	1700
4	400	967	1767

PSSs are installed on G1 and G3 to mitigate local oscillations, while the information of TCSC and SVC will be accordingly explained in Section 4.6.1 and Section 4.6.2. The other details of the two-area test system can be found in Appendix A.

4.6.1. Damping Controller Design of TCSC

The TCSC is installed on Line 8 with a 25% compensation of the line reactance for steady state operation. The upper and lower boundary of the TCSC compensation is 35% and 15%. The controller output will be connected to the reactance reference of the TCSC so that the power flow on Line 8 can be controlled to provide extra damping during oscillations.

Eigenvalue Analysis and LMI Pole Placement Region

Eigenvalue analysis is conducted to inspect the damping characteristics of the open-loop systems under different operating points. The dominant oscillatory modes for the two-area system with TCSC are listed below:

Table 4-2 Oscillatory modes of the two-area system with TCSC

Operating Points	Mode 1		Mode 2		Mode 3	
	ζ	ω (Hz)	ζ	ω (Hz)	ζ	ω (Hz)
1	18.2%	1.162	20.1%	1.176	6.50%	0.681
2	18.4%	1.160	19.3%	1.174	6.29%	0.678
3	18.1%	1.158	19.8%	1.170	6.29%	0.669
4	18.4%	1.155	18.8%	1.169	6.05%	0.664

According to Table 4-2, it is known that the two-area system with TCSC has three dominant oscillatory modes: Mode 1 and 2 are local oscillatory modes with sufficient damping since PSSs are installed in both areas; Mode 3 is a weakly damped inter-area oscillatory mode ($\zeta \approx 6\%$) which doesn't meet the system damping requirement.

In this case, it is expected that the damping ratio ζ of Mode 3 can be increased to an acceptable level with the design of a TCSC damping controller. To this end, an LMI region, as illustrated in Figure 4-2, is assigned for the pole placement.

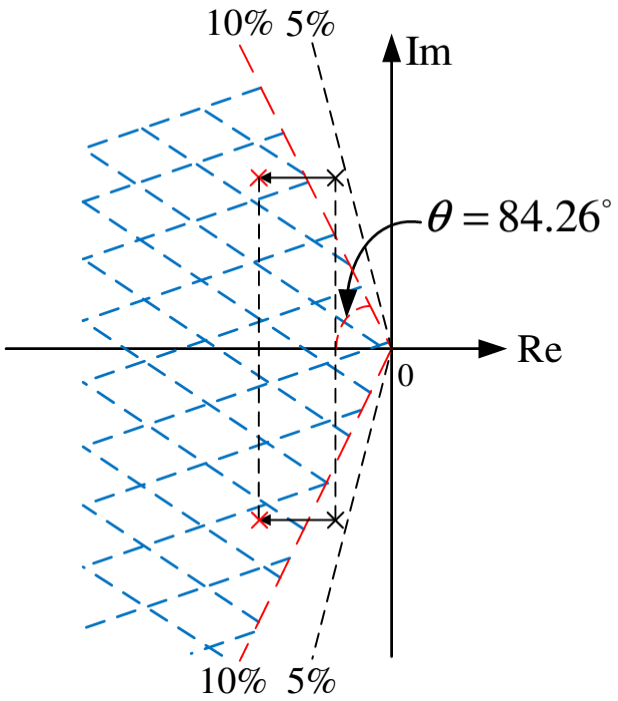

Figure 4-2 The LMI pole placement region

According to (3.5), the corresponding coefficients for the above LMI pole placement region are

$$\alpha = 0,\ \beta = \begin{bmatrix} 0.9950 & -0.1000 \\ 0.1000 & 0.9950 \end{bmatrix} \tag{4.3}$$

Remark: The settling time $T_s \cong 4/\zeta\omega$ of an inter-area oscillatory mode is expected to be controlled within 10 seconds for such a small system. In this case, the settling time for Mode 3 is around 15 seconds. By moving the eigenvalues of Mode 3 to their left in a conic sector with at least 10% damping ratio, the system damping requirements should be satisfied.

Selection of the Feedback Signal

Figure 4-3 illustrates the participation factors of different rotor angles and speeds to Mode 3 under operating point 4. It should noticed that the participation factors have been normalized with a maximum value of 1.0 so that different type of states can be comparable to each other.

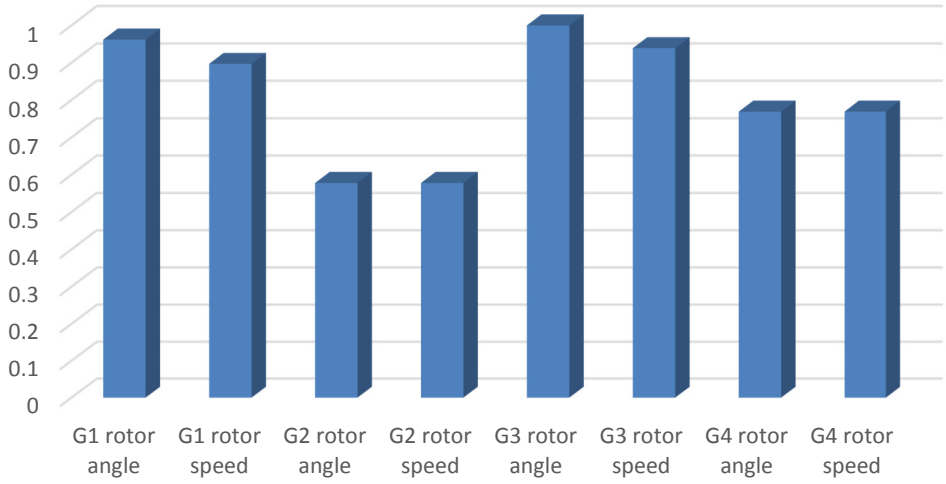

Figure 4-3 Participation factors of different generators to Mode 3

It can be seen that the most participated system states to Mode 3 are the rotor angles and speeds of G1 and G3; in other words, the inter-area oscillation is mainly caused by G1 oscillating against G3. Since the two-area system is considerably small and the mode shape of Mode 3 is quite straightforward, the rotor speed deviation is adopted here as the feedback signal for the TCSC damping controller. To increase the observability of Mode 3, a combination of G1 and G3 rotor speed deviations is used as the feedback signal:

$$\Delta y = \Delta\omega_1 - \Delta\omega_3 \tag{4.4}$$

The feedback signal in (4.4) was also used in [89]; it has been proven to be effective for FACTS damping controller designs in the two-area system.

System Order Reduction

The synchronous generator with excitation system, PSS, and TCSC are in the order of 7, 3 and 1. Therefore, the two-area four-generator system with two PSSs and one TCSC is in the order of 35. The full-order system is then reduced to a 7^{th} order system by balanced truncation model reduction. The eigenvalues of the order-reduced system at operating point 4 are presented in Table 4-3 to examine the validity of the system order reduction. The corresponding frequency responses are demonstrated in Figure 4-4. From Table 4-3 and Figure 4-4, it is known that the system order reduction is successful as the order-reduced system doesn't lose much information within 0.1~2.0 Hz.

Table 4-3 Eigenvalues of the reduced system at operating point 4

Eigenvalues	ζ	ω (Hz)
-0.253±4.170i	**6.04%**	**0.665**
-1.310±7.270i	17.8%	1.176
-6.420±12.70i	45.0%	2.276
-22.700	/	/

Forming the State-space Realizations

The objective of control effort optimization is included to formulate the synthesis problem; as only one augmented output is considered here, its weight function is simply set to be scalar 1. The state-space realizations with H_2 output are

$$\begin{aligned} \dot{x} &= A_i x + B_i u \\ z_2 &= u \\ y &= C_i x + w \\ i &= 1,2,3,4. \end{aligned} \tag{4.5}$$

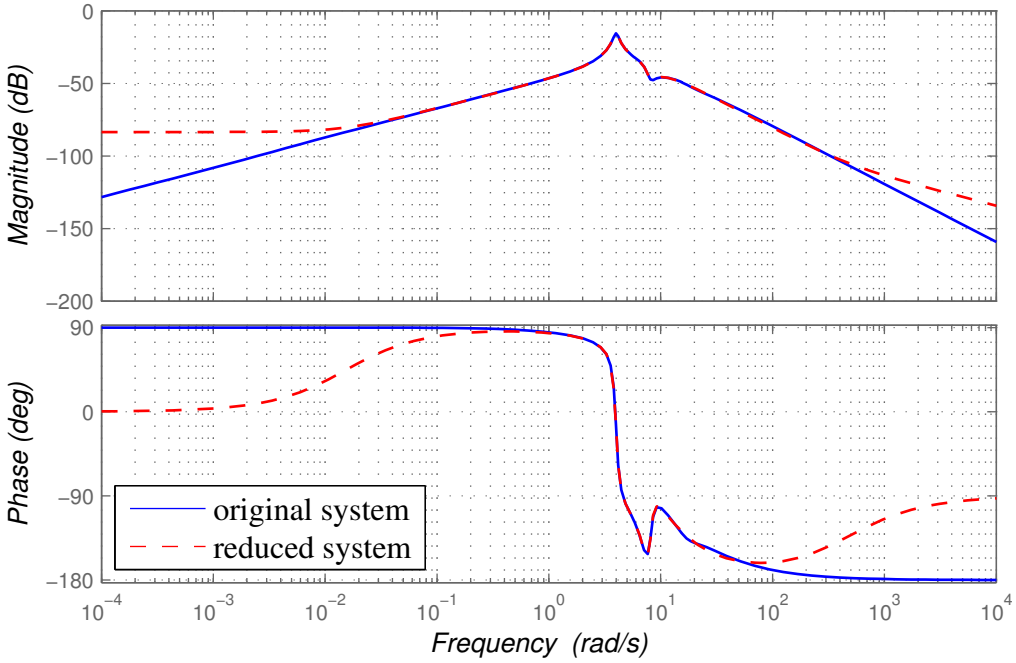

Figure 4-4 Frequency responses: origianl system v.s. reduced system at operating point 4

where $A_i \in \Re^{7\times7}$, $B_i \in \Re^{7\times1}$ and $C_i \in \Re^{1\times7}$.

Finding the Controller through Two-step Approach

Firstly, find the state-feedback controller K by solving (3.46); the optimization problem can be solved by function *mincx* in MATLAB and controller K is determined by optimal solutions $X^* \in \Re^{7\times7}$ and $Y^* \in \Re^{1\times7}$ as follows:

$$K = Y^*(X^*)^{-1} = [-0.5 \quad -19.9 \quad -346.6 \quad -4387.9 \quad -21855.0 \quad -146310.0 \quad -3979.4] \tag{4.6}$$

Secondly, plug the state-feedback controller into the output-feedback controller ($C_c = K$) to find the controller variables A_c and B_c by solving (3.54); the optimization problem can also be solved by function *mincx* in MATLAB and controller variable A_c and B_c are consequently determined by the optimal solutions $Y^* \in \Re^{7\times7}$, $Z^* \in \Re^{7\times7}$ and $G^* \in \Re^{7\times1}$ as follows:

$$A_c = (Y^*)^{-1} Z^*$$

$$= \begin{bmatrix} -32.5 & -443.3 & -2127.4 & 15359.8 & 74227.3 & 2230075.3 & -1614292.1 \\ 0.8 & -9.7 & -245.2 & -2669.7 & -17508.3 & -112735.8 & -97136.7 \\ 0.0 & -0.9 & -42.0 & -658.5 & -3431.9 & -30176.0 & -8747.0 \\ 0.0 & 0.2 & 6.2 & 77.8 & 412.9 & 3523.3 & 1188.7 \\ 0.0 & 0.0 & -0.4 & -4.2 & -30.0 & -231.5 & -121.8 \\ 0.0 & 0.0 & 0.0 & -0.1 & 0.7 & -6.1 & 4.6 \\ 0.0 & 0.0 & 0.0 & 0.1 & 0.6 & 5.9 & 2.6 \end{bmatrix} \quad (4.7)$$

$$B_c = (Y^*)^{-1} G^* = \begin{bmatrix} -56.1432 & 1.9804 & 0.5663 & -0.0656 & 0.0043 & 0.0001 & 0.0000 \end{bmatrix}^T \quad (4.8)$$

At last, the controller transfer function $tf(A_c, B_c, C_c, 0)$ is determined as:

$$G_{TCSC}(s) = \frac{-29.91(s^2 + 25.65s - 23.40)(s^2 + 14.83s + 314.54)(s^2 + 2.57s + 55.51)}{(s + 0.44)(s^2 + 26.87s + 789.07)(s^2 + 10.49s + 139.07)(s^2 + 1.97s + 55.14)} \quad (4.9)$$

Linear Close-loop System Performance

Eigenvalue analysis is performed for each full-order linear close-loop system with the obtained TCSC damping controller (4.9) to examine its damping control performance. Figure 4-5 shows the eigenvalue plots of the open-loop system and the close-loop system at operating point 4. It is clear that the weakly damped system eigenvalues have been moved to the desired LMI region as we expected.

A comparison of inter-area oscillatory modes between the open-loop and close-loop system under multiple system operating points is shown in Table 4-4. It can be seen that the damping ratio of the inter-area oscillatory mode has been increased to a satisfactory level under each system operating point, thus the TCSC damping controller is considered to be robust against different power flow patterns in a set range.

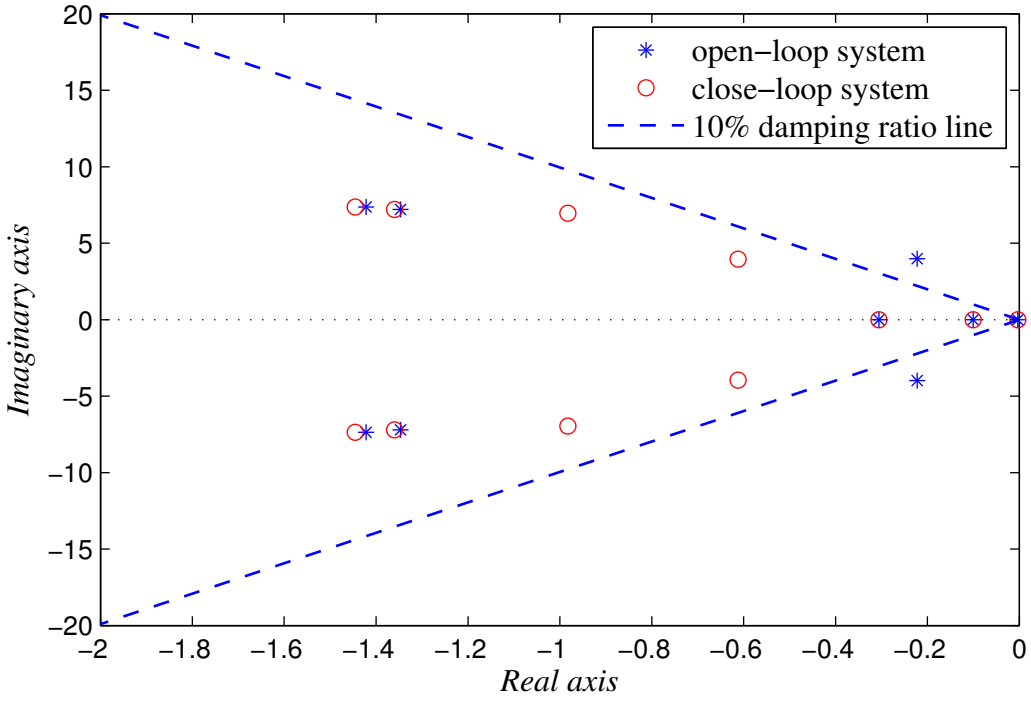

Figure 4-5 Eigenvalue plots: the open-loop system v.s. the close-loop system

Table 4-4 Inter-area oscillatory modes of the open-loop system and the close-loop system

Operating points	Open-loop system		Close-loop system	
	ζ	ω (Hz)	ζ	ω (Hz)
1	6.50%	0.681	11.5%	0.684
2	6.29%	0.678	12.0%	0.679
3	6.29%	0.669	13.5%	0.672
4	6.05%	0.664	14.1%	0.665

4.6.2. Damping Controller Design of SVC

The SVC is installed on Bus 7 with a rated capacity of ±100Mvar; by means of injecting and absorbing reactive power, it is able to regulate the voltage at Bus 7. For steady state operation, the voltage at Bus 7 is set to $V_{B7} = 1.0$ p.u. The damping controller output is added to the voltage reference of the SVC internal voltage regulator so that the voltage at V_{B7} can be continuously controlled to provide extra damping during oscillations.

Eigenvalue Analysis and LMI Pole Placement Region

The dominant oscillatory modes of the two-area system with SVC under different operating points are presented in Table 4-5. It is easy to see that the open-loop system has two well damped local oscillatory modes (Mode 1 and 2) and one weakly damped inter-area oscillatory mode (Mode 3).

Table 4-5 Oscillatory modes of the two-area system with SVC

Operating Points	Mode 1		Mode 2		Mode 3	
	ζ	ω (Hz)	ζ	ω (Hz)	ζ	ω (Hz)
1	18.6%	1.169	20.6%	1.185	5.69%	0.640
2	18.8%	1.170	19.9%	1.181	5.51%	0.636
3	18.5%	1.169	20.5%	1.176	5.48%	0.627
4	19.8%	1.171	18.5%	1.172	5.26%	0.621

The same LMI region, as shown in Figure 4-2, is assigned here for pole placement so that the damping ratio of Mode 3 can be increased with the design of SVC damping controller.

Selection of the Feedback Signal

Participation factors of different generator rotor angles and speeds are calculated for Mode 3; the same conclusion can be drawn that the inter-area oscillatory mode is highly related to the generator rotor angles and speeds of G1 and G3. Therefore, the same feedback signal $\Delta y = \Delta\omega_1 - \Delta\omega_3$ is selected for the SVC damping controller.

System Order Reduction

According to Section 2.3, the dynamics of SVC is in the order of 3, hence the two-area system with SVC will be in the order of 37. Balanced truncation model reduction is applied here so

that the full-order system can be reduced to a 7th order system. To examine the validity of the system order reduction, the eigenvalues of the order-reduced system at operating point 4 are presented in Table 4-6; the corresponding frequency responses are illustrated in Figure 4-6.

Table 4-6 Eigenvalues of the reduced system at operating point 4

Eigenvalues	ζ	ω (Hz)
-0.206±3.900i	**5.26%**	**0.622**
-1.260±7.330i	17.0%	1.184
-13.000	/	/
-4.290±13.80i	29.7%	2.292

From Table 4-6 and Figure 4-6, it can be seen that the 7th order system is very close to the full-order system within the frequency range of the inter-area oscillations. Thus, the system order reduction is considered to be acceptable for the SVC damping controller design.

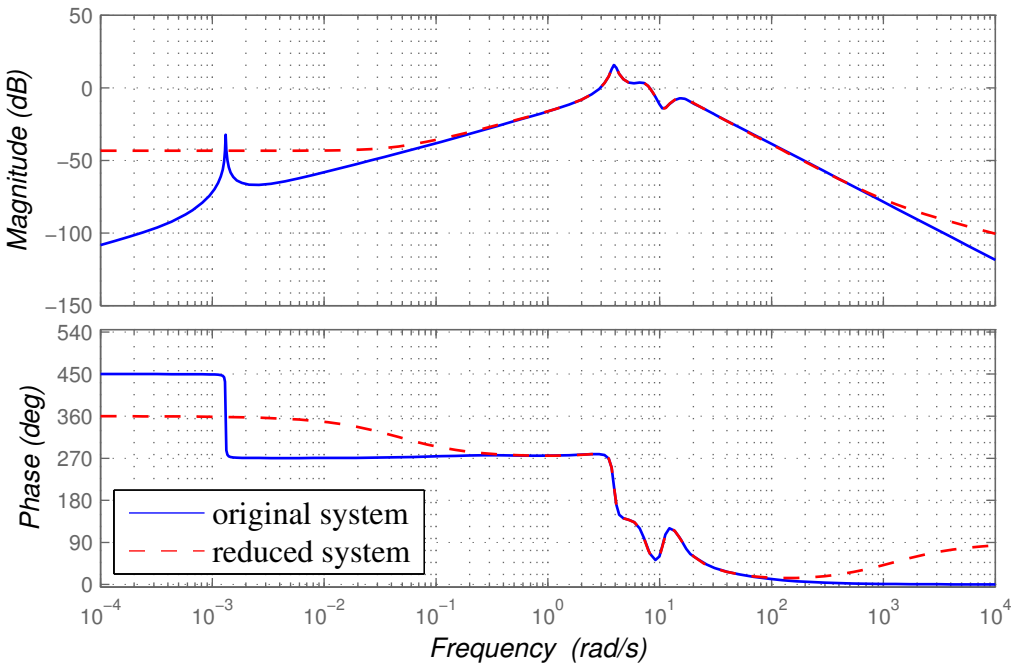

Figure 4-6 Frequency responses: origianl system v.s. reduced system at operating point 4

Forming the State-space Realizations

To include the objective of control effort optimization, state-space realizations with augmented H_2 output are formed in the exact same way as that have been done for the systems with TCSC.

Finding the Controller through Two-step Approach

The controller variables A_c, B_c, C_c are systematically determined through the two-step approach:

$$A_c = \begin{bmatrix} -3.86e3 & -5.37e5 & -4.34e6 & -7.67e7 & -3.60e8 & -1.41e9 & -1.24e8 \\ 750.58 & 1.04e5 & 8.48e5 & 1.49e7 & 7.03e7 & 2.75e8 & 2.39e7 \\ 31.22 & 4.36e3 & 3.53e4 & 6.23e5 & 2.92e6 & 1.14e7 & 9.96e5 \\ -29.31 & -4.09e3 & -3.31e4 & -5.85e5 & -2.75e6 & -1.07e7 & -9.36e5 \\ -2.05 & -28.82 & -233.16 & -4.11e3 & -1.93e4 & -7.57e4 & -6.55e3 \\ 0.78 & 109.15 & 883.05 & 1.55e4 & 7.32\,e\,4 & 2.87e5 & 2.49e4 \\ 0.39 & 55.51 & 449.12 & 7.92e3 & 3.72e4 & 1.45e5 & 1.26e4 \end{bmatrix} \tag{4.10}$$

$$B_c = \begin{bmatrix} -4536.90 & 885.34 & 36.88 & -34.62 & -0.24 & 0.92 & 0.16 \end{bmatrix}^T \tag{4.11}$$

$$C_c = \begin{bmatrix} -0.61 & -14.47 & -261.91 & -2793.30 & -14844.00 & -87981.00 & 1078.10 \end{bmatrix} \tag{4.12}$$

And the controller transfer function $tf(A_c, B_c, C_c, 0)$ is determined as:

$$G_{SVC}(s) = \frac{2.9150(s^2 + 2.00e5s + 2.00e6)(s^2 + 8.59s + 213.28)(s^2 + 2.50s + 56.00)}{(s + 1.68e5)(s^2 + 22.46s + 590.45)(s^2 + 3.40s + 100.55)(s^2 + 5.45s + 27.48)} \tag{4.13}$$

Linear Close-loop System Performance

The eigenvalue plots of the open-loop system and the close-loop system under operating point 4 are compared in Figure 4-7. It is easy to see that the eigenvalues of the close-loop system inter-area oscillatory mode has been moved to the desire LMI region with the obtained SVC

damping controller.

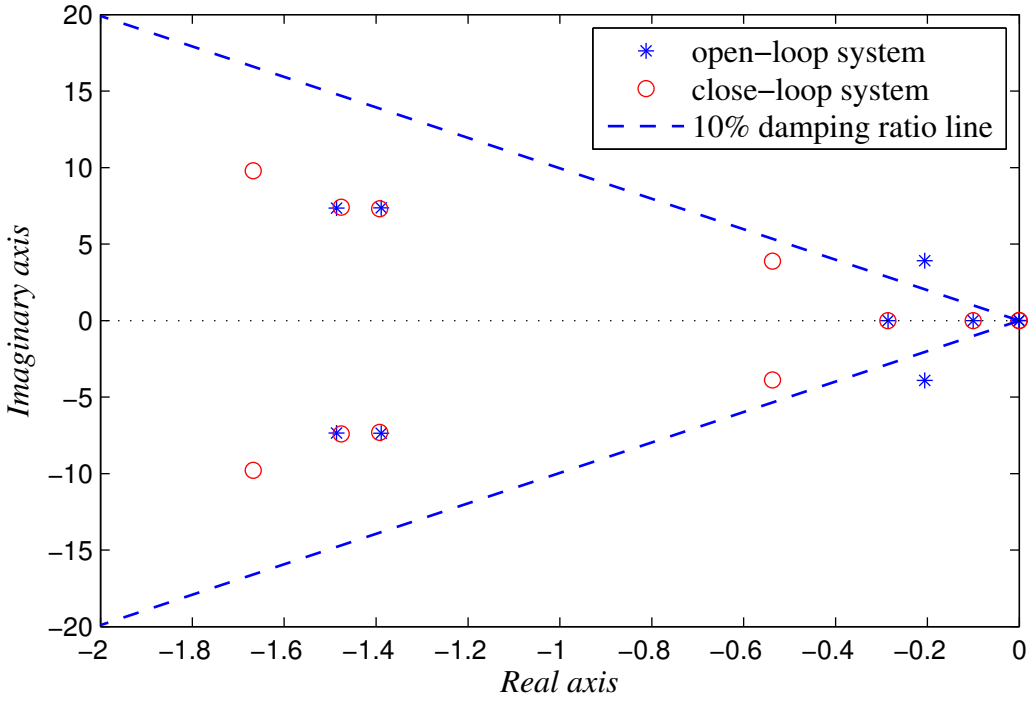

Figure 4-7 Eigenvalue plots: the open-loop system v.s. the close-loop system

To examine the robustness of the SVC damping controller, eigenvalue analysis is carried out on the full-order linear close-loop systems under multiple operating points. The inter-area oscillatory modes of the open-loop and close-loop systems are compared in Table 4-7. It can be seen that the damping ratio of the inter-area oscillatory mode has been adequately improved under each operating point which indicates that the obtained SVC damping controller is robust against different operating conditions as expected.

Table 4-7 Inter-area oscillatory modes of the open-loop system and the close-loop system

Operating points	Open-loop system		Close-loop system	
	ζ	ω (Hz)	ζ	ω (Hz)
1	5.69%	0.640	13.0%	0.639
2	5.51%	0.636	13.0%	0.635
3	5.48%	0.627	13.7%	0.630
4	5.26%	0.621	13.7%	0.624

4.6.3. Simulation Case Studies

Real-time simulations are conducted on RTDS to validate the performance of the obtained TCSC and SVC damping controllers. The controllers are tested under multiple system operating scenarios with three different types of disturbances: excitation system disturbance, system post-fault disturbance and system load variation. A wash-out filter block with the time constant of 10s is installed for each obtained FACTS damping controller to make sure that the damping control only contribute to a certain low frequency band.

Case 1: Excitation System Disturbance

The disturbance is generated by giving a small impulse to the excitation system voltage reference V_{ref} at G3. The small impulse has a constant magnitude of 1.10p.u. (the initial value of V_{ref} is 1.03p.u) and lasts for 200ms. The responses of power flow on Line 7 under operating 1 and 4 to the excitation system disturbance are illustrated in Figure 4-8.

Case 2: System Post-fault Disturbance

The system is tested in a post-fault condition in this case. The disturbance is generated by the circuit breaker tripping and auto-reclosing when the fault occurs and is cleared. The fault is a 3-phase to ground fault on Line 7 which lasts 20ms until Line 7 is tripped and it is cleared 60ms after the line trip and then the circuit breaker is auto-reclosed. The power flow responses on Line 7 at operating point 1 and 4 in the post-fault condition are illustrated in Figure 4-9.

Case 3: System Load Variation

In this case, the system is tested with load variations. The disturbance is generated by load

increasing or load shedding at Bus 7 and 8. It should be noticed that the four operating points considered in the controller design stage are actually based on different load configurations. Therefore, operating point switching can be simply interpreted as load variations. Figure 4-10 shows the power flow responses on Line 7 when the system switches from operating point 1 to operating 4.

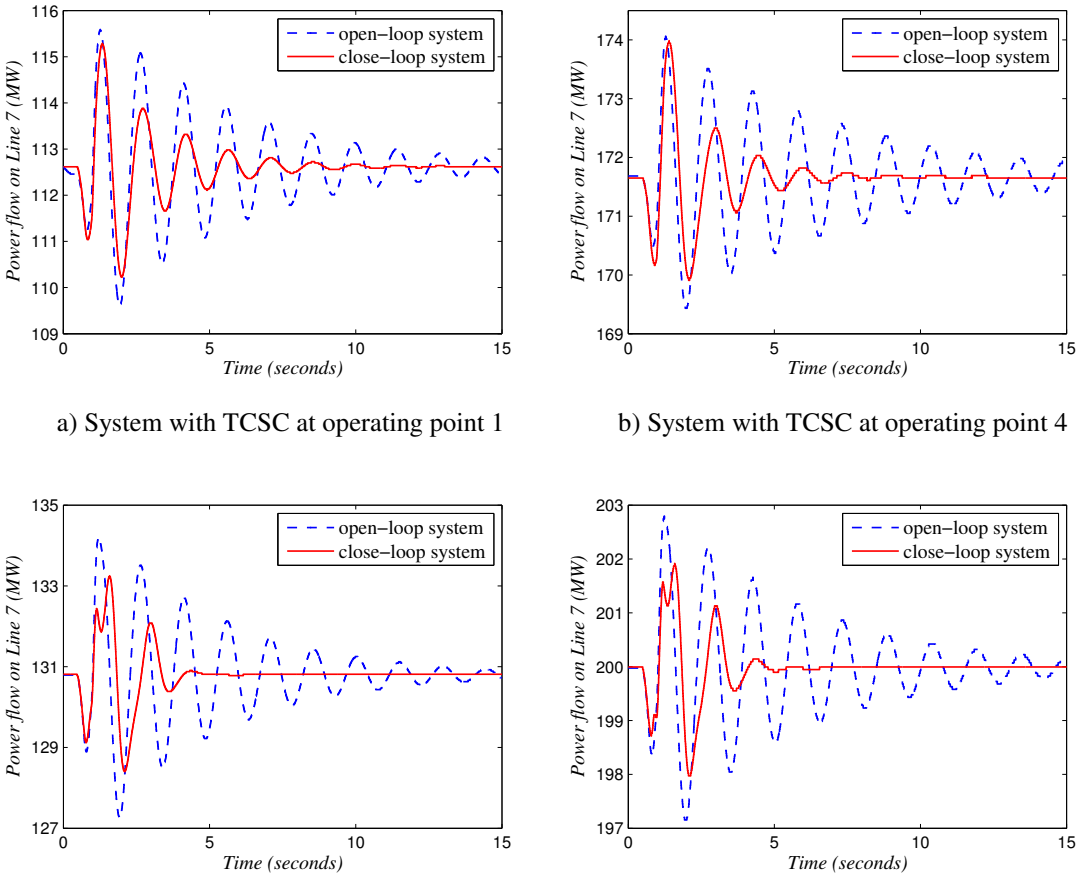

a) System with TCSC at operating point 1

b) System with TCSC at operating point 4

c) System with SVC at operating point 1

d) System with SVC at operating point 4

Figure 4-8 Power flow responses to excitation disturbance

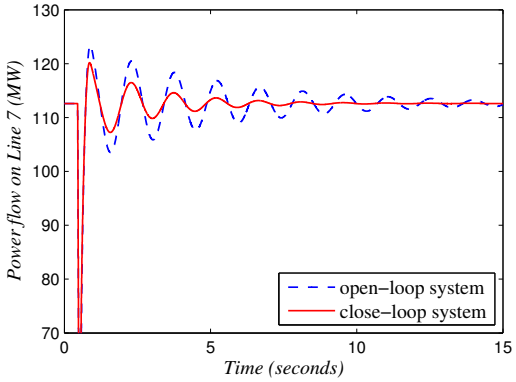

a) System with TCSC at operating point 1

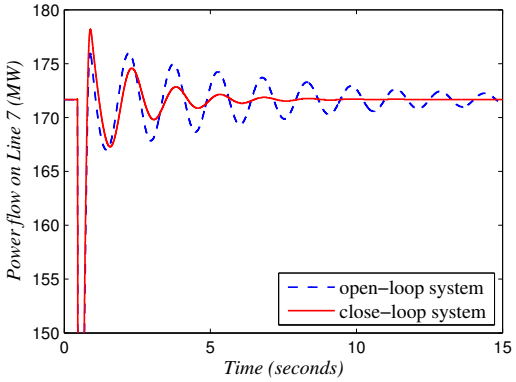

b) System with TCSC at operating point 4

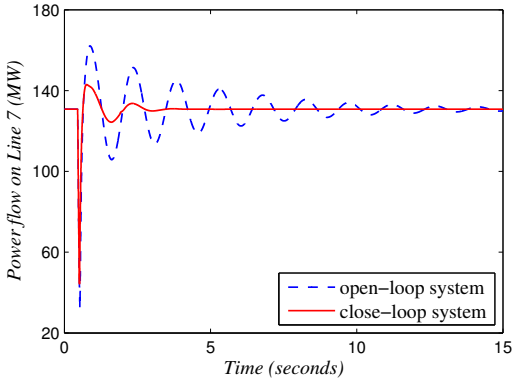

c) System with SVC at operating point 1

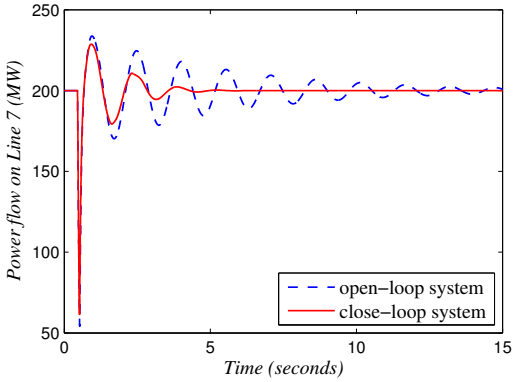

d) System with SVC at operating point 4

Figure 4-9 Power flow responses at post-fault condition

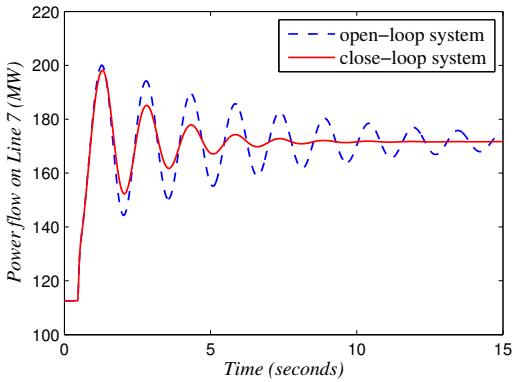

a) System with TCSC

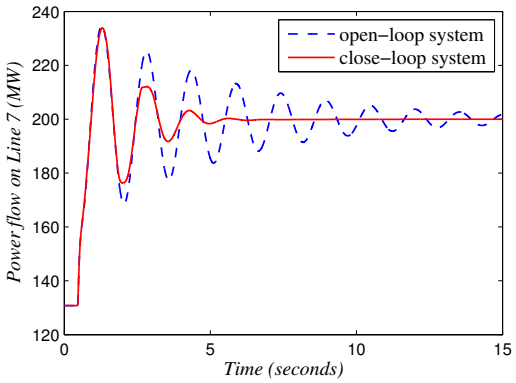

b) System with SVC

Figure 4-10 Power flow responses when system switches from operating 1 to operating 4

Discussion

From the above simulation results, it is known that the proposed FACTS damping controllers are capable of improving system damping of inter-area oscillations against different types of disturbances. The settling time of the inter-area oscillations in each case has been significantly reduced which completely fulfils the system damping requirement. The results also show that the controllers are robust enough to work under multiple system operating conditions which coincides with the eigenvalue analysis results.

4.7. Applications on a Five-area System

The FACTS damping controller designs are implemented on a five-area system [11] to further explore the feasibility of the design approach proposed in Chapter 3. The five-area system is a simplified equivalent system of the New York-New England (NYPS-NETS) interconnected system. A single line diagram of the system is illustrated in Figure 4-11.

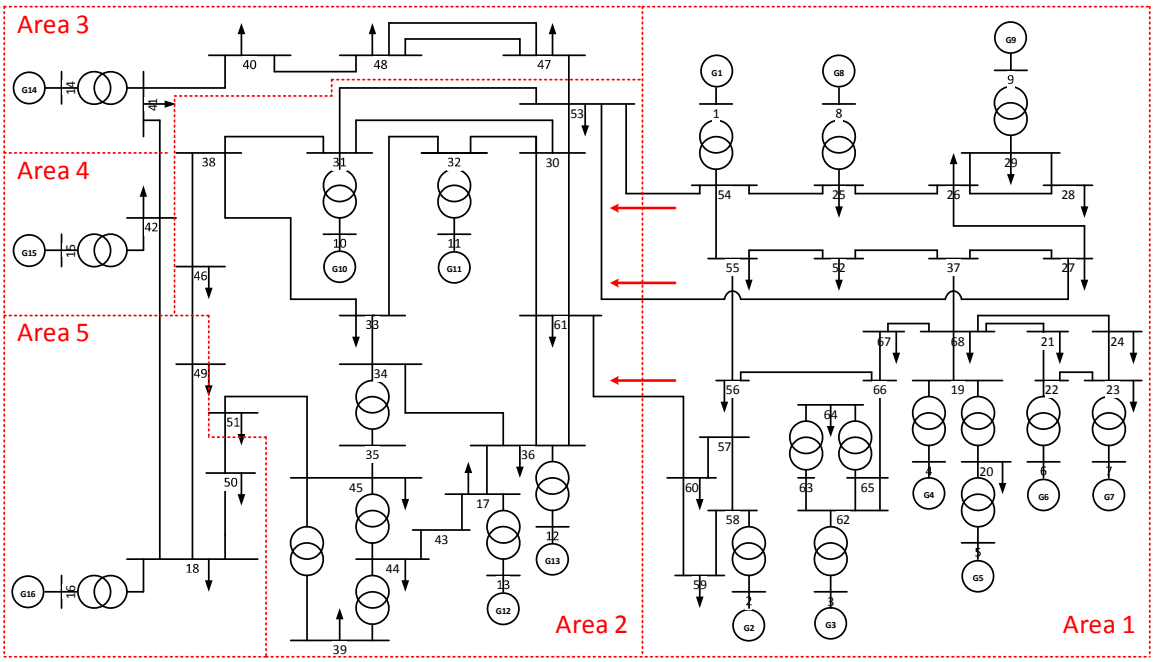

Figure 4-11 Five-area, 16-generator 68-bus system

There are three transmission corridors Line 53-54, Line 53-27 and Line 60-61 between Area 1 and Area 2. Multiple system operating points can be generated by changing the power flows between Area 1 and Area 2 and it is easily achievable through load variations within these two areas. Table 4-8 lists the operating points that have been included in the multi-model system for FACTS damping controller designs.

Table 4-8 Multiple operating points for the five-area system

Operating points	Active power transferred in MW (Area 1 → Area 2)
1	100
2	300
3	500
4	700

PSS are installed on G1-G12 to damp out local oscillations, full details of the five -area system can be found in Appendix B.

4.7.1. Damping Controller Design of TCSC

A TCSC is installed between Bus 18 and 50 to provide 40% line compensation for steady state operation as Line 18-50 is a heavily loaded transmission corridor connecting Area 2 and Area 5. The upper and lower boundary of the TCSC compensation level are 50% and 20%.

Eigenvalue Analysis and LMI Pole Placement Region

The five-area system has dozens of local oscillatory modes, however, the local oscillation problems are not our concern as they already have been properly addressed with the installation of PSSs. In the following designs, the main attention will be focused on the damping of inter-area oscillatory modes.

Table 4-9 shows the dominant inter-area oscillatory modes of the open-loop systems with TCSC. It can be seen that there are four weakly damped inter-area oscillatory modes in the five-area system. The damping ratios of these inter-area oscillatory modes are all below 10%, especially the second and fourth mode.

The LMI region, as shown in Figure 4-2, is assigned here for pole placement so that all weakly damped inter-area oscillatory modes can be moved to a region with at least 10% damping ratio through the TCSC damping controller design.

Table 4-9 Inter-area oscillatory modes of the five-area system with TCSC

Operating Points	Mode 1		Mode 2		Mode 3		Mode 4	
	ζ	ω (Hz)	ζ	ω (Hz)	ζ	ω (Hz)	ζ	ω (Hz)
1	7.33%	0.391	2.95%	0.541	8.76%	0.636	3.88%	0.804
2	7.23%	0.390	2.95%	0.540	8.74%	0.632	3.88%	0.804
3	7.13%	0.390	2.96%	0.540	8.68%	0.628	3.88%	0.804
4	7.03%	0.390	2.99%	0.540	8.57%	0.622	3.88%	0.804

Selection of the Feedback Signal

To investigate the mode shapes of the oscillations, participation factors are calculated for each inter-area oscillatory mode. Figure 4-12 shows the participation factors of different generator rotor speeds under operating point 2. From Figure 4-12, it is known that mode 1 is between Area 1, 2 and Area 3, 4, 5; mode 2 is between Area 3 and Area 5; mode 3 is between Area 1, 2 and Area 5; mode 4 is between Area 3, 5 and Area 4. Due to the complexity of the mode shapes, it is difficult to select a feedback signal from generator states simply based on their participation factors. In this case, the candidate feedback signal will be selected from system line currents based on modal residue calculations.

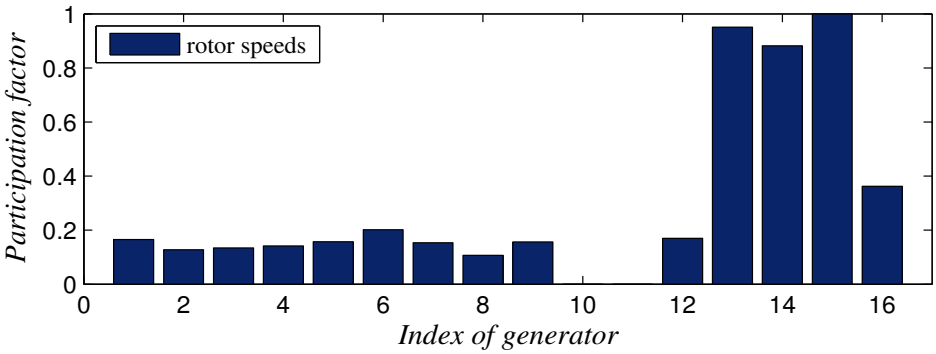

a) Participation factors of inter-area oscillatory mode 1

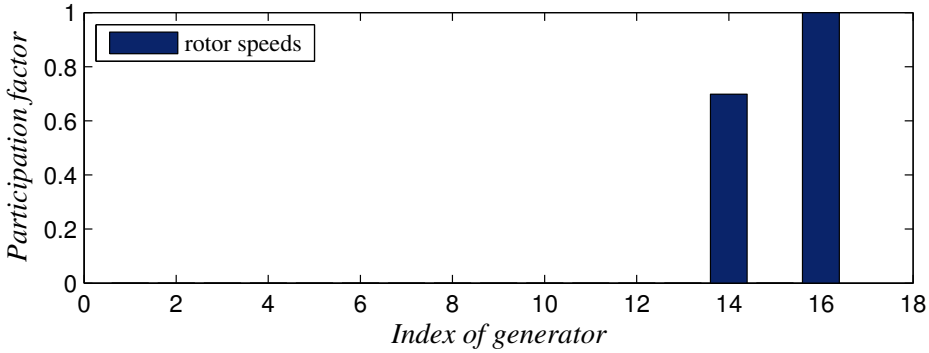

b) Participation factors of inter-area oscillatory mode 2

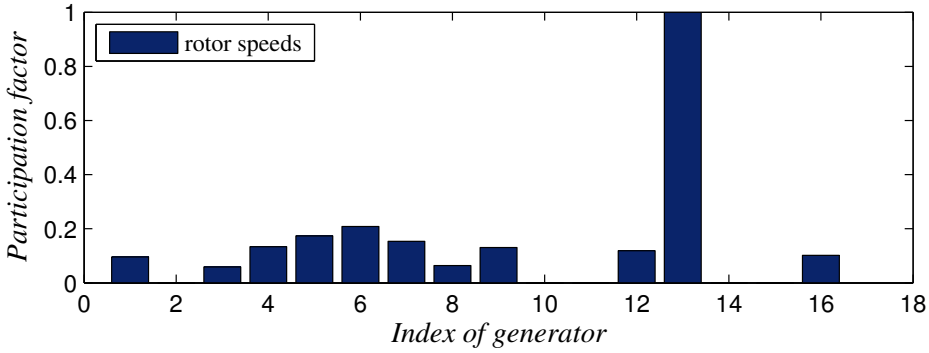

c) Participation factors of inter-area oscillatory mode 3

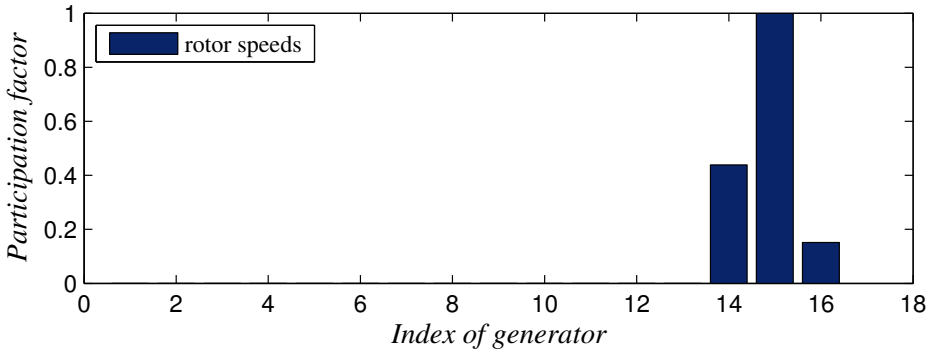

d) Participation factors of inter-area oscillatory mode 4

Figure 4-12 Participation factors of different generators to the inter-area oscillatory modes

Modal residues are calculated for each inter-area oscillatory mode with system outputs of different line currents to compare the observability of each line current signal. The modal residues at operating point 2 are illustrated in Figure 4-13.

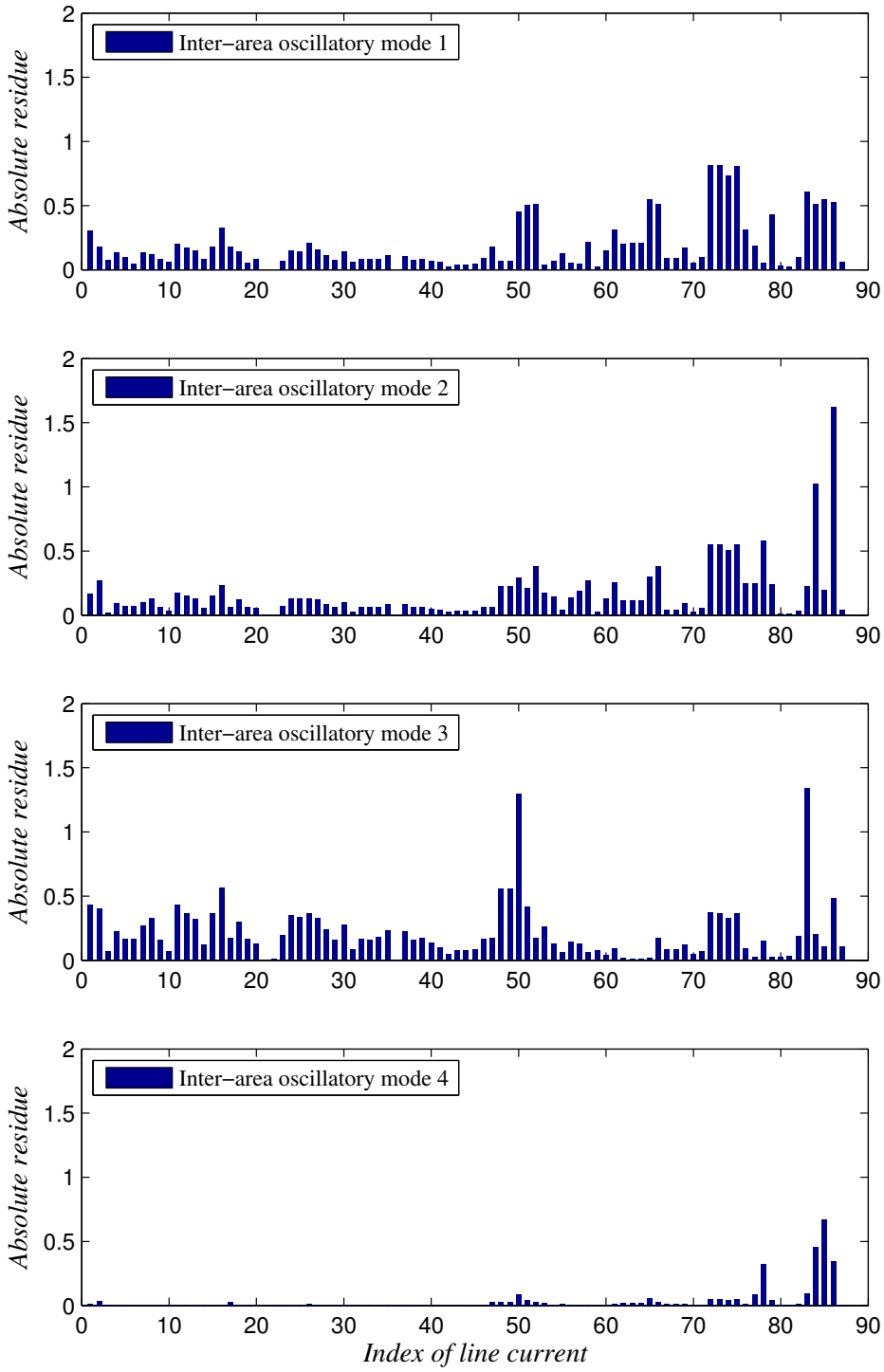

Figure 4-13 Absolute residue values with different line currents as system output

It is expected that the candidate feedback signal would have relatively high residue value upon all four inter-area oscillatory modes; besides, it also should be locally measureable (i.e. the current signal should be close to the TCSC). Thus, the current on Line 75 (Line 50-51, the line adjacent to the TCSC) is selected as the feedback signal for the TCSC damping controller.

Remark: According to Figure 4-13, it is noticed that the current of Line 75 has small contribution to inter-area oscillatory mode 4. This is acceptable since, if the design is a decentralized local control, a single FACTS damping controller might not be able to cover all dominant oscillatory modes of the system. Therefore, the TCSC damping controller design will mainly focus on the damping of the first three inter-area oscillatory modes.

System Order Reduction

The five-area system with TCSC is in the order of 149, balanced truncation model reduction is applied to simplify the system. The reduced system is in the order of 7, and the eigenvalues of the reduced system at operating point 2 are presented in Table 4-10 for validation.

It should be noticed that the order-reduced system only includes the first three inter-area oscillatory modes as the system (with the selected output) has low observability on inter-area oscillatory mode 4 and it is removed in the system order reduction.

Table 4-10 Eigenvalues of the reduced system at operating point 2

Mode Index	Eigenvalues	ζ	ω (Hz)
1	-0.182±2.450i	7.41%	0.392
2	-0.103±3.400i	3.03%	0.541
3	-0.304±3.900i	7.77%	0.622
/	-20.100	/	/

Figure 4-14 illustrates the corresponding frequency responses of the full-order system and

order-reduced system under operating point 2. Obviously, the system order reduction is valid as the order-reduced system is almost identical to the full-order system within the freqeuncy range of our interests.

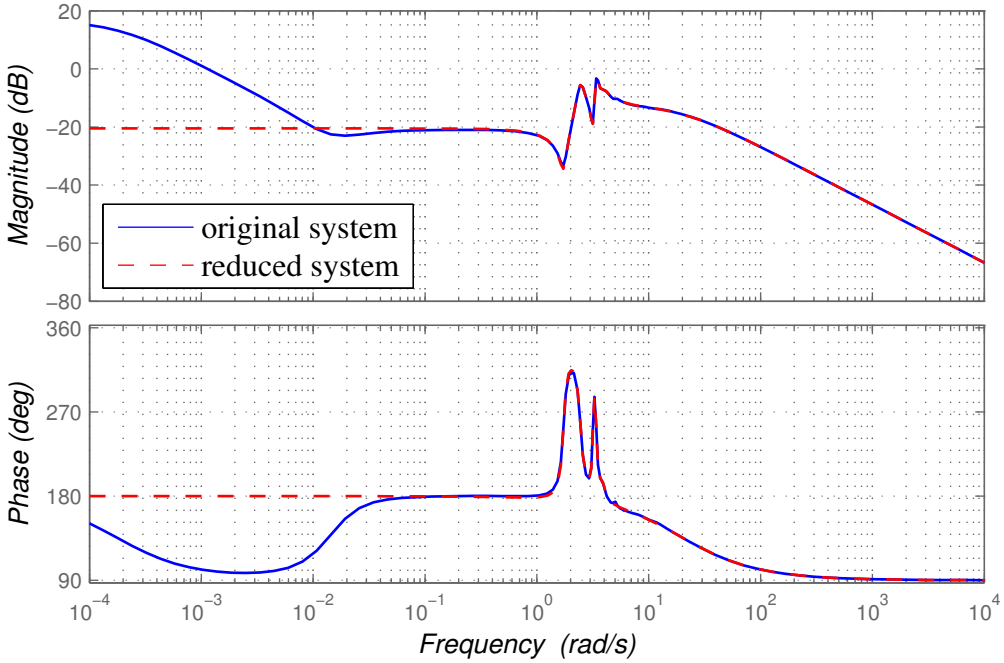

Figure 4-14 Frequency responses: origianl system v.s. reduced system at operating point 2

Forming the State-space Realizations

Similar to the two-area system applications, state-space realizations with augmented H_2 output are formulated for control effort optimization.

Finding the Controller through Two-step Approach

The controller variables A_c, B_c and C_c are systematically determined through the two-step approach:

$$A_c = \begin{bmatrix} -43.32 & -103.15 & -1288.71 & -1657.08 & -11216.36 & -6672.50 & -26940.79 \\ 2.89 & -4.52 & 43.65 & -110.75 & 321.83 & -605.31 & 807.31 \\ 0.19 & 1.91 & 4.33 & 16.29 & 11.99 & 67.52 & -91.13 \\ 0.00 & 0.59 & 1.66 & 12.70 & 5.43 & 62.21 & -13.27 \\ 0.06 & -0.03 & 1.67 & 0.10 & 14.30 & -5.56 & 35.95 \\ -0.02 & -0.07 & -0.48 & -1.33 & -2.68 & -6.03 & -4.47 \\ -0.01 & 0.00 & -0.21 & 0.10 & -1.75 & 1.66 & -4.18 \end{bmatrix} \quad (4.14)$$

$$B_c = \begin{bmatrix} -52.92 & 5.50 & 0.42 & -0.07 & 0.16 & -0.03 & -0.02 \end{bmatrix}^T \quad (4.15)$$

$$C_c = \begin{bmatrix} -1.03 & -21.93 & -45.51 & -455.72 & -328.78 & -2037.71 & 17.97 \end{bmatrix} \quad (4.16)$$

And the controller transfer function $tf(A_c, B_c, C_c, 0)$ is determined as:

$$G_{TCSC}(s) = \frac{-37.87(s^2 + 9.68s - 204.31)(s^2 + 0.88s + 14.73)(s^2 + 0.46s + 6.18)}{(s + 21.42)(s^2 + 4.21s + 10.28)(s^2 + 0.90s + 14.79)(s^2 + 0.20s + 6.52)} \quad (4.17)$$

Linear Close-loop System Performance

Eigenvalue analysis is carried out on the full-order close-loop systems to validate the control performance of the obtained TCSC damping controller (4.17). Figure 4-15 shows the eigenvalue plots of the open-loop system and the close-loop system under operating point 2.

Evidently, the eigenvalues of inter-area oscillatory mode 1, 2 and 3 have been moved to the left side of the 10% damping boundary line; while the eigenvalues of inter-area oscillatory mode 4 remain in the same position.

Table 4-11 presents the inter-area oscillatory modes of the close-loop systems with controller (4.17) under multiple operating points. From Table 4-11, it is confirmed that the obtained TCSC damping controller adequately improves the damping ratios of inter-area oscillatory mode 1, 2 and 3 under all considered operating points. Thus, the proposed TCSC damping controller is

considered to be robust within a certain range of power flow variations (Area 1→Area 2: 100 MW~700 MW).

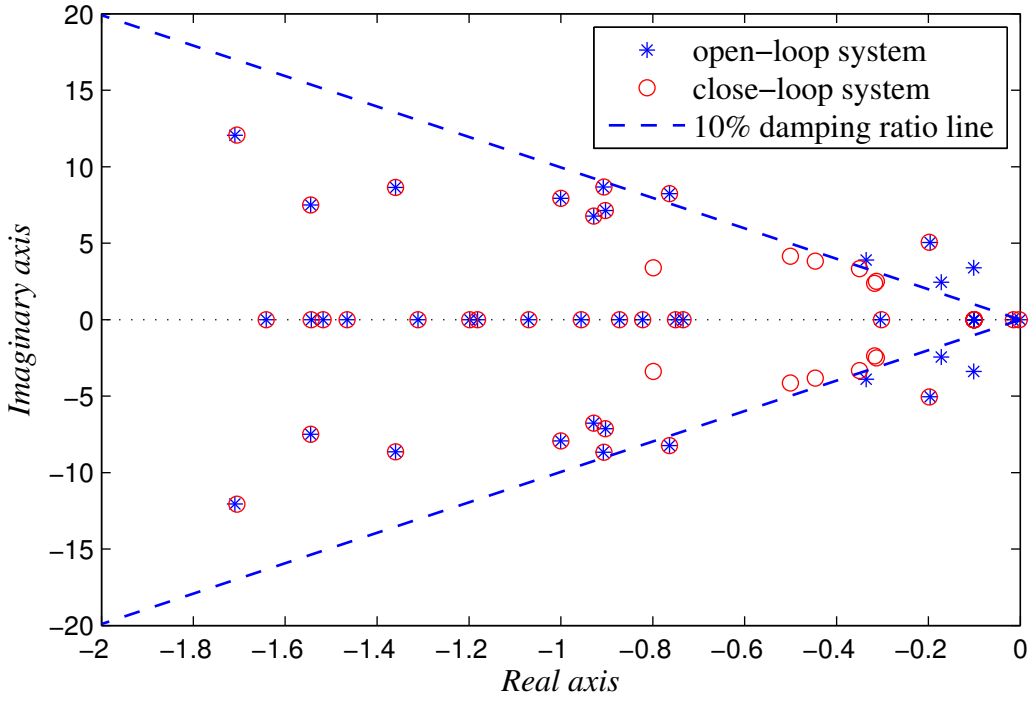

Figure 4-15 Eigenvalue plots: the open-loop system v.s. the close-loop system

Table 4-11 Inter-area oscillatory modes of the close-loop system

Operating points	Mode 1		Mode 2		Mode 3		Mode 4	
	ζ	ω (Hz)	ζ	ω (Hz)	ζ	ω (Hz)	ζ	ω (Hz)
1	**12.8%**	0.401	**10.5%**	0.538	**11.8%**	0.613	3.91%	0.807
2	**12.7%**	0.401	**10.5%**	0.536	**11.8%**	0.613	3.91%	0.805
3	**12.6%**	0.401	**10.4%**	0.535	**11.7%**	0.613	3.91%	0.805
4	**12.4%**	0.403	**10.3%**	0.535	**11.6%**	0.614	3.91%	0.805

4.7.2. Damping Controller Design of SVC

An SVC with the capacity of ±100 Mvar is installed on Bus 18 for voltage regulation so that the bus voltage can be maintained at 1.0 p.u. when large amount of power is injecting from Area 5 to Area 2.

Eigenvalue Analysis and LMI Pole Placement Region

Table 4-12 shows the dominant inter-area oscillatory modes of the open-loop systems with SVC. Similar to the five-area system with TCSC, the system with SVC also has four weakly damped inter-area oscillatory modes; among which, the second and fourth mode are particularly lack of damping. Therefore, the same LMI pole placement region, as shown in Figure 4-2, will be assigned here for the SVC damping controller design.

Table 4-12 Inter-area oscillatory modes of the five-area system with SVC

Operating points	Mode 1		Mode 2		Mode 3		Mode 4	
	ζ	ω (Hz)	ζ	ω (Hz)	ζ	ω (Hz)	ζ	ω (Hz)
1	7.35%	0.376	2.63%	0.530	9.16%	0.629	3.88%	0.802
2	7.23%	0.374	2.63%	0.530	9.14%	0.627	3.88%	0.802
3	7.12%	0.374	2.63%	0.528	9.08%	0.622	3.89%	0.802
4	7.01%	0.374	2.65%	0.528	8.98%	0.618	3.89%	0.802

Selection of the Feedback Signal

Participation factors are calculated to investigate the mode shapes of the inter-area oscillations. Figure 4-16 shows the participation factors of different generator rotor speeds and angles under operating point 2. It can be concluded that inter-area oscillatory mode 1 is between Area 1, 2 and Area 3, 4, 5; inter-area oscillatory the mode 2 is between Area 3 and Area 5; inter-area oscillatory mode 3 is between Area 1, 2 and Area 5; inter-area oscillatory mode 4 is between Area 3, 5 and 4.

In order to find the most suitable feedback signal, modal residues are calculated for each inter-area oscillatory mode with system outputs of different line currents. Figure 4-17 shows the modal residues at operating point 2.

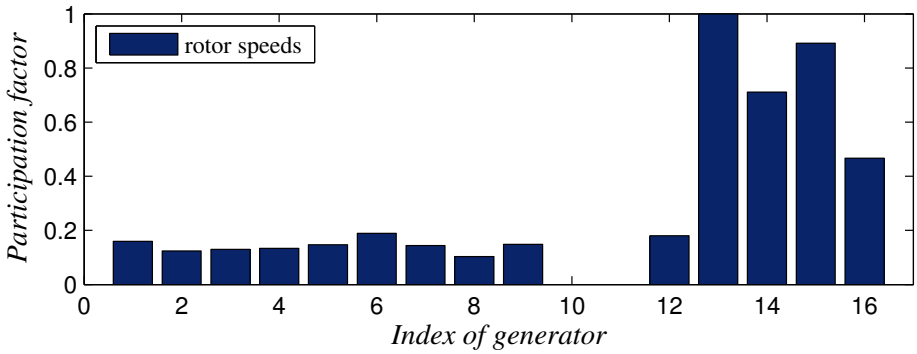

a) Participation factors of inter-area oscillatory mode 1

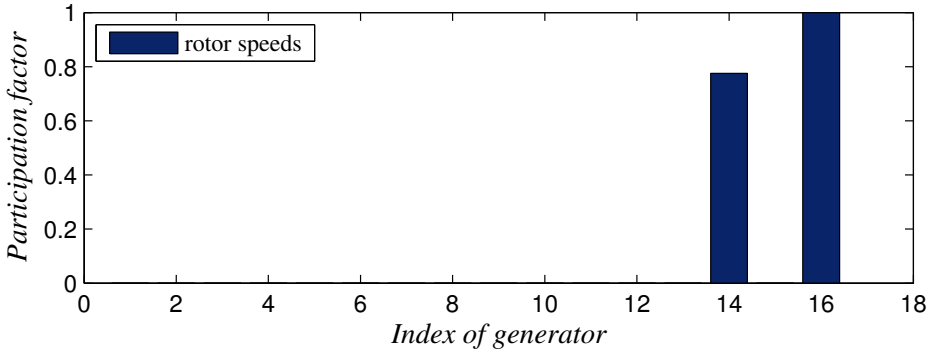

b) Participation factors of inter-area oscillatory mode 2

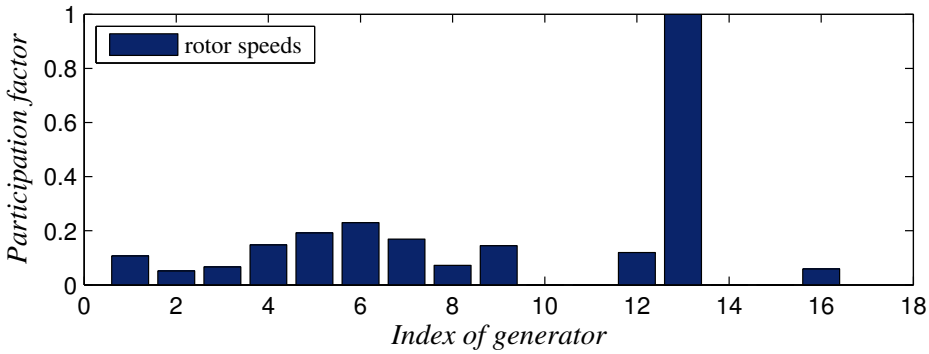

c) Participation factors of inter-area oscillatory mode 3

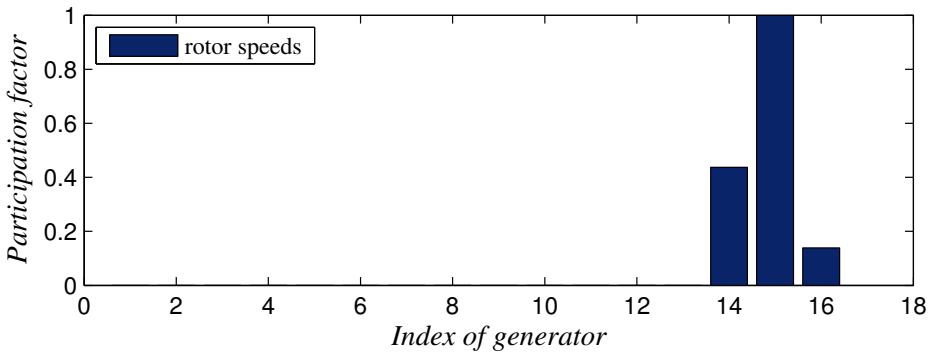

d) Participation factors of inter-area oscillatory mode 4

Figure 4-16 Participation factors of different generators to the inter-area oscillatory modes

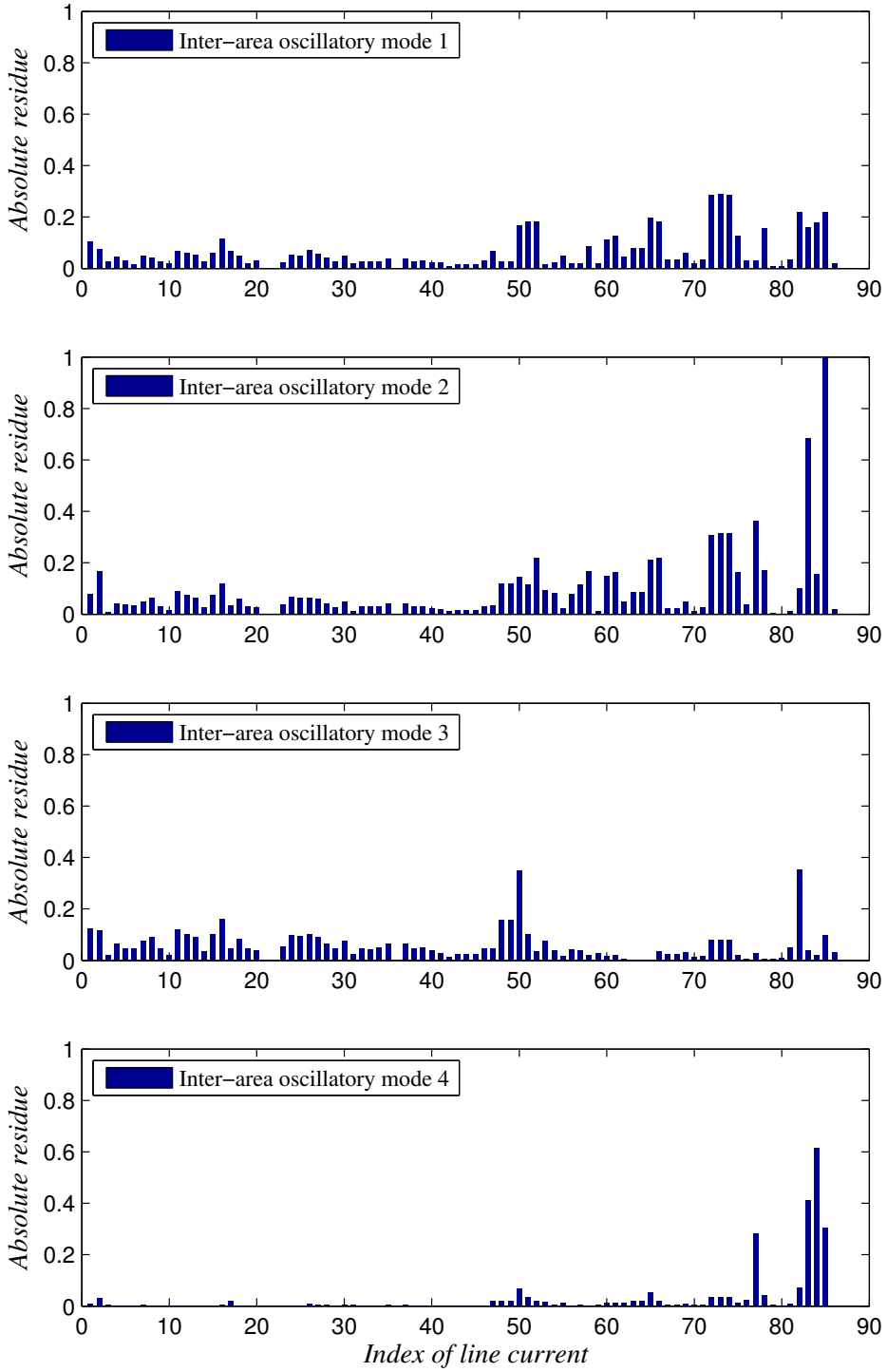

Figure 4-17 Absolute residue values with different line currents as system output

It can be seen from Figure 4-17 that, the SVC installed on Bus 18 has less contribution to the damping of inter-area oscillatory mode 1 and 3 as the absolute residue values for these two modes are relatively low no matter which line current is selected as the output. Therefore, the

damping control will mainly focus on inter-area oscillatory mode 2 and 4.

To this end, the current on Line 85 (Line 16-18) is selected as the feedback signal since it has the highest residue values upon inter-area oscillatory mode 2 and 4 and it is also locally measurable.

Remark: The absolute residue value of the current on Line 85 is 0.025 for inter-area oscillatory mode 3; this indicates that inter-area oscillatory mode 3 is hardly observable with the feedback signal we selected. According to Table 4-12, the damping ratio of inter-area oscillatory mode 3 is relatively high (approximately 9%), thus it is tolerable to not include inter-area oscillatory mode 3 in the pole placement as long as the designed SVC damping controller doesn't cause any deterioration to it.

System Order Reduction

The five-area system with SVC is in the order of 153, balanced truncation model reduction is applied here to simplify the open-loop systems. The simplified system is in the order of 7, and the eigenvalues of the order-reduced systems at operating point 2 are presented in Table 4-13 for validation.

Table 4-13 Eigenvalues of the reduced system at operating point 2

Mode Index	Eigenvalues	ζ	ω (Hz)
/	-1.51	/	/
1	-1.82e-1±2.30i	7.91%	0.368
2	-8.95e-2±3.32i	2.69%	0.528
4	-1.97e-1±5.02i	3.92%	0.799

It can be seen that the order-reduced system includes the information of inter-area oscillatory mode 1, 2 and 4, which coincides with the system modal residue results.

Figure 4-18 illustrates the corresponding frequency responses of the full-order system and the order-reduced system. Apparently, the system order reduction is acceptable as the order-reduced system doesn't lose much information within the frequency range of our interests.

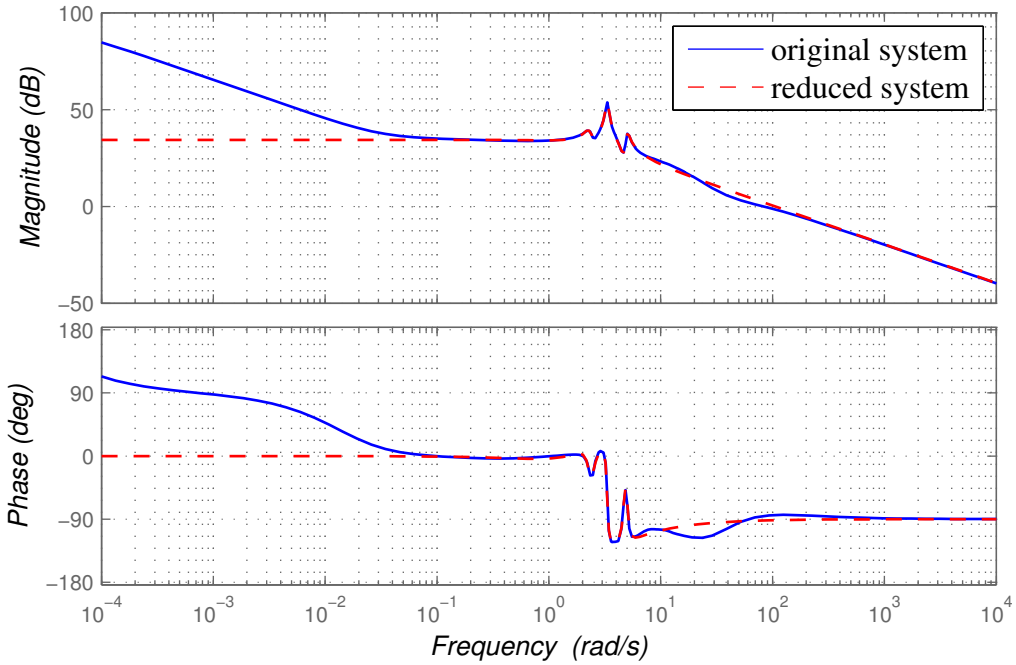

Figure 4-18 Frequency responses: origianl system v.s. reduced system at operating point 2

Forming the State-space Realizations

State-space realizations are formulated in the same way as that has been presented in the previous applications, the H_2 performance will be included here by creating augmented output for control effort optimization.

Finding the Controller through Two-step Approach

The controller variables A_c, B_c and C_c are methodically determined through the two-step approach:

$$A_c = \begin{bmatrix} -1.04 & -54.15 & -56.91 & -912.65 & -1453.50 & -4137.42 & -6702.80 \\ -0.09 & -6.95 & -47.17 & -196.71 & -576.75 & -982.14 & -1769.10 \\ -0.16 & 1.06 & -4.33 & 7.88 & 4.50 & 65.12 & 159.42 \\ 0.04 & 0.26 & 2.86 & 7.13 & 21.70 & 35.04 & 63.15 \\ 0.01 & 0.03 & 0.40 & 1.42 & 1.65 & 0.65 & -2.67 \\ 0.00 & -0.02 & -0.17 & -0.57 & -0.75 & -2.67 & -4.44 \\ 0.00 & 0.00 & -0.03 & -0.07 & -0.19 & 0.73 & -0.09 \end{bmatrix} \quad (4.18)$$

$$B_c = \begin{bmatrix} -2.73 & -0.61 & 0.09 & 1.87e-02 & -2.14e-03 & -1.19e-03 & -1.04e-04 \end{bmatrix} \quad (4.19)$$

$$C_c = \begin{bmatrix} -1.46 & -3.54 & -36.99 & -68.33 & -181.18 & -238.56 & -10.50 \end{bmatrix} \quad (4.20)$$

The controller transfer function $tf(A_c, B_c, C_c, 0)$ is determined as:

$$G_{SVC}(s) = \frac{1.84(s^2 - 0.83s - 3.30)(s^2 + 0.76s + 12.83)(s^2 + 0.48s + 5.54)}{(s + 1.75)(s^2 + 3.03s + 19.40)(s^2 + 1.02s + 14.24)(s^2 + 0.49s + 5.54)} \quad (4.21)$$

Linear Close-loop System Performance

Eigenvalue analysis is conducted on the full-order close-loop systems to validate the control performance of the obtained SVC damping controller (4.21). Figure 4-19 shows the eigenvalue plots of the open-loop system and the close-loop system under operating point 2.

It is obvious that the eigenvalues of the inter-area oscillatory mode 1, 2 and 4 have been moved to the left side of the 10% damping boundary line (or close to the 10% line). It also can be seen that the eigenvalues of inter-area oscillatory mode 3 are already close to the 10% damping line in the open-loop system, and they have been slightly moved towards the 10% damping line in the close-loop system.

Table 4-14 presents the inter-area oscillatory modes of the close-loop systems under multiple operating points. It is clear that the damping ratios of inter-area oscillatory mode 1, 2 and 4

have been improved to a satisfactory level under all considered operating points by the obtained SVC damping controller; besides, the close-loop systems also show slight improvement on inter-area oscillatory mode 3 although it is not covered in the pole placement.

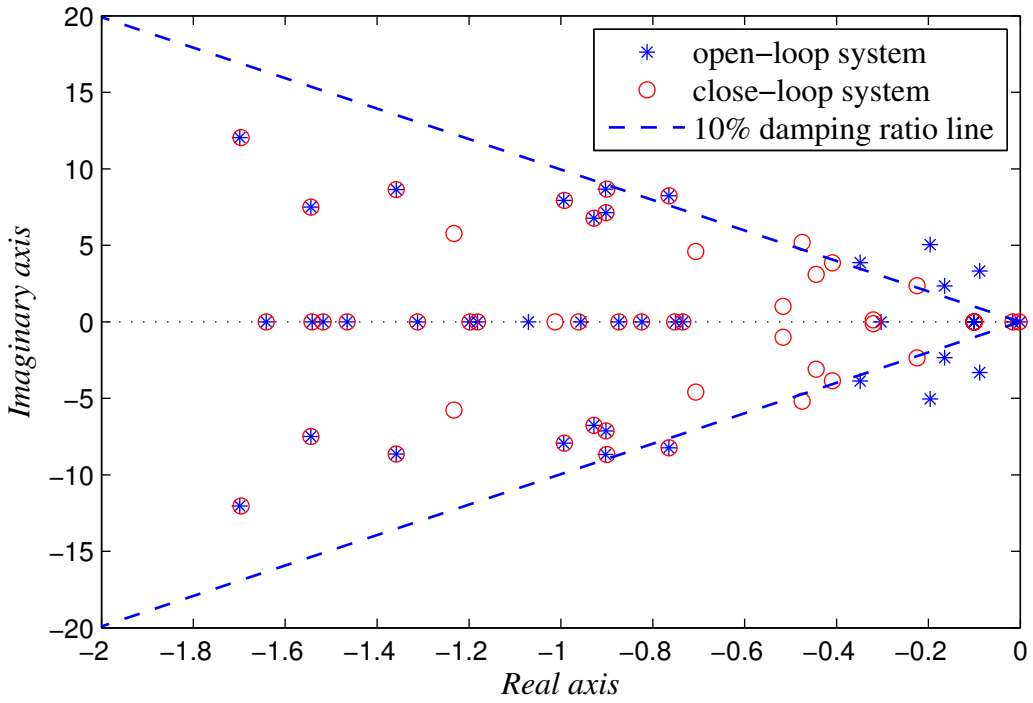

Figure 4-19 Eigenvalue plots: the open-loop system v.s. the close-loop system

Table 4-14 Inter-area oscillatory modes of the close-loop system

Operating points	Mode 1		Mode 2		Mode 3		Mode 4	
	ζ	ω (Hz)	ζ	ω (Hz)	ζ	ω (Hz)	ζ	ω (Hz)
1	**9.64%**	0.374	**13.0%**	0.541	10.6%	0.624	**9.45%**	0.830
2	**9.62%**	0.374	**13.0%**	0.541	10.5%	0.621	**9.42%**	0.830
3	**9.61%**	0.374	**13.1%**	0.541	10.4%	0.618	**9.39%**	0.828
4	**9.62%**	0.372	**13.2%**	0.539	10.2%	0.613	**9.36%**	0.828

4.7.3. Simulation Case Studies

Real-time simulations are carried out on RTDS to evaluate the performance of the obtained

TCSC and SVC damping controllers. The controllers are tested under different system operating scenarios with two types of disturbances: excitation system disturbance and system line outage. Wash-out filters are installed for each FACTS damping controller.

Case 1: Excitation System Disturbance

In this case, the controllers are tested under small excitation system disturbance. The disturbance is generated by giving a small impulse on the excitation system voltage reference V_{ref} at G13. The small impulse raises the magnitude of V_{ref} from 1.01 p.u. to 1.05 p.u. for 200ms. The power flow responses on Line 50-51 to the excitation system disturbance are illustrated in Figure 4-20.

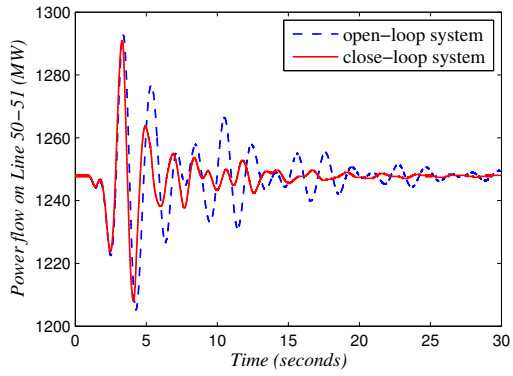

a) System with TCSC at operating point 2

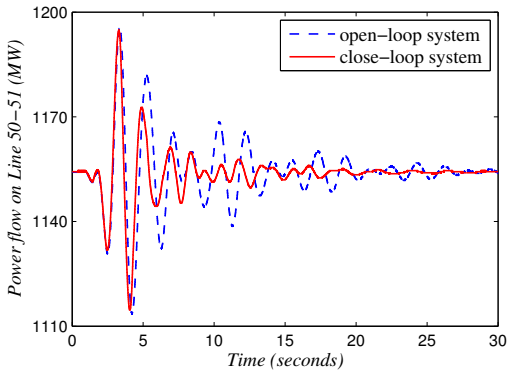

b) System with TCSC at operating point 4

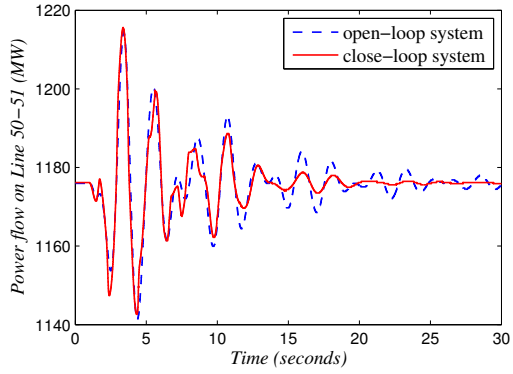

a) System with SVC at operating point 2

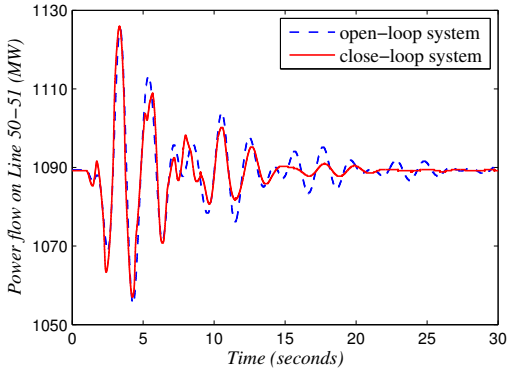

b) System with SVC at operating point 4

Figure 4-20 Power flow responses to excitation system disturbance

Case 2: System Line Outage

In this case, the controllers are tested under disturbance caused by line outage: a three-phase to ground fault occurs on Line 53-27 (one of the three transmission corridors between Area 1 and Area 2), the faulted line is immediately tripped by the protection system and stays outage for the rest of the time. The power flow responses on Line 53-54 and Line 60-61 (the other two transmission corridors between Area 1 and Area 2) after the outage incident are illustrated in Figure 4-21.

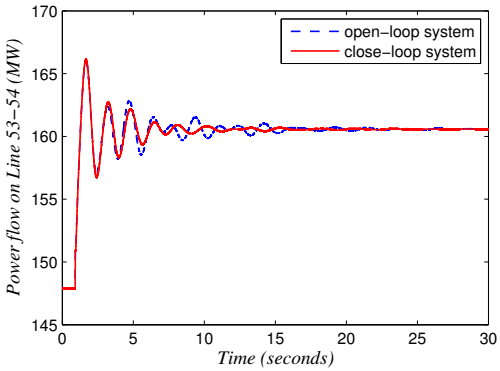

a) System with TCSC at operating point 2

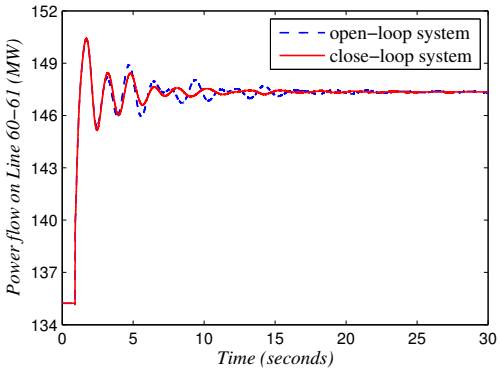

b) System with TCSC at operating point 2

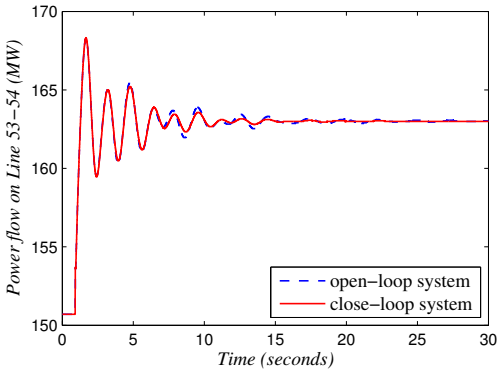

a) System with SVC at operating point 2

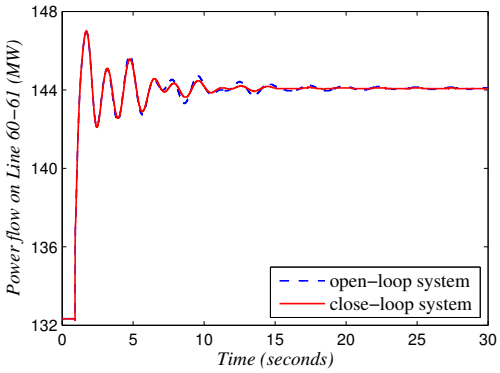

b) System with SVC at operating point 2

Figure 4-21 Power flow responses after Line 53-27 is at outage

Discussion

The simulation results in Figure 4-20 and Figure 4-21 show that the proposed FACTS damping

controllers are robust enough to work under multiple operating points with respect to different types of disturbances. With the proposed FACTS damping controllers, the inter-area oscillations can be effectively suppressed and the system settling time after disturbances can be greatly reduced.

4.7.4. Control Performance: TCSC vs. SVC

The overall performance of a FACTS damping controller is related to many factors such as the installation location of the FACTS, choice of feedback signal, controller design algorithm, etc. In general, it is very hard to judge which type of FACTS device is more effective in inter-area oscillation damping. However, under certain preconditions, such as the TCSC and SVC damping controller designs presented in this chapter, the controllers are comparable in terms of their performance.

According to the linear close-loop system performance as presented in Table 4-11 and Table 4-14, it can be concluded that, for the five-area system applications, the proposed SVC damping controller is superior to the proposed TCSC damping controller as its the overall damping capability is better. This is mainly because the mode that the SVC controller cannot cover already has sufficient damping in the open-loop system, while the mode that the TCSC cannot cover is weakly damped.

However, the real-time simulation results in Figure 4-20 and Figure 4-21 show that the performance of the proposed TCSC and SVC damping controllers is relatively close, where the dominance of the SVC controller is hardly observable. Figure 4-22 shows the susceptance responses of the TCSC and SVC to the excitation system disturbance. It can be seen that that the SVC damping controller actually requires much more control effort than the TCSC damping

controller does to damp out the oscillations due to the fact that TCSC can directly regulate the power flow while SVC cannot. Therefore, the actual damping performance of the SVC is very much limited to its rated capacity. In other words, the controllability of TCSC is considerably better than SVC in low frequency oscillation damping. Furthermore, the SVC damping controller is also limited to system load types and is not recommended for systems with constant power loads in real practice as the modulation of bus voltage may bring adverse effects to the loads.

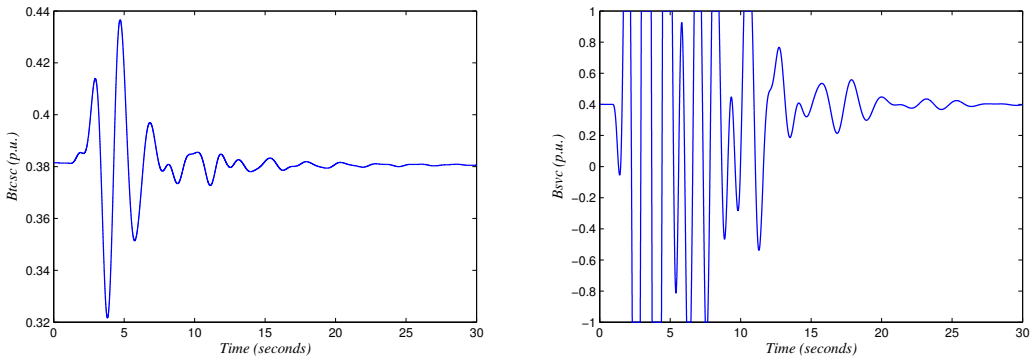

a) TCSC b) SVC

Figure 4-22 Susceptance of the TCSC and SVC after excitation disturbance

4.7.5. Control Performance: Multi-Model Approach vs. Nominal Model Approach

As most of the conventional robust damping control approaches are nominal model based, it is interesting to make a comparison of damping control performance between the nominal modal system approach (as elaborated in Chapter 3) and the proposed multi-model system approach.

From Table 4-9 and Table 4-12, it is known that the four system operating points included in the multi-model system are actually quite close to each other although the power flow exchange between Area 1 and 2 varies a lot (from 100MW to 700MW). To further distinguish the operating points from one to another, the active power generations of Area 3 and 5 will be

accordingly changed. And the new multi-model system is formulated based on the operating points listed in Table 4-15.

Table 4-15 Multiple operating points for FACTS damping controller designs

Operating points	TCSC	SVC
	Active power generated by G16 in MW	Active power generated by G14 in MW
Nominal	3500	1785
Off-nominal	4000	1485

In the controller design stage, the nominal operating point is used in the conventional nominal modal system approach, while both nominal and off-nominal operating points are used in the multi-model system approach.

Control Performance with TCSC

Table 4-16 - Table 4-18 present the dominant inter-area oscillatory modes of the open-loop system and the close-loop systems with two different TCSC damping controllers.

Table 4-16 Inter-area oscillatory modes of the open-loop system with TCSC

Operating points	Mode 1		Mode 2		Mode 3		Mode 4	
	ζ	ω (Hz)	ζ	ω (Hz)	ζ	ω (Hz)	ζ	ω (Hz)
Nominal	7.23%	2.56	3.89%	3.47	8.24%	4.02	3.99%	5.06
Off-nominal	7.23%	2.45	2.95%	3.39	8.74%	3.97	3.88%	5.05

Table 4-17 Inter-area oscillatory modes of the close-loop system with multi-model TCSC damping controller

Operating points	Mode 1		Mode 2		Mode 3		Mode 4	
	ζ	ω (Hz)	ζ	ω (Hz)	ζ	ω (Hz)	ζ	ω (Hz)
Nominal	12.4%	2.49	8.90%	3.48	11.3%	4.23	4.10%	5.08
Off-nominal	**11.8%**	2.66	**11.4%**	3.28	**13.2%**	3.87	4.03%	5.08

Table 4-18 Inter-area oscillatory modes of the close-loop system with nominal model TCSC damping controller

Operating points	Mode 1		Mode 2		Mode 3		Mode 4	
	ζ	ω (Hz)	ζ	ω (Hz)	ζ	ω (Hz)	ζ	ω (Hz)
Nominal	10.8%	2.51	9.06%	3.45	11.5%	3.83	4.04%	5.07
Off-nominal	**9.92%**	2.63	**8.75%**	3.26	**11.5%**	3.85	3.92%	5.07

It can be observed that, under nominal operating point, the damping capabilities of both TCSC damping controllers are relatively close. Meanwhile, the multi-model TCSC damping controller shows great advantage under off-nominal operating point as the damping ratios of inter-area oscillatory mode 1, 2 and 3 have been adequately increased to above 10%. The nominal-model TCSC damping controller shows a certain degree of robustness under off-nominal operating point but its damping capability is relatively weaker than that of the multi-model TCSC damping controller.

Control Performance with SVC

The inter-area oscillatory modes of the open-loop system and the close-loop systems with different SVC damping controllers are presented in Table 4-19, Table 4-20 and Table 4-21.

Table 4-19 Inter-area oscillatory modes of the open-loop system with SVC

Operating points	Mode 1		Mode 2		Mode 3		Mode 4	
	ζ	ω (Hz)	ζ	ω (Hz)	ζ	ω (Hz)	ζ	ω (Hz)
Nominal	7.23%	2.35	2.63%	3.33	9.14%	3.94	3.88%	5.04
Off-nominal	7.24%	2.46	2.77%	3.39	8.96%	3.97	3.98%	5.06

Table 4-20 Inter-area oscillatory modes of the close-loop system with multi-model SVC damping controller

Operating points	Mode 1		Mode 2		Mode 3		Mode 4	
	ζ	ω (Hz)	ζ	ω (Hz)	ζ	ω (Hz)	ζ	ω (Hz)
Nominal	**10.4%**	2.39	**15.7%**	3.22	11.1%	3.88	**9.96%**	5.250
Off-nominal	**10.3%**	2.49	**14.2%**	3.31	11.0%	3.91	**10.0%**	5.26

Table 4-21 Inter-area oscillatory modes of the close-loop system with nominal model SVC damping controller

Operating points	Mode 1		Mode 2		Mode 3		Mode 4	
	ζ	ω (Hz)	ζ	ω (Hz)	ζ	ω (Hz)	ζ	ω (Hz)
Nominal	**8.98%**	2.35	**12.8%**	3.47	10.3%	3.92	**9.42%**	5.24
Off-nominal	**9.46%**	2.43	**11.7%**	3.46	10.3%	3.95	**9.19%**	5.29

It can be seen that the multi-model SVC damping controller shows better damping capability under both nominal and off-nominal operating points.

4.8. Summary

In this chapter, the designs of robust TCSC and SVC damping controllers were presented. The controller designs were successively implemented on a two-area system and a five-area system to explore the generality and feasibility of the BMI-based multi-objective multi-model system approach that had been proposed in Chapter 3. To ensure the effectiveness of designs, investigations were also carried out in the aspect of feedback signal selection and system order reduction.

The damping performance of the obtained robust TCSC and SVC damping controllers were firstly evaluated through full-order linear close-loop system eigenvalue analyses. The corresponding numerical results indicated that the proposed method was not only effective but also robust as the damping ratios of the objective inter-area oscillatory modes were adequately improved under all considered system operating points. Comparisons were also made between the proposed multi-model controllers and conventional nominal model controllers in terms of close-loop system performance. It was clear that the proposed multi-model controllers had better damping performance under off-nominal system operating points.

To further evaluate the performance of the proposed FACTS damping controllers, real-time simulation tests were conducted on RTDS under multiple system operating points with different types of disturbances. The simulation results indicated that the obtained controllers could significantly increase the system damping and reduce the oscillation settling time under different system operating conditions. And it was also known that, the performance of the damping controllers was also bounded by the capacity of the FACTS devices. In the five-area system applications, the SVC obviously required more control effort than the TCSC which could degrade its actual damping capability due to the limitations of its susceptance.

CHAPTER 5 COORDINATED DESIGN OF MULTIPLE FACTS DAMPING CONTROLLERS VIA THE SEQUENTIAL APPROACH

Abbreviations

BMI	Bilinear Matrix Inequality
FACTS	Flexible AC Transmission System
LMI	Linear Matrix Inequality
MIMO	Multiple-Input and Multiple-Output
RTDS	Real-Time Digital Simulator
SISO	Single-Input and Single-Output
SVC	Static VAR Compensator
TCSC	Thyristor Controlled Series Compensator

5.1. Introduction

The robust damping controller designs presented in Chapter 4 concentrated on systems with single FACTS device where the open-loop plants are modelled as SISO systems. For systems

with multiple FACTS devices, it is also possible to develop similar BMI-based robust damping control schemes based on MIMO systems to improve the system damping against inter-area oscillations. This is also known as the coordination damping control of multiple FACTS devices.

Finding an MIMO output-feedback controller for multiple FACTS devices could potentially improve the damping of multiple dominant inter-area oscillatory modes. However, solving the MIMO control problem can be much more difficult regarding multiple control variables; moreover, the MIMO output-feedback controller design, which is inherently centralized, will create strong cross-coupling between multiple inputs and outputs. This could reduce the reliability of the controller as one failure input signal can easily compromise the entire control action. From the security point of view, it is better to have multiple FACTS damping controllers designed in a decoupled manner so that the failure of one controller won't degrade the performance of another.

This chapter presents the coordinated design of multiple FACTS damping controllers via the sequential approach. This approach allows the controllers to be designed sequentially without extra decoupling process. The BMI-based multi-objective multi-model system approach elaborated in Chapter 3 is adopted here for the controller design of each FACTS device. The design is then applied to a five-area system with two FACTS devices (a TCSC and an SVC). Linear system analysis and real-time simulations are finally carried out to investigate the feasibility of the proposed coordination control scheme and the performance of the obtained FACTS damping controllers.

5.2. The Sequential Design Approach

The sequential design approach has been adopted in many research studies regarding different

types of damping control strategies [47, 72, 90], and it is also applicable for the BMI-based multi-objective multi-model system approach. The concept of the sequential design approach is depicted in Figure 5-1.

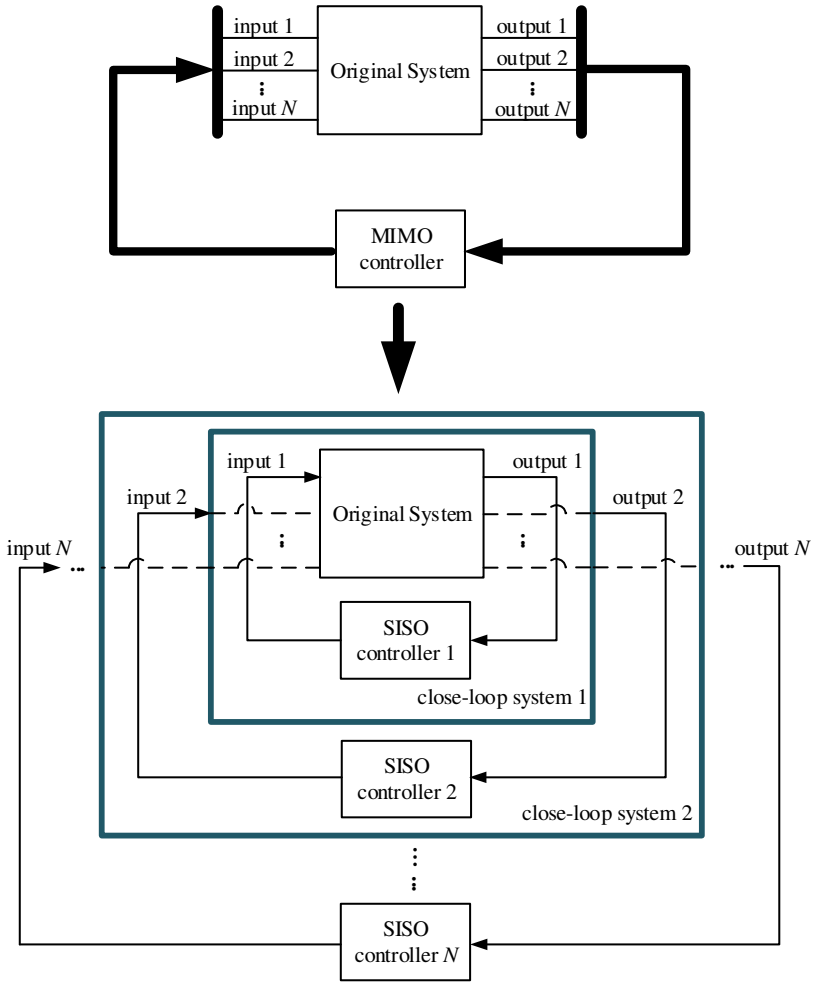

Figure 5-1 Schematic diagram of the sequential approach

Instead of finding a centralized MIMO output-feedback controller, a series of SISO output-feedback controllers are designed sequentially to reduce adverse effect between different FACTS devices (i.e. the next SISO output-feedback controller is designed based on the close-loop system with the previous SISO output-feedback controller). The controller design of each FACTS device follows the same procedures as that has been elucidated in Chapter 4, where

regional pole placement and H_2 performance are simultaneously considered under both nominal and off-nominal operating points.

5.3. Coordinated Design of Robust FACTS Damping Controllers

5.3.1. Test System

The coordinated design in this section involves two FACTS devices: an SVC and a TCSC. The five-area, 16-generator 68-bus system in Figure 4-11 will be used as the test system. To ensure the robustness of the damping control design, the multi-model system includes two operating points as illustrated in Table 5-1.

Table 5-1 Operating points of the multi-model system

Operating points	Power transfer Area 5 → Area 2 (MW)
Nominal	1150
Off-nominal	1250

Eigenvalue analysis is conducted to investigate the weakly damped inter-area oscillatory modes of the five-area system. The results in Table 5-2 show that the system has four inter-area oscillatory modes, among which, the first, second and fourth mode at around 0.4Hz, 0.5Hz and 0.8Hz are notably lack of damping.

Table 5-2 Inter-area oscillatory modes of the five-area system without FACTS

Operating points	Mode 1		Mode 2		Mode 3		Mode 4	
	ζ	ω (Hz)	ζ	ω (Hz)	ζ	ω (Hz)	ζ	ω (Hz)
Nominal	5.88%	0.40	2.49%	0.55	8.33%	0.65	3.52%	0.81
Off-nominal	5.87%	0.40	2.34%	0.54	8.39%	0.65	3.50%	0.81

The mode shape of each inter-area oscillatory mode is plotted in Figure 5-2 based on the

participation factors of different generator rotor speeds. It is easy to see that mode 1 is between Area 1, 2 and Area 3, 4, 5; mode 2 is between Area 3 and Area 5; mode 3 is between Area 1 and Area 2; mode 4 is between Area 3, 5 and Area 4.

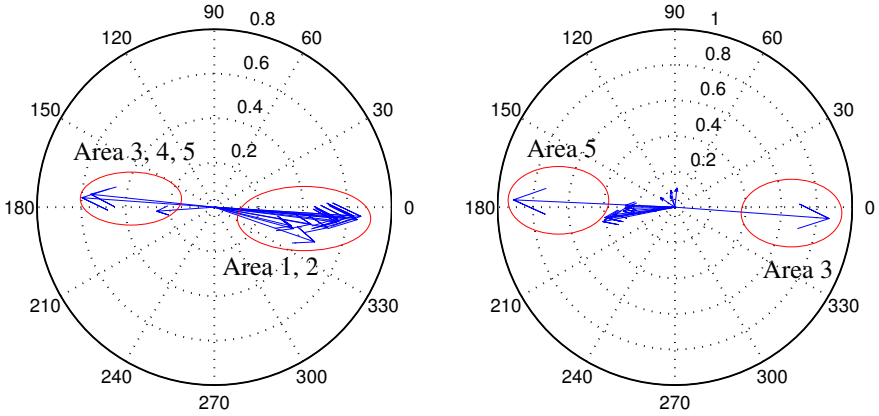

Inter−area oscillatory mode 1

Inter−area oscillatory mode 2

Inter−area oscillatory mode 3

Inter−area oscillatory mode 4

Figure 5-2 Mode shapes of the inter-area oscillatory modes

5.3.2. Installation Locations of FACTS and Choice of Feedback Signals

According to the mode shapes, the four inter-area oscillatory modes can be geographically classified as two types: the modes (mode 1 and 3) highly correlated with Area 1 and 2 and the modes (mode 2 and 4) highly correlated with Area 3, 4 and 5. As the controllability of a certain

FACTS damping controller to a particular inter-area oscillatory mode is usually decided by its installation location, it is presumed that we need at least two FACTS devices to cover the four inter-area oscillatory modes. For the above reasons, a TCSC is installed on Line 53-54 to damp the inter-area oscillatory mode 1 and 3; an SVC is installed on Bus 51 to damp the inter-area oscillatory mode 2 and 4.

The feedback signal for each FACTS damping controller is cautiously selected from signals with invaluable information of the objective inter-area oscillatory modes. A good feedback signal not only increases the feasibility of the design but also reduces the damping control effort. System line current has already been proven to be an effective feedback signal in Chapter 4; it will be used again in the following coordinated designs.

To find the most suitable line current signal, modal residues are calculated for each inter-area modes with different line currents; a higher modal residue value indicates higher observability of a particular inter-area oscillatory mode in the corresponding line current.

Figure 5-3 shows the absolute residue values of different FACTS devices with different line currents. It can be observed that the SVC damping controller has great dominance in the damping of inter-area oscillatory mode 2 and 4 due to high residue values upon these two modes; while, for the same reason, the TCSC damping controller shows great potential for the damping of inter-area oscillatory mode 1 and 3.

Current signals with high residues upon mode 1, 3 and mode 2, 4 will be accordingly selected as the feedback signals for the TCSC and SVC damping controllers; moreover, in order to reduce the adverse interactions between different controllers, the residues of a feedback signal for the modes that the controller not intend to cover should be kept as low as possible.

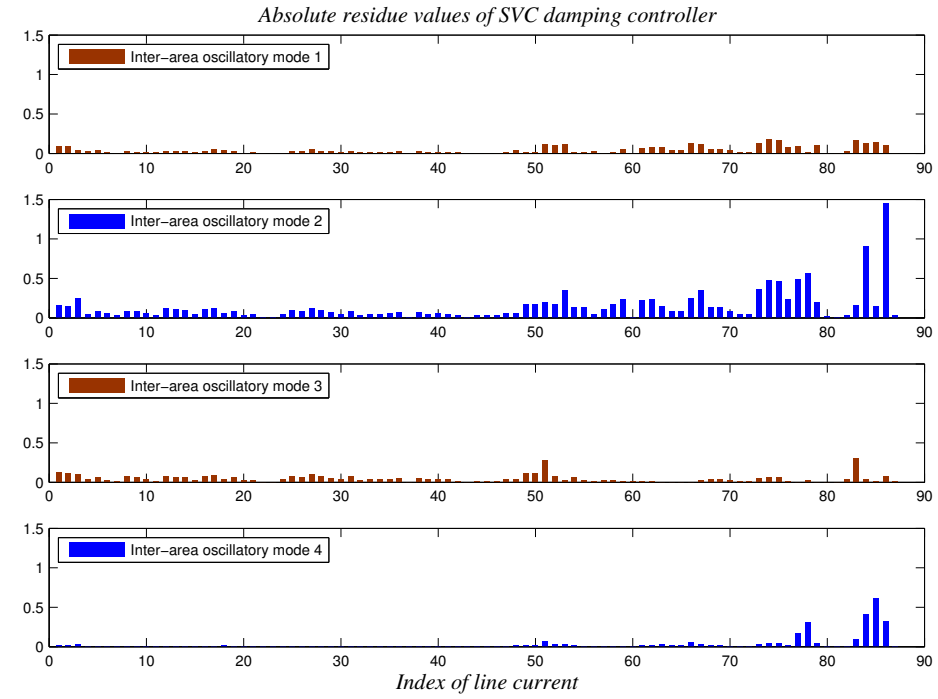

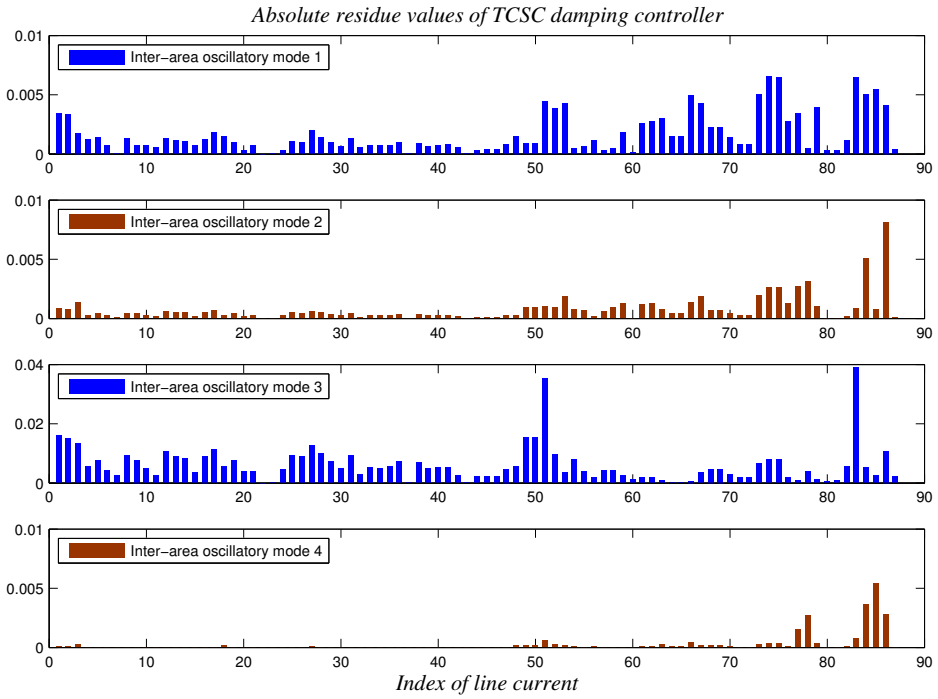

Figure 5-3 Absolute residue values of FACTS damping controllers

As a result, current on Line 86 (Line 16-18) is selected as the feedback signal for the SVC damping controller; current on Line 83 (Line 13-17) is selected as the feedback signal for the TCSC damping controller. With the above selections of feedback signals, the decentralized coordination control is no longer local; however, with the help of wide-area measurement techniques, the control is applicable with remote signals.

5.3.3. Damping Controller Design of SVC

The sequential design approach initially starts with the damping controller design of the SVC. The open-loop system is in the order of 152. Balanced truncation model reduction is employed here to reduce the system to a 7^{th} order system. The eigenvalues presented in Table 5-3, show that the order-reduced system sufficiently captures the damping characteristics of the inter-area oscillatory mode 2 and 4.

Table 5-3 Eigenvalues of the order reduced system

Operating points	Eigenvalues	Damping ratio ζ	Damping frequency ω
Nominal	- 0.216 ± 2.46i	8.75 %	0.39
	- 0.079 ± 3.43i	**2.29 %**	**0.55**
	- 0.185 ± 5.06i	**5.06 %**	**0.81**
	-24.4	/	/
Off-nominal	- 0.230 ± 2.43i	9.43 %	0.39
	- 0.084 ± 3.45i	**2.44 %**	**0.55**
	- 0.175 ± 5.06i	**3.47 %**	**0.81**
	-24.3	/	/

The frequency responses of the full order systems and the order-reduced systems are compared under nominal operating point in Figure 5-4. The bode diagrams show that the system order reduction is adequate as the reduced system doesn't lose much information within the frequency range of our interest.

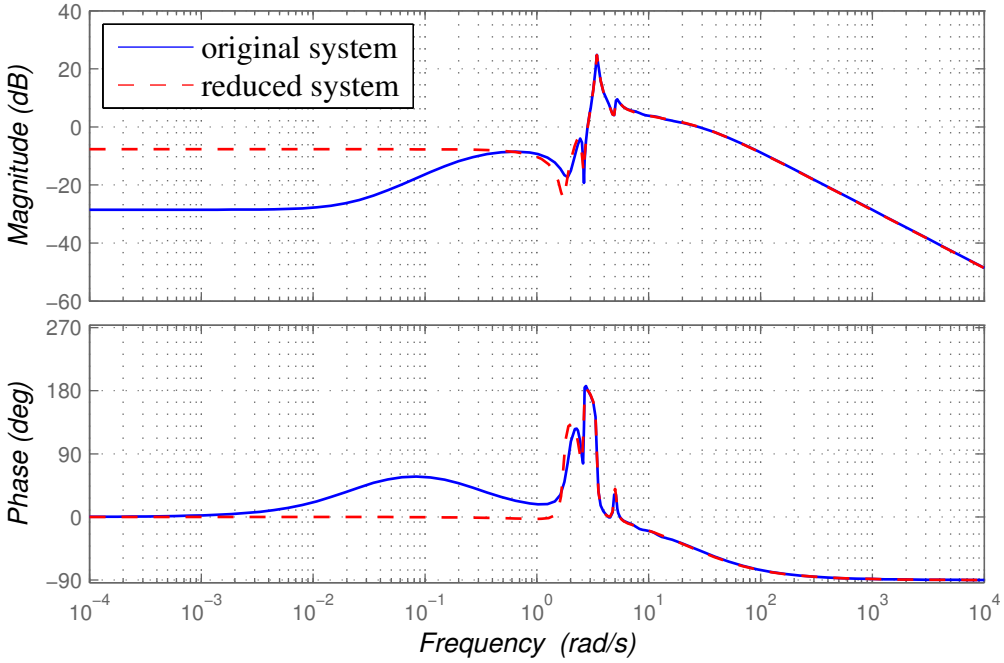

Figure 5-4 Frequency responses: origianl system v.s. reduced system, nominal operating point

State-space realizations are formed with the order-reduced systems to incorporate control effort optimization. The damping ratio boundary for the pole placement is set to 8% to guarantee sufficient damping of the inter-area oscillatory mode 2 and 4 in the close-loop systems.

The output-feedback controller variables are determined systematically through the two-step approach:

$$A_c = \begin{bmatrix} -56.39 & 125.73 & -675.33 & 5341.24 & 16730.74 & 36401.16 & 111023.26 \\ 2.63 & -2.36 & -34.58 & -98.77 & -2147.90 & -985.09 & -11972.27 \\ 1.23 & -4.81 & 7.61 & -191.22 & -526.18 & -1188.30 & -3048.74 \\ -0.26 & 0.96 & 1.01 & 33.04 & 168.09 & 222.50 & 960.91 \\ -0.01 & 0.09 & -0.29 & 3.82 & -2.38 & 15.09 & -11.74 \\ 0.04 & -0.17 & 0.06 & -5.68 & -19.69 & -36.36 & -116.34 \\ -0.01 & 0.03 & 0.02 & 1.12 & 5.00 & 8.38 & 27.62 \end{bmatrix} \quad (5.1)$$

$$B_c = \begin{bmatrix} 3.5110 & -0.2315 & -0.0928 & 0.0235 & 0.0005 & -0.0030 & 0.0006 \end{bmatrix}$$

$$C_c = [-1.19 \quad -30.06 \quad -57.33 \quad -724.15 \quad -452.87 \quad -3261.81 \quad 89.13]$$

And the corresponding controller transfer function is given in (5.2).

$$T_{svc}(s) = \frac{0.8477(s^2 + 4.5564s - 115.1025)(s^2 + 1.6433s + 21.6314)(s^2 + 1.4284s + 7.9315)}{(s + 23.8780)(s^2 + 2.8174s + 24.9007)(s^2 + 1.4407s + 19.2210)(s^2 + 1.0805s + 5.2297)} \tag{5.2}$$

5.3.4. Damping Controller Design of TCSC

With controller (5.2), the feedback loop of the SVC is closed. The sequential design approach then moves on to the TCSC. The open-loop system for the TCSC damping controller design is in the order of 159 (the order of the original system plus the order of the SVC damping controller); it is reduced to a 7th order system by balanced truncation modal reduction. Eigenvalues of the order-reduced system are presented in Table 5-4. It is clear that the order-reduced system has full information on inter-area oscillatory mode 1 and 3. Same conclusion can also be drew from the system frequency responses as illustrated in Figure 5-5.

Table 5-4 Eigenvalues of the order reduced system

Operating points	Eigenvalues	Damping ratio ζ	Damping frequency ω
Nominal	**- 0.148 ± 2.53i**	**5.84 %**	**0.40**
	- 0.395 ± 4.20i	**9.38 %**	**0.67**
	- 0.813 ± 7.90i	10.2 %	1.26
	-29.2	/	/
Off-nominal	**- 0.142 ± 2.55i**	**5.54 %**	**0.40**
	- 0.387 ± 4.21i	**9.17 %**	**0.67**
	- 0.826 ± 7.89i	10.4 %	1.26
	-29.0	/	/

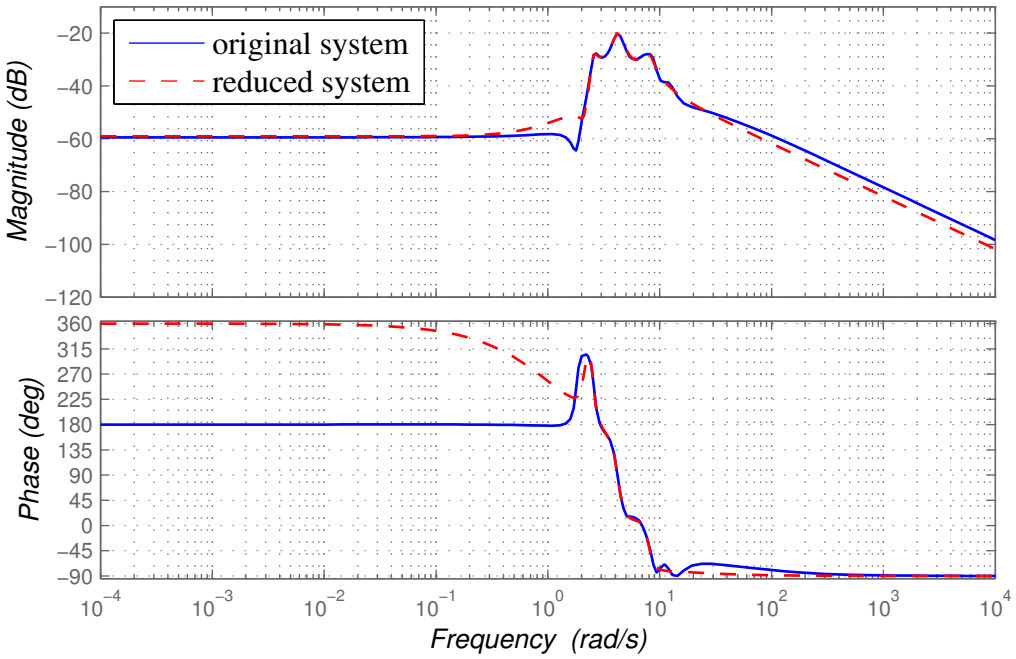

Figure 5-5 Frequency responses: origianl system v.s. reduced system, nominal operating point

A 10% damping ratio boundary is assigned for the pole placement. By means of the two-step method, the output-feedback controller is consequently determined as:

$$A_c = \begin{bmatrix} -5.71 & -98.16 & -395.98 & -2126.05 & -6027.86 & -10775.64 & -20799.08 \\ 0.95 & -0.12 & -3.32 & 7.61 & -37.97 & 6.12 & -228.38 \\ -0.04 & 0.87 & -1.77 & -1.67 & -13.54 & -12.94 & -20.98 \\ 0.00 & 0.01 & 1.31 & -1.11 & 3.62 & -2.81 & 24.07 \\ 0.00 & 0.02 & 0.24 & 1.24 & 1.67 & 1.71 & 1.94 \\ 0.00 & 0.00 & -0.04 & 0.18 & 0.65 & 0.59 & -2.70 \\ 0.00 & 0.00 & -0.04 & -0.05 & -0.28 & 0.70 & -0.38 \end{bmatrix} \tag{5.3}$$

$$B_c = \begin{bmatrix} -1.0438 & 0.9636 & 0.1926 & -0.1073 & -0.0249 & 0.0156 & 0.0032 \end{bmatrix}$$

$$C_c = \begin{bmatrix} -0.43 & -2.21 & -35.85 & -123.32 & -493.71 & -1148.83 & 15.76 \end{bmatrix}$$

And the corresponding controller transfer function is given in (5.4)

$$T_{tcsc}(s)=\frac{-0.9632(s^2-36.1446-33.0655)(s^2+1.2608s+0.3285)(s^2+0.7360s+18.2576)}{(s+0.5067)(s^2+1.6477s+0.6787)(s^2+1.0133s+19.5599)(s^2+1.0042s+6.1391)} \quad (5.4)$$

5.3.5. Linear Close-loop System Performance

The inter-area oscillatory modes of the close-loop systems are compared in Table 5-5 - Table 5-7: It is obvious that the close-loop systems with the TCSC damping controller shows significant damping improvement on mode 1 and 3, while the close-loop systems with the SVC damping controller shows great damping improvement on mode 2 and 4. Moreover, when both FACTS damping controllers are installed, the damping ratios of all inter-area oscillatory modes are increased to a satisfactory level. This indicates that the coordinated design is successful.

Table 5-5 Dominant inter-area modes of the system with SVC damping controller

Operating points	Mode 1		Mode 2		Mode 3		Mode 4	
	ζ	ω (Hz)	ζ	ω (Hz)	ζ	ω (Hz)	ζ	ω (Hz)
Nominal	6.56%	0.40	**10.6%**	0.51	9.60%	0.66	**9.78%**	0.80
Off-nominal	6.22%	0.41	**10.4%**	0.52	9.47%	0.67	**9.14%**	0.81

Table 5-6 Dominant inter-area modes of the system with TCSC damping controller

Operating points	Mode 1		Mode 2		Mode 3		Mode 4	
	ζ	ω (Hz)	ζ	ω (Hz)	ζ	ω (Hz)	ζ	ω (Hz)
Nominal	**12.3%**	0.42	2.38%	0.55	**9.42%**	0.65	3.51%	0.81
Off-nominal	**11.7%**	0.42	2.54%	0.55	**9.36%**	0.66	3.53%	0.81

Table 5-7 Dominant inter-area modes of the system with TCSC and SVC damping controllers

Operating points	Mode 1		Mode 2		Mode 3		Mode 4	
	ζ	ω (Hz)	ζ	ω (Hz)	ζ	ω (Hz)	ζ	ω (Hz)
Nominal	**11.0%**	0.43	**10.8%**	0.51	**10.5%**	0.66	**9.84%**	0.80
Off-nominal	**10.6%**	0.43	**10.5%**	0.51	**10.4%**	0.66	**9.15%**	0.81

Figure 5-6 illustrates the eigenvalue plots of the systems under both nominal and off-nominal operating conditions. It is clear that the coordinated design works adequately fine under both operating points and the eigenvalues of those weakly damped inter-area oscillatory modes have been moved to a region of higher damping ratios.

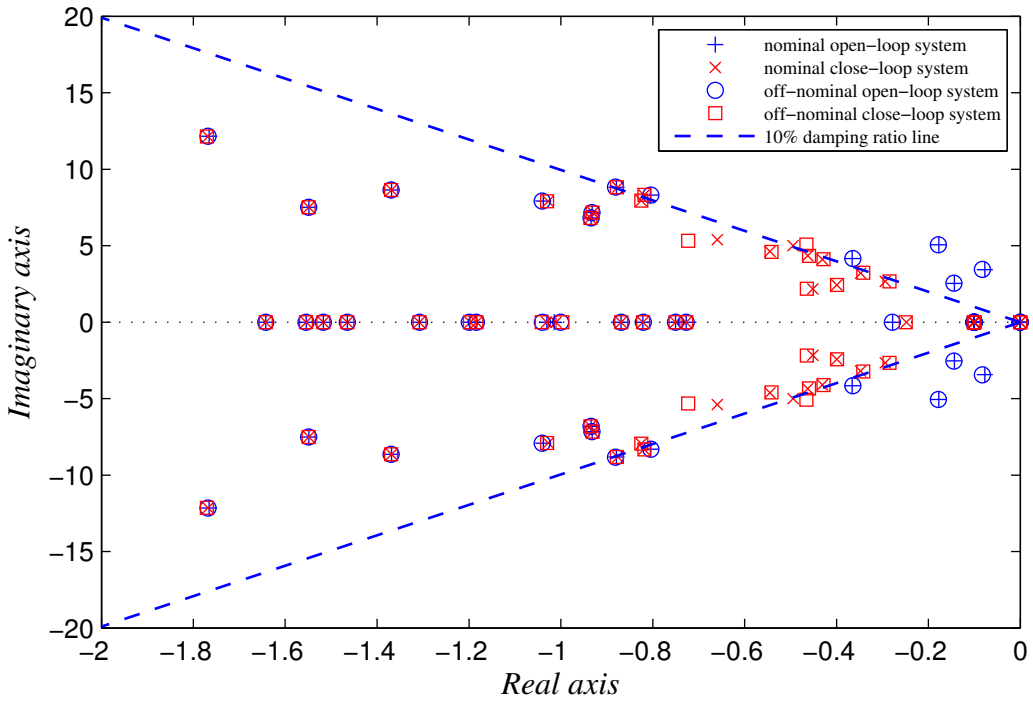

Figure 5-6 Eigenvalue plots: open-loop systems v.s. close-loop systems

5.3.6. Nominal Model Controllers

Under the same system configurations, a SVC damping controller and a TCSC damping controller are sequentially designed based on the nominal operating point in Table 5-1. The controllers are designed in the same sequence with the same control objectives. The optimization problem is solved by MATLAB function *hinfmix*.

The inter-area oscillatory modes of the close-loop systems with nominal model FACTS damping controllers are shown in Table 5-8. Evidently, the nominal model FACTS damping

controllers are able to work under the off-nominal operating point with a certain degree of robustness. However, their damping performance is relatively poor comparing to that of the multi-model FACTS damping controllers.

Table 5-8 Dominant inter-area modes of the system with nominal model damping controllers

Operating points	Mode 1		Mode 2		Mode 3		Mode 4	
	ζ	ω (Hz)	ζ	ω (Hz)	ζ	ω (Hz)	ζ	ω (Hz)
Nominal	**9.83%**	0.43	**9.92%**	0.54	**9.64%**	0.66	**9.00%**	0.83
Off-nominal	**9.41%**	0.43	**9.51%**	0.54	**9.52%**	0.66	**8.19%**	0.82

5.4. Simulation Case Studies

The FACTS damping controllers presented in (5.2) and (5.4) are validated by real-time simulations conducted on the RTDS with the sampling frequency of 15μs.

A wash-out block with the time constant of 10s is added to each controller as a band-pass filter for inter-area oscillation damping. According to [91], the transferring time of the PMU measurement packages varies from several milliseconds to 100ms; hence, delay unit blocks with the time constant of 10s (100ms delay) are added to the feedback signals to simulate the transmission delays of the wide-area remote signals.

System responses are investigated under both nominal and off-nominal operating conditions subject to different types of disturbances: excitation system disturbance, load variation and line outage. The case studies are presented as follows:

5.4.1. Excitation System Disturbance

The disturbance is generated by a small impulse on the excitation system voltage reference. In

this case, the excitation system voltage reference at G14 is raised from 1.01p.u. to 1.10p.u. for 200ms. The corresponding power flow responses at Line 50-51 to the disturbance are illustrated in Figure 5-7 and Figure 5-8.

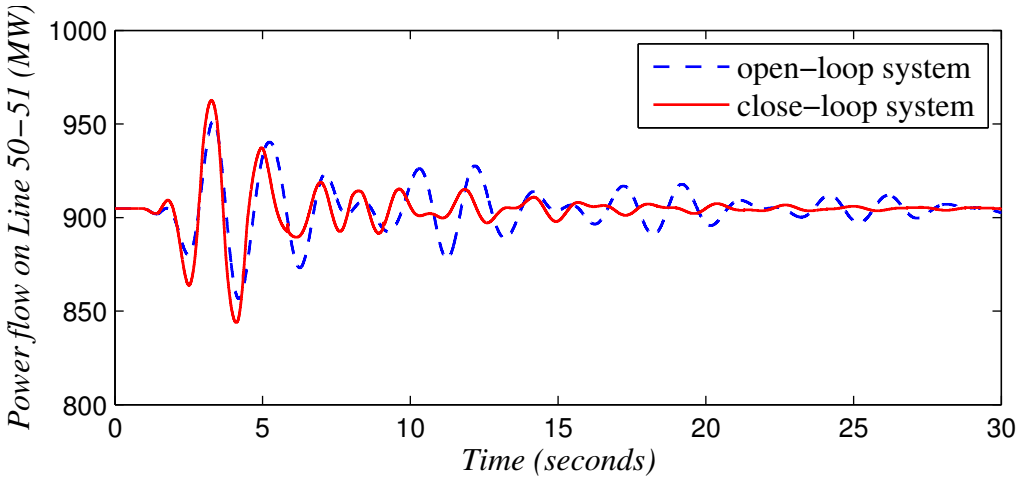

Figure 5-7 Power flow responses to excitation disturbance at nominal operating condition

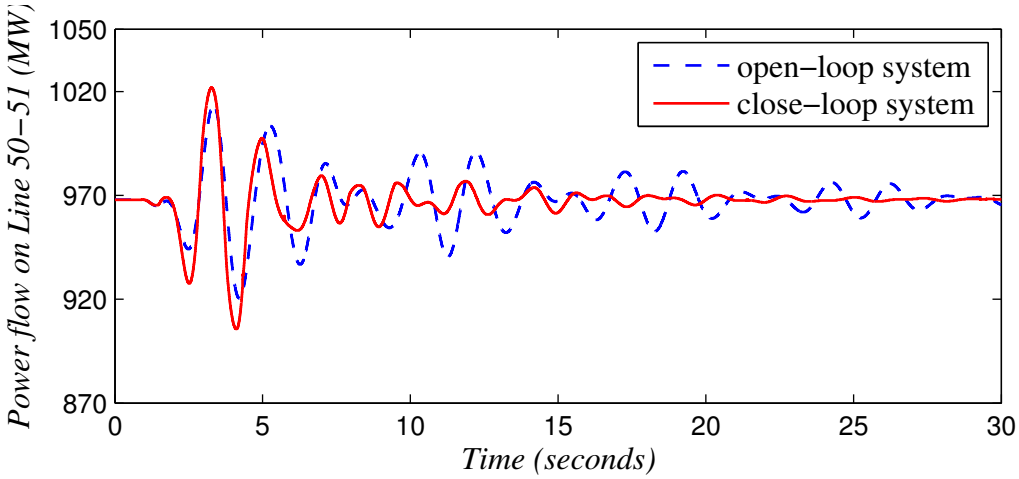

Figure 5-8 Power flow responses to excitation disturbance at off-nominal operating condition

5.4.2. Load Variation

Load variation is a common cause of low frequency oscillation during normal system operations. Figure 5-9 and Figure 5-10 illustrate the power flow responses on Line 41-42 when load at Bus 41 suddenly increases from 800MW to 1000MW.

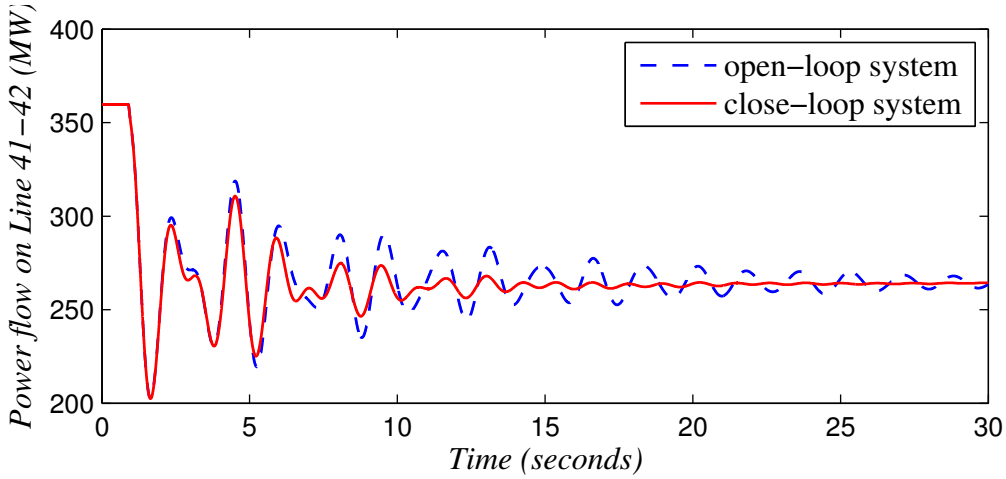

Figure 5-9 Power flow responses to load increasing at nominal operating condition

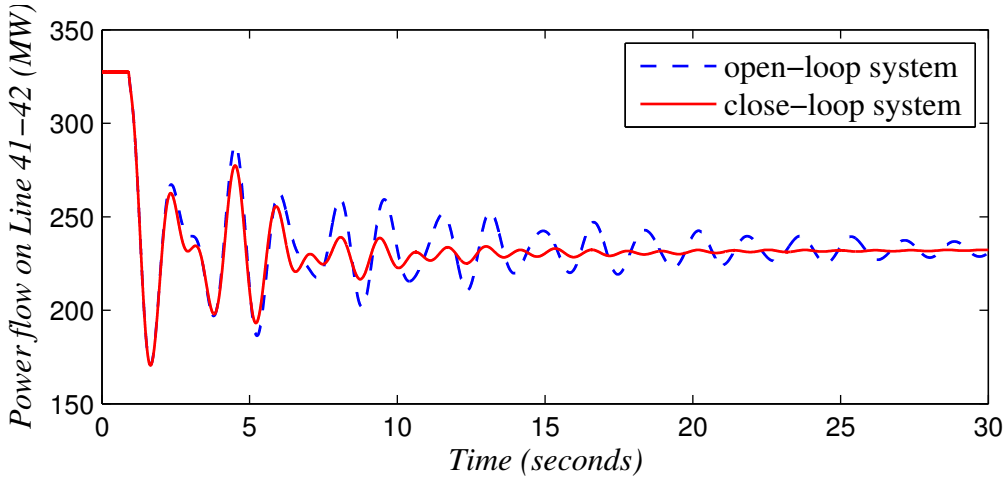

Figure 5-10 Power flow responses to load increasing at off-nominal operating condition

5.4.3. Transmission Line outage

Transmission line outages caused by system faults or maintenance activities are considered to be large disturbances. In this case, a three-phase to ground fault occurs on Line 27-53, the line is tripped immediately after the incident and stays outage for the rest of the time. The corresponding power flow responses on Line 53-54 are illustrated as follows:

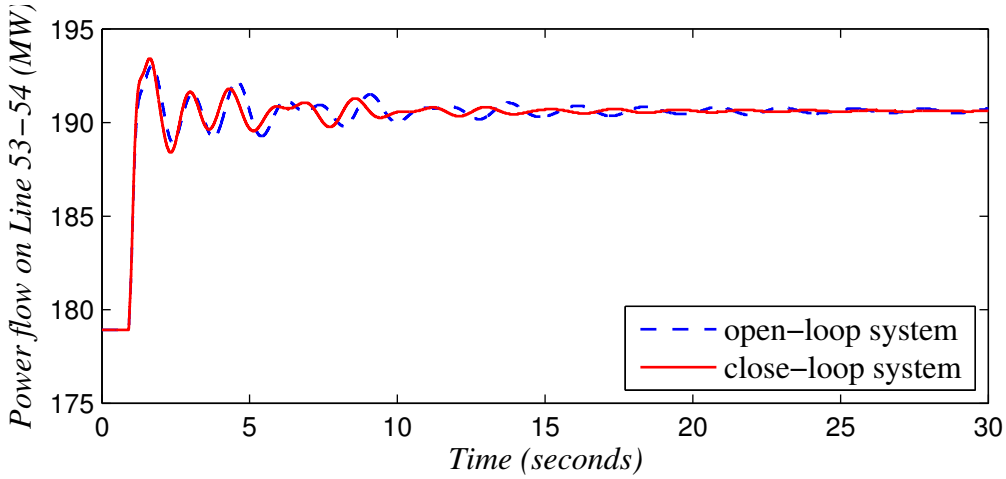

Figure 5-11 Power flow responses to Line 27-53 outage at nominal operating condition

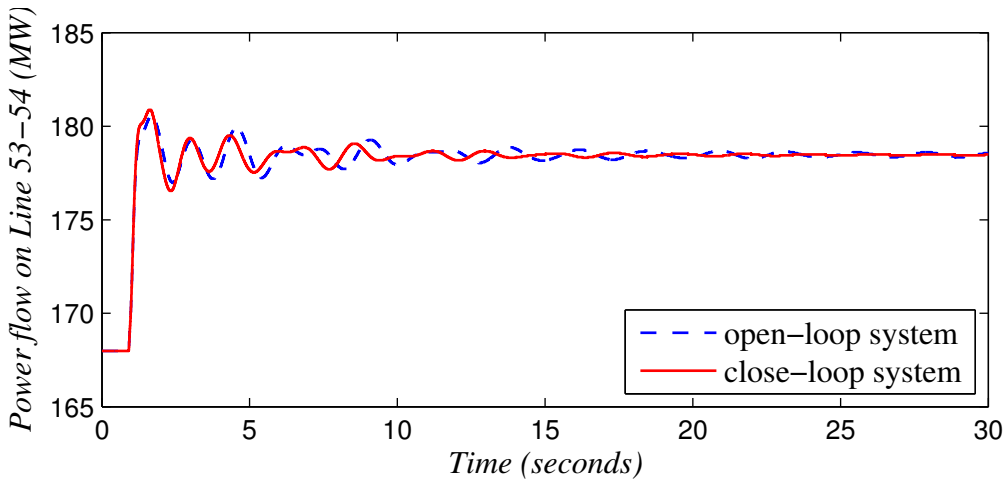

Figure 5-12 Power flow responses to Line 27-53 outage at off-nominal operating condition

The above simulation results show that the coordinated designed FACTS damping controllers are able to provide sufficient damping against inter-area oscillations; the system power flow oscillations aroused by various types of disturbances can be adequately damped out within 15-20 seconds. The controllers also show significant robustness as the damping performance are almost the same under both nominal and off-nominal operating conditions. Besides, the results also indicate that the robust coordinated damping design is compatible with wide-area remote signals, although the transmission delays are not considered in the controller design stages.

5.5. Summary

This chapter presented the coordinated design of multiple FACTS damping controllers. The design could be naturally considered as finding an MIMO output-feedback controller. However, a centralized MIMO design not only increased the computational complexity but also reduced the controller reliability as it could create strong coupling between different feedback signals. To overcome the above difficulties, multiple FACTS damping controllers were designed through a sequential approach: the first controller was designed based on the open-loop system, then the second controller was designed based on the close-loop system with the first controller, and so on. BMI-based multi-objective multi-model system approach was incorporated in each loop of the sequential approach to assure the overall effectiveness and robustness of the coordinated design.

The coordinated design was implemented on a five-area, 16-generator 68-bus system with an SVC and a TCSC. In pursuit of better control performance, wide-area remote signals were selected as feedback signals based on modal residues. The eigenvalue analysis results of the linear close-loop systems clearly showed that the damping ratios of all four inter-area

oscillatory modes were effectively improved with the installation of both FACTS damping controllers. Real-time simulation results demonstrated that the proposed coordinated design had great robustness to work against different disturbances under both nominal and off-nominal operating conditions. Besides, the controllers were also compatible with wide-area remote signals of minor transmission delays.

CHAPTER 6 CONCLUSTION AND FUTURE WORK

6.1. Conclusion

Today, the incremental power electric demand and generation are gradually pushing the existing power transmission system towards its working limits. Reinforcement of the transmission grid is a vital and yet challenging task in consideration of power system operation in the long term. Instead of building new lines, utilization of FACTS devices provides a more cost-efficient solution to the improvement of transmission system capability. Furthermore, the great flexibility and controllability of FACTS are also beneficial for the power system stability operation. This thesis presented the robust damping control of power systems with FACTS for the enhancement of system small-signal stability against low frequency oscillations. The main efforts can be concluded in the following aspects:

1. The small-signal models of the power system with FACTS were presented. In system modelling stage, the electromechanical transient of synchronous generators and FACTS components was sufficiently considered along with the system static power flows. The small-signal dynamics of the entire system was properly linearized and expressed in LTI state-space equations. A multi-model system consisting of a series of linear models under different system

operating points was formed for the robust damping control design.

2. The damping improvement of low frequency oscillations can be attained by designing appropriate supplementary FACTS controllers. The two basic requirements for the FACTS damping controller designs are: *a*) the controller should effectively increase the damping ratio of the weakly damped oscillatory modes; *b*) the controller should be robust against system uncertainties. To satisfy the above requirements, a BMI-based multi-objective multi-model system approach was proposed for the design of FACTS damping controllers. The approach has the following benefits:

1) The control objective of damping improvement is formulated as regional pole placement in BMI constraints and the generalized Lyapunov criterion [77] is used to ensure the close-loop system stability. The BMI-based formulation is straightforward and easy for understanding.
2) Both unstructured and structured system uncertainties can be considered in the problem formulation: For control effort optimization and disturbance rejection (unstructured uncertainties), the minimization of norm bounded sensitivities between disturbance and certain system outputs is adopted and it is formulated as an optimization problem with BMI constraints. Along with the BMI constraints of damping improvement, the robust damping control problem is formulated as a synthesis BMI optimization problem. To assure the robustness under certain off-nominal system operating conditions (structured uncertainties), multiple sets of BMI constraints can be formed with respect to different linear models.
3) The synthesis BMI optimization problem with respect to a nominal model system (single system model under nominal operating point) can be linearized by the

parameterizations of Lyapunov matrix and system matrix variables so it can be solved by convex LMI solvers. But the method is not applicable for a multi-model system as the matrix variables are varying with respect to different system models. To find a common output-feedback controller for a multi-model system, a two-step method is employed here so that the controller parameters can be systematically determined without direct matrix variable parameterizations.

3. The proposed BMI-based multi-objective multi-model system approach has been individually applied to the controller designs of two FACTS devices: a TCSC and an SVC. The designs were successively implemented on a two-area system and a five-area system, where regional pole placement and control effort optimization were simultaneously considered under each selected system operating point.

The feedback signals of the controllers were selected based on participation factors and modal residues. For the two-area system, a combination of two rotor speed deviations with high participation factors to the dominant oscillatory mode was used as the controller input; while for the five-area system, local line current signals with high observability over multiple dominant oscillatory modes were used as the feedback signals. To reduce the computational complexity, optimization was carried out on the order-reduced systems. Therefore, the order of the controllers obtained from BMI optimization was the same as that of the order-reduced systems. However, further reduction could still be applied to the controllers if necessary.

Eigenvalue analysis results of the full-order linear close-loop systems showed that the proposed controllers could adequately improve the damping ratios of one or multiple dominant oscillatory modes under several preselected system operating points. Besides, compared to the controllers designed via the nominal model system approach, the proposed controllers exhibited

better performance especially under off-nominal system operating points. The results also indicated that, for large systems such as the five-area system, one FACTS damping controller might be insufficient to damp out all dominant oscillatory modes. Real-time simulations were conducted on RTDS to evaluate the obtained controllers. The simulation results showed that the controllers were capable of maintaining system performance and stability under different system operating conditions with respect to various types of disturbances.

4. As an extension of the proposed BMI-based multi-objective multi-model system approach, its application to the coordinated design of multiple FACTS robust damping controllers was also explored. The sequential design method was adopted here so that a series of SISO controllers could be designed in a sequence without much cross-coupling between different FACTS devices.

The coordinated design was implemented on a five-area system with an SVC and a TCSC to improve the damping of four weakly damped inter-area oscillatory modes. To reduce the adverse interactions between different FACTS controllers, feedback signals were carefully selected based on modal residue studies. Instead of using local measurable signals, wide-area remote signals were introduced so that each FACTS device could cover two of the four dominant modes.

Eigenvalue analysis results showed that the coordinated design sufficiently improved system damping over four dominant oscillatory modes under all considered system operating points. The control performance of the obtained FACTS damping controllers were validated through real-time simulations on RTDS. Numerical simulation results indicated that the design was successful in terms of effectiveness and robustness.

6.2. Future Work

Based on the work presented in this thesis, future research studies can be carried out in a number of aspects:

1. The real-time simulations used for controller validation were based on detailed models of power system and FACTS devices. From the simulation results, it was known that the controller designs conducted on linear systems with equivalent models of FACTS devices were effective in most of the cases. However, the real-time simulations also revealed the limitation of the prevailing damping control methods based on reduced system models as they might be less effective in real practice because of the system simplification. It is interesting to consider the power system and FACTS models with more details in the controller design stage to further improve the effectiveness of the linear damping controller designs for real power systems.

2. As the synthesis BMI optimization problem is non-convex and systematically solved with Lyapunov matrix partitions in two steps, the obtained solutions can be conservative and may not be locally optimized. Therefore, it is of great interest to explore the possibility of using other algorithms or nonlinear solvers such as PENBMI [92] to find optimal solutions for such problem.

3. In Chapter 5, the simulation results showed that the designed FACTS damping controllers were compatible with remote signals of small time delay (100ms) although the delay was not considered in the design stage. However, for WAMS with sizeable time delay, it is better to have the delay issue properly addressed in the controller designs. As that has been elaborated in [93], the robust damping control problem with time delay could also be formulated using the mixed-sensitivity approach, hence the BMI-based design approach proposed in this study

should also be applicable to the above problem.

4. Compared with the traditional AC transmission systems, the HVDC systems have great benefits in the following aspects [94]: a) lower transmission losses for long distances; b) better interconnection between systems with different voltage levels and frequencies; c) greater controllability on power flows. Furthermore, the VSC-based HVDC systems are able to provide independent control of real and reactive power. As the power flow modulation mechanism of the HVDC systems is very similar to that of FACTS, it is interesting to extend the proposed robust damping control approach to the designs of HVDC supplementary damping controllers. Besides, the proposed coordinated design approach can also be extended to the multi-terminal HVDC systems.

APPENDIX A

Two-area system data

A.1 Generator Parameters

	G1	G2	G3	G4
Rated MVA	900	900	900	900
X_{Li}	0.2	0.2	0.2	0.2
R_{si}	0	0	0	0
X_{di}	1.8	1.8	1.8	1.8
X'_{di}	0.3	0.3	0.3	0.3
X''_{di}	0.25	0.25	0.25	0.25
T'_{doi}	8	8	8	8
T''_{doi}	0.03	0.03	0.03	0.03
X_{qi}	1.7	1.7	1.7	1.7
X'_{qi}	0.55	0.55	0.55	0.55
X''_{qi}	0.25	0.25	0.25	0.25
T'_{qoi}	0.4	0.4	0.4	0.4
T''_{qoi}	0.05	0.05	0.05	0.05
H_i	6.5	6.5	6.175	6.175

A.2 Static AC exciter and PSS Parameters

Static AC exciter				
	G1	G2	G3	G4
K_{Ai}	200	200	200	200
T_{Ai}	0.05	0.05	0.05	0.05

PSS		
	G1	G3
K_{pss}	10	10
T_w	10	10
T_a	0.05	0.05
T_b	0.02	0.02
T_c	0.08	0.08
T_d	0.015	0.015

A.3 Transmission Line Parameters

Line index	From bus	To bus	Resistance (p.u.)	Reactance (p.u.)	Line charging (p.u.)
1	1	5	0	0.0167	0
2	2	6	0	0.0167	0
3	3	10	0	0.0167	0
4	4	9	0	0.0167	0
5	5	6	0.0025	0.025	0.0437
6	9	10	0.0025	0.025	0.0437
7	6	7	0.001	0.01	0.0175
8	8	9	0.001	0.01	0.0175
9	7	8	0.022	0.22	0.3850
10	7	8	0.022	0.22	0.3850

A.4 Generation Parameters

Generator index	Active power (MW)	Reactive power (Mvar)
G1	700	114.3
G2	700	178.4
G3	700	114.3
G4	700	178.4

A.5 Load Parameters

Bus index	Active load (MW)	Reactive load (Mvar)	Reactive compensation (Mvar)
7	1067	100	280
8	1667	100	350

APPENDIX B

Five-area system data

B.1 Generator Parameters

	Rated MVA	X_{Li}	R_{si}	X_{di}	X'_{di}	X''_{di}	T'_{doi}	T''_{doi}	X_{qi}	X'_{qi}	X''_{qi}	T'_{qoi}	T''_{qoi}	H_i
G1	2200	0.0125	0	1.8	0.56	0.45	10.20	0.05	1.24	0.50	0.45	1.50	0.035	2.33
G2	800	0.035	0	1.8	0.43	0.31	6.56	0.05	1.72	0.37	0.31	1.50	0.035	4.95
G3	800	0.0304	0	1.8	0.38	0.32	5.70	0.05	1.71	0.36	0.32	1.50	0.035	4.96
G4	800	0.0295	0	1.8	0.30	0.24	5.69	0.05	1.77	0.27	0.24	1.50	0.035	4.16
G5	700	0.027	0	1.8	0.36	0.27	5.40	0.05	1.69	0.33	0.27	0.44	0.035	4.77
G6	900	0.0224	0	1.8	0.35	0.28	7.30	0.05	1.71	0.32	0.28	0.40	0.035	4.91
G7	800	0.0322	0	1.8	0.30	0.24	5.66	0.05	1.78	0.27	0.24	1.50	0.035	4.33
G8	800	0.028	0	1.8	0.35	0.28	6.70	0.05	1.74	0.31	0.28	0.41	0.035	3.92
G9	1000	0.0298	0	1.8	0.49	0.38	4.79	0.05	1.75	0.43	0.38	1.96	0.035	4.04
G10	1200	0.0199	0	1.8	0.49	0.43	9.37	0.05	1.22	0.48	0.43	1.50	0.035	2.91
G11	1600	0.0103	0	1.8	0.25	0.17	4.10	0.05	1.73	0.21	0.17	1.50	0.035	2.01
G12	1900	0.022	0	1.8	0.55	0.45	7.40	0.05	1.69	0.50	0.45	1.50	0.035	5.18
G13	12000	0.003	0	1.8	0.33	0.24	5.90	0.05	1.74	0.30	0.24	1.50	0.035	4.08
G14	10000	0.0017	0	1.8	0.29	0.23	4.10	0.05	1.73	0.25	0.23	1.50	0.035	3.00
G15	10000	0.0017	0	1.8	0.29	0.23	4.10	0.05	1.73	0.25	0.23	1.50	0.035	3.00
G16	11000	0.0041	0	1.8	0.36	0.28	7.80	0.05	1.69	0.30	0.28	1.50	0.035	4.45

B.2 Static AC exciter and PSS Parameters

Static AC exciter								
	G1	G2	G3	G4	G5	G6	G7	G8
K_{Ai}	100	100	100	100	100	100	100	100
T_{Ai}	0.01	0.01	0.01	0.01	0.01	0.01	0.01	0.01
	G9	G10	G11	G12	G13	G14	G15	G16
K_{Ai}	100	100	100	100	100	100	100	100
T_{Ai}	0.01	0.01	0.01	0.01	0.01	0.01	0.01	0.01

PSS												
	G1	G2	G3	G4	G5	G6	G7	G8	G9	G10	G11	G12
K_{pss}	10	10	10	10	10	10	10	10	10	10	5	11
T_w	10	10	10	10	10	10	10	10	10	10	10	10
T_a	0.1	0.08	0.08	0.08	0.08	0.1	0.08	0.08	0.08	0.1	0.08	0.10
T_b	0.02	0.02	0.02	0.02	0.02	0.02	0.02	0.02	0.02	0.02	0.03	0.02
T_c	0.08	0.08	0.08	0.08	0.08	0.1	0.08	0.08	0.05	0.1	0.05	0.10
T_d	0.02	0.02	0.02	0.02	0.02	0.02	0.02	0.02	0.01	0.02	0.01	0.02

B.3 Transmission line Parameters

Line index	From bus	To bus	Resistance (p.u.)	Reactance (p.u.)	line charging (p.u.)	Tap ratio
1	53	54	0.007	0.0822	0.3493	
2	53	30	0.0008	0.0074	0.48	
3	54	55	0.0013	0.0151	0.2572	
4	54	25	0.007	0.0086	0.146	
5	54	1	0	0.0181	0	1.025
6	55	56	0.0013	0.0213	0.2214	
7	55	52	0.0011	0.0133	0.2138	
8	56	57	0.0008	0.0128	0.1342	
9	56	66	0.0008	0.0129	0.1382	
10	57	58	0.0002	0.0026	0.0434	
11	57	60	0.0008	0.0112	0.1476	
12	58	59	0.0006	0.0092	0.113	
13	58	63	0.0007	0.0082	0.1389	
14	58	2	0	0.025	0	1.070
15	59	60	0.0004	0.0046	0.078	
16	60	61	0.0023	0.0363	0.3804	
17	61	30	0.0019	0.0183	0.29	
18	62	63	0.0004	0.0043	0.0729	
19	62	65	0.0004	0.0043	0.0729	
20	62	3	0	0.02	0	1.070
21	64	63	0.0016	0.0435	0	1.060
22	64	65	0.0016	0.0435	0	1.060
23	65	66	0.0009	0.0101	0.1723	
24	66	67	0.0018	0.0217	0.366	
25	67	68	0.0009	0.0094	0.171	
26	68	37	0	0	0	
27	68	19	0	0	0	

Line index	From bus	To bus	Resistance (p.u.)	Reactance (p.u.)	line charging (p.u.)	Tap ratio
28	68	21	0.0008	0.0135	0.2548	
29	68	24	0.0003	0.0059	0.068	
30	37	52	0.0007	0.0082	0.1319	
31	37	27	0.0013	0.0173	0.3216	
32	19	20	0.0007	0.0138	0	1.060
33	19	4	0.0007	0.0142	0	1.070
34	20	5	0.0009	0.018	0	1.009
35	21	22	0.0008	0.014	0.2565	
36	22	23	0.0006	0.0096	0.1846	
37	22	6	0	0.0143	0	1.025
38	23	24	0.0022	0.035	0.361	
39	23	7	0.0005	0.0272	0	
40	25	26	0.0032	0.0323	0.531	
41	25	8	0.0006	0.0232	0	1.025
42	26	27	0.0014	0.0147	0.2396	
43	26	28	0.0043	0.0474	0.7802	
44	26	29	0.0057	0.0625	1.029	
45	28	29	0.0014	0.0151	0.249	
46	29	9	0.0008	0.0156	0	1.025
47	61	30	0.0019	0.0183	0.29	
48	61	36	0.0022	0.0196	0.34	
49	61	36	0.0022	0.0196	0.34	
50	36	17	0.0005	0.0045	0.32	
51	34	36	0.0033	0.0111	1.45	
52	35	34	0.0001	0.0074	0	0.946
53	33	34	0.0011	0.0157	0.202	
54	32	33	0.0008	0.0099	0.168	
55	30	31	0.0013	0.0187	0.333	
56	30	32	0.0024	0.0288	0.488	
57	53	31	0.0016	0.0163	0.25	
58	31	38	0.0011	0.0147	0.247	
59	33	38	0.0036	0.0444	0.693	
60	38	46	0.0022	0.0284	0.43	
61	46	49	0.0018	0.0274	0.27	
62	53	47	0.0013	0.0188	1.31	
63	47	48	0.0025	0.0268	0.4	
64	47	48	0.0025	0.0268	0.4	
65	48	40	0.002	0.022	1.28	
66	35	45	0.0007	0.0175	1.39	
67	17	43	0.0005	0.0276	0	
68	43	44	0.0001	0.0011	0	

Line index	From bus	To bus	Resistance (p.u.)	Reactance (p.u.)	line charging (p.u.)	Tap ratio
69	44	45	0.0025	0.073	0	
70	39	44	0	0.0411	0	
71	39	45	0	0.0839	0	
72	45	51	0.0004	0.0105	0.72	
73	50	18	0.0012	0.0288	2.06	
74	50	51	0.0009	0.0221	1.62	
75	49	18	0.0076	0.1141	1.16	
76	18	42	0.004	0.06	2.25	
77	42	41	0.004	0.06	2.25	
78	41	40	0.006	0.084	3.15	
79	31	10	0	0.026	0	1.040
80	32	11	0	0.013	0	1.040
81	36	12	0	0.0075	0	1.040
82	17	13	0	0.0033	0	1.040
83	41	14	0	0.0015	0	1.000
84	42	15	0	0.0015	0	1.000
85	18	16	0	0.003	0	1.000
86	53	27	0.032	0.32	0.41	1.000

B.4 Generation Parameters

Generator index	Active power (MW)	Reactive power (Mvar)
G1	250	77.04
G2	545	192.74
G3	650	212.11
G4	632	132.33
G5	505	174.01
G6	700	256.30
G7	560	121.38
G8	540	22.40
G9	800	22.31
G10	500	-0.42
G11	1000	40.31
G12	1350	117.65
G13	4051	862.04
G14	1785	-38.27
G15	1000	68.79
G16	4000	143.55

B.5 Load Parameters

Bus index	Active power (MW)	Reactive power (Mvar)
17	6000.00	300.00
18	2470.00	123.00
20	680.00	103.00
21	174.00	115.00
23	148.00	85.00
25	224.00	47.00
26	139.00	17.00
27	281.00	76.00
28	206.00	28.00
29	284.00	27.00
39	267.00	12.60
40	65.63	23.53
41	1000.00	250.00
42	1150.00	250.00
44	267.55	4.84
45	208.00	21.00
46	150.70	28.50
47	203.12	32.59
48	241.20	2.20
49	164.00	29.00
52	158.00	30.00
53	252.70	118.56
55	322.00	2.00
56	500.00	184.00
59	234.00	84.00
60	522.00	177.00
61	104.00	125.00
64	9.00	88.00
67	320.00	153.00
68	329.00	32.00

LIST OF PUBLICATIONS

[1] J. Deng, X.-P. Zhang and C. Li, "Coordinated Design of Multiple Robust FACTS Damping Controllers: A BMI-based Sequential Approach For Multi-Model Systems," *IEEE Transactions on Power Systems*, 2014, (submitted).

[2] J. Deng and X.-P. Zhang, "Robust Damping Control of Power Systems With TCSC: A Multi-Model BMI Approach With H_2 Performance," *IEEE Transactions on Power Systems*, 2014, DOI: 10.1109/TPWRS.2013.2292067 (accepted for publication).

[3] J. Deng and X.-P. Zhang, "Robust damping control of power system with TCSC using a multi-model system approach," *10th IET International Conference on AC and DC Power Transmission (ACDC 2012)*, Dec. 4-5 2012.

LIST OF REFERENCES

[1] M. Hoel and S. Kverndokk, "Depletion of fossil fuels and the impacts of global warming," *Resource and Energy Economics,* vol. 18, pp. 115-136, 1996.

[2] M. Chino, H. Nakayama, H. Nagai, H. Terada, G. Katata, and H. Yamazawa, "Preliminary estimation of release amounts of 131I and 137Cs accidentally discharged from the Fukushima Daiichi nuclear power plant into the atmosphere," *Journal of nuclear science and technology,* vol. 48, pp. 1129-1134, 2011.

[3] WWEA, "Half-year Report 2011," *The World Wind Energy Association*, 2011.

[4] WWEA, "Half-year Report 2013," *The World Wind Energy Association*, 2013.

[5] RenewableUK, (March 2014), "UK Wind Energy Database Statistics," Available: http://www.renewableuk.com/

[6] ENSG, "Our Electricity Transmission Network: A Vision For 2020," *The Electricity Networks Strategy Group*, 2012.

[7] NGC, "UK Future Energy Scenarios," *National Grid*, 2013.

[8] X.-P. Zhang, C. Rehtanz, and B. Pal, *Flexible AC Transmission Systems: Modelling and Control*, Springer, 2006.

[9] N. G. Hingorani and L. Gyugyi, *Understanding FACTS: Concepts and Technology of Flexible AC Transmission Systems*, Wiley, 2000.

[10] P. Kundur, N. J. Balu, and M. G. Lauby, *Power System Stability and Control*, McGraw-hill, 1994.

[11] G. Rogers, *Power System Oscillations*, Kluwer Academic Publishers, 2000.

[12] K. Prasertwong, N. Mithulananthan, and D. Thakur, "Understanding low-frequency oscillation in power systems," *International Journal of Electrical Engineering Education,* vol. 47, pp. 248-262, 2010.

[13] P. L. Dandeno, A. N. Karas, K. R. McClymont, and W. Watson, "Effect of High-Speed Rectifier Excitation Systems on Generator Stability Limits," *IEEE Transactions on Power Apparatus and Systems,* vol. PAS-87, pp. 190-201, 1968.

[14] F. R. Schleif, H. D. Hunkins, G. E. Martin, and E. E. Hattan, "Excitation control to improve powerline stability," *IEEE Transactions on Power Apparatus and Systems,* pp. 1426-1434, 1968.

[15] G. Berube, L. Hajagos, and R. Beaulieu, "Practical utility experience with application of power system stabilizers," *IEEE PES Working Group Panel Presentation on Power System Stabilizers,* 1999.

[16] F. W. Keay and W. H. South, "Design of a Power System Stabilizer Sensing Frequency Deviation," *IEEE Transactions on Power Apparatus and Systems,* vol. PAS-90, pp. 707-713, 1971.

[17] W. Watson and G. Manchur, "Experience with Supplementary Damping Signals for Generator Static Excitation Systems," *IEEE Transactions on Power Apparatus and Systems,* vol. PAS-92, pp. 199-203, 1973.

[18] E. V. Larsen and D. A. Swann, "Applying Power System Stabilizers Part I: General Concepts," *IEEE Transactions on Power Apparatus and Systems,* vol. PAS-100, pp. 3017-3024, 1981.

[19] P. Kundur, M. Klein, G. Rogers, and M. S. Zywno, "Application of power system stabilizers for enhancement of overall system stability," *IEEE Transactions on Power Systems,* vol. 4, pp. 614-626, 1989.

[20] M. Klein, G. J. Rogers, S. Moorty, and P. Kundur, "Analytical investigation of factors influencing power system stabilizers performance," *IEEE Transactions on Energy Conversion,* vol. 7, pp. 382-390, 1992.

[21] M. Parsa and J. Toyoda, "Implementation of a hybrid power system stabilizer," *IEEE Transactions on Power Systems,* vol. 4, pp. 1463-1469, 1989.

[22] R. Grondin, I. Kamwa, L. Soulieres, J. Potvin, and R. Champagne, "An approach to PSS design for transient stability improvement through supplementary damping of the common low-frequency," *Power Systems, IEEE Transactions on,* vol. 8, pp. 954-963, 1993.

[23] Y. Zhang, O. P. Malik, and G. P. Chen, "Artificial neural network power system stabilizers in multi-machine power system environment," *IEEE Transactions on Energy Conversion,* vol. 10, pp. 147-155, 1995.

[24] G. J. Li, T. T. Lie, C. B. Soh, and G. H. Yang, "Decentralised nonlinear H_∞ control for stability enhancement in power systems," *IEE Proceedings: Generation, Transmission and Distribution,* vol. 146, pp. 19-24, 1999.

[25] H. Quinot, H. Bourles, and T. Margotin, "Robust coordinated AVR+PSS for damping large scale power systems," *IEEE Transactions on Power Systems,* vol. 14, pp. 1446-1451, 1999.

[26] R. Mohan Mathur and R. K. Varma, *Thyristor-Based FACTS Controllers for Electrical Transmission Systems*, Wiley-IEEE Press, 2002.

[27] R. L. Lee, M. J. Beshir, A. T. Finley, D. R. Hayes, J. C. Hsu, H. R. Peterson*, et al.*, "Application of static VAr compensators for the dynamic performance of the Mead-Adelanto and Mead-Phoenix transmission projects," *IEEE Transactions on Power Delivery,* vol. 10, pp. 459-466, 1995.

[28] C. Gama, "Brazilian North-South Interconnection control-application and operating experience with a TCSC," in *1999 IEEE Power Engineering Society Summer Meeting*, vol. 2, pp. 1103-1108 1999.

[29] S. Arabi, H. Hamadanizadeh, and B. Fardanesh, "Convertible static compensator performance studies on the NY State transmission system," in *2002 IEEE Power Engineering Society Summer Meeting*, vol. 1, p. 232 2002.

[30] A. M. Simoes, D. C. Savelli, P. C. Pellanda, N. Martins, and P. Apkarian, "Robust Design of a TCSC Oscillation Damping Controller in a Weak 500-kV Interconnection Considering Multiple Power Flow Scenarios and External Disturbances," *IEEE Transactions on Power Systems,* vol. 24, pp. 226-236, 2009.

[31] L. Tain-Syh, H. Yuan-Yih, G. Tzong-Yih, L. Jiann-Tyng, and H. Chiung-Yi, "Application of thyristor-controlled series compensators to enhance oscillatory stability and transmission capability of a longitudinal power system," *IEEE Transactions on Power Systems,* vol. 14, pp. 179-185, 1999.

[32] Y. N. Yu, *Electric Power System Dynamics*, Academic Press, 1983.

[33] W. G. Heffron and R. A. Phillips, "Effect of a Modern Amplidyne Voltage Regulator on Underexcited Operation of Large Turbine Generators [includes discussion]," *Power Apparatus and Systems, Part III. Transactions of the American Institute of Electrical Engineers,* vol. 71, 1952.

[34] H. F. Wang and F. J. Swift, "A unified model for the analysis of FACTS devices in damping power system oscillations. I. Single-machine infinite-bus power systems," *IEEE Transactions on Power Delivery,* vol. 12, pp. 941-946, 1997.

[35] H. F. Wang, F. J. Swift, and M. Li, "A unified model for the analysis of FACTS devices in damping power system oscillations. II. Multi-machine power systems," *IEEE Transactions on Power Delivery,* vol. 13, pp. 1355-1362, 1998.

[36] H. F. Wang, "A unified model for the analysis of FACTS devices in damping power system oscillations. III. Unified power flow controller," *IEEE Transactions on Power Delivery,* vol. 15, pp. 978-983, 2000.

[37] E. V. Larsen, J. J. Sanchez-Gasca, and J. H. Chow, "Concepts for design of FACTS controllers to damp power swings," *IEEE Transactions on Power Systems,* vol. 10, pp. 948-956, 1995.

[38] N. Yang, Q. Liu, and J. D. McCalley, "TCSC controller design for damping interarea oscillations," *IEEE Transactions on Power Systems,* vol. 13, pp. 1304-1310, 1998.

[39] I. R. Petersen and R. Tempo, "Robust control of uncertain systems: Classical results and recent developments," *Automatica*.

[40] G. Zames, "Feedback and optimal sensitivity: Model reference transformations, multiplicative seminorms, and approximate inverses," *IEEE Transactions on Automatic Control,* vol. 26, pp. 301-320, 1981.

[41] H. Kwakernaak, "Robust control and H_∞ - optimization - Tutorial paper," *Automatica,* vol. 29, pp. 255-273, 3// 1993.

[42] J. C. Doyle, K. Glover, P. P. Khargonekar, and B. A. Francis, "State-space solutions to standard H_2 and H_∞ control problems," *IEEE Transactions on Automatic Control,* vol. 34, pp. 831-847, 1989.

[43] G. N. Taranto, J. K. Shiau, J. H. Chow, and H. A. Othman, "Robust decentralised design for multiple FACTS damping controllers," *IEE Proceedings: Generation, Transmission and Distribution,* vol. 144, pp. 61-67, 1997.

[44] C. Scherer, "The Riccati inequality and state-space H_∞ - optimal control," *Univ. Wnrzburg, Germany,* 1990.

[45] C. Y. Chung, C. T. Tse, A. K. David, and A. B. Rad, "A new H_∞ based PSS design using numerator - denominator perturbation representation," *Electric Power Systems Research,* vol. 52, pp. 37-42, 10/1/ 1999.

[46] B. Pal, "Robust damping of interarea oscillations with unified power-flow controller," *IEE Proceedings: Generation, Transmission and Distribution,* vol. 149, pp. 733-738, 2002.

[47] B. Chaudhuri, B. C. Pal, A. C. Zolotas, I. M. Jaimoukha, and T. C. Green, "Mixed-sensitivity approach to H_∞ control of power system oscillations employing multiple FACTS devices," *IEEE Transactions on Power Systems,* vol. 18, pp. 1149-1156, 2003.

[48] B. Chaudhuri and B. C. Pal, "Robust damping of multiple swing modes employing global stabilizing signals with a TCSC," *IEEE Transactions on Power Systems,* vol. 19, pp. 499-506, 2004.

[49] R. Majumder, B. C. Pal, C. Dufour, and P. Korba, "Design and real-time implementation of robust FACTS controller for damping inter-area oscillation," *IEEE Transactions on Power Systems,* vol. 21, pp. 809-816, 2006.

[50] L. Yong, C. Rehtanz, S. Ruberg, L. Longfu, and C. Yijia, "Wide-Area Robust Coordination Approach of HVDC and FACTS Controllers for Damping Multiple Interarea Oscillations," *IEEE Transactions on Power Delivery,* vol. 27, pp. 1096-1105, 2012.

[51] M. M. Farsangi, Y. H. Song, and M. Tan, "Multi-objective design of damping controllers of FACTS devices via mixed H_2/H_∞ with regional pole placement," *International Journal of Electrical Power & Energy Systems,* vol. 25, pp. 339-346, 2003.

[52] D. McFarlane and K. Glover, "A loop-shaping design procedure using H_∞ synthesis," *IEEE Transactions on Automatic Control,* vol. 37, pp. 759-769, 1992.

[53] Z. Chuanjiang, M. Khammash, V. Vittal, and Q. Wenzheng, "Robust power system stabilizer design using H_∞ loop shaping approach," *IEEE Transactions on Power Systems,* vol. 18, pp. 810-818, 2003.

[54] R. Majumder, B. Chaudhuri, H. El-Zobaidi, B. C. Pal, and I. M. Jaimoukha, "LMI approach to normalised H_∞ loop-shaping design of power system damping controllers," *IEE Proceedings: Generation, Transmission and Distribution,* vol. 152, pp. 952-960, 2005.

[55] B. Chaudhuri, S. Ray, and R. Majumder, "Robust low-order controller design for multi-modal power oscillation damping using flexible AC transmission systems devices," *IET Generation, Transmission & Distribution,* vol. 3, pp. 448-459, 2009.

[56] J. Kennedy and R. Eberhart, "Particle swarm optimization," in *1995 IEEE International Conference on Neural Networks*, vol. 4, pp. 1942-1948, 1995.

[57] D. P. Ke and C. Y. Chung, "An Inter-Area Mode Oriented Pole-Shifting Method With Coordination of Control Efforts for Robust Tuning of Power Oscillation Damping Controllers," *IEEE Transactions on Power Systems,* vol. 27, pp. 1422-1432, 2012.

[58] A. L. B. Do Bomfim, G. N. Taranto, and D. M. Falcao, "Simultaneous tuning of power system damping controllers using genetic algorithms," *IEEE Transactions on Power Systems,* vol. 15, pp. 163-169, 2000.

[59] I. Kamwa, G. Trudel, and L. Gerin-lajoie, "Robust design and coordination of multiple damping controllers using nonlinear constrained optimization," *IEEE Transactions on Power Systems,* vol. 15, pp. 1084-1092, 2000.

[60] Z. Wang, C. Y. Chung, K. P. Wong, and C. T. Tse, "Robust power system stabiliser design under multi-operating conditions using differential evolution," *IET Generation, Transmission & Distribution,* vol. 2, pp. 690-700, 2008.

[61] R. A. Jabr, B. C. Pal, and N. Martins, "A Sequential Conic Programming Approach for the Coordinated and Robust Design of Power System Stabilizers," *IEEE Transactions on Power Systems,* vol. 25, pp. 1627-1637, 2010.

[62] C. Li-Jun and I. Erlich, "Simultaneous coordinated tuning of PSS and FACTS damping controllers in large power systems," *IEEE Transactions on Power Systems,* vol. 20, pp. 294-300, 2005.

[63] R. A. Ramos, L. F. C. Alberto, and N. G. Bretas, "A new methodology for the coordinated design of robust decentralized power system damping controllers," *IEEE Transactions on Power Systems,* vol. 19, pp. 444-454, 2004.

[64] C. F. Xue, X. P. Zhang, and K. R. Godfrey, "Design of STATCOM damping control with multiple operating points: a multimodel LMI approach," *IEE Proceedings: Generation, Transmission and Distribution,* vol. 153, pp. 375-382, 2006.

[65] B. R. Barmish and E. Jury, "New tools for robustness of linear systems," *IEEE Transactions on Automatic Control,* vol. 39, pp. 2525-2525, 1994.

[66] B. R. Barmish, "A generalization of Kharitonov's four-polynomial concept for robust stability problems with linearly dependent coefficient perturbations," *IEEE Transactions on Automatic Control,* vol. 34, pp. 157-165, 1989.

[67] D. D. Simfukwe, B. C. Pal, R. A. Jabr, and N. Martins, "Robust and low-order design of flexible ac transmission systems and power system stabilisers for oscillation damping," *IET Generation, Transmission & Distribution,* vol. 6, pp. 445-452, 2012.

[68] I. Kamwa, R. Grondin, and Y. Hebert, "Wide-area measurement based stabilizing control of large power systems-a decentralized/hierarchical approach," *Power Systems, IEEE Transactions on,* vol. 16, pp. 136-153, 2001.

[69] G. T. Heydt, C. C. Liu, A. G. Phadke, and V. Vittal, "Solution for the crisis in electric power supply," *Computer Applications in Power, IEEE,* vol. 14, pp. 22-30, 2001.

[70] A. C. Zolotas, B. Chaudhuri, I. M. Jaimoukha, and P. Korba, "A Study on LQG/LTR Control for Damping Inter-Area Oscillations in Power Systems," *IEEE Transactions on Control Systems Technology,* vol. 15, pp. 151-160, 2007.

[71] Y. Pipelzadeh, B. Chaudhuri, and T. C. Green, "Control Coordination Within a VSC HVDC Link for Power Oscillation Damping: A Robust Decentralized Approach Using Homotopy," *IEEE Transactions on Control Systems Technology,* vol. 21, pp. 1270-1279, 2013.

[72] B. Pal and B. Chaudhuri, *Robust Control in Power Systems*, Springer, 2005.

[73] P. W. Sauer and A. Pai, *Power System Dynamics and Stability*, Prentice Hall, 1998.

[74] W. Price, C. Taylor, and G. Rogers, "Standard load models for power flow and dynamic performance simulation," *IEEE Transactions on power systems,* vol. 10, 1995.

[75] M. Noroozian, L. Angquist, M. Ghandhari, and G. Andersson, "Improving power system dynamics by series-connected FACTS devices," *IEEE Transactions on Power Delivery,* vol. 12, pp. 1635-1641, 1997.

[76] R. C. Dorf, *Modern control systems*, Addison-Wesley Longman Publishing Co., Inc., 1995.

[77] M. Chilali and P. Gahinet, " H_∞ design with pole placement constraints: an LMI approach," *IEEE Transactions on Automatic Control,* vol. 41, pp. 358-367, 1996.

[78] H. K. Khalil and J. Grizzle, *Nonlinear systems*, Prentice hall 2002.

[79] T. Iwasaki and R. E. Skelton, "All controllers for the general H_∞ control problem: LMI existence conditions and state space formulas," *Automatica,* vol. 30, pp. 1307-1317, 1994.

[80] P. P. Khargonekar and M. A. Rotea, "Mixed H_2/H_∞ control: a convex optimization approach," *IEEE Transactions on Automatic Control* vol. 36, pp. 824-837, 1991.

[81] S. Skogestad and I. Postlethwaite, *Multivariable feedback control: analysis and design*, John Wiley, 2005.

[82] B. D. Anderson and S. Vongpanitlerd, *Network analysis and synthesis: a modern systems theory approach*, Prentice-Hall 1973.

[83] S. Kanev, C. Scherer, M. Verhaegen, and B. De Schutter, "Robust output-feedback controller design via local BMI optimization," *Automatica,* vol. 40, pp. 1115-1127, 2004.

[84] Y.-N. Yu and Q.-h. Li, "Pole-placement power system stabilizers design of an unstable nine-machine system," *IEEE Transactions on Power Systems,* vol. 5, pp. 353-358, 1990.

[85] M. Safonov and R. Chiang, "A Schur method for balanced-truncation model reduction," *IEEE Transactions on Automatic Control,* vol. 34, pp. 729-733, 1989.

[86] K. Zhou, J. C. Doyle, and K. Glover, *Robust and optimal control* vol. 272, Prentice Hall, 1996.

[87] R. Kuffel, J. Giesbrecht, T. Maguire, R. P. Wierckx, and P. McLaren, "RTDS-a fully digital power system simulator operating in real time," in *1995 IEEE Conference Proceedings on Communications, Power, and Computing, WESCANEX 95*, vol. 2, pp. 300-305 vol.2, 1995.

[88] P. Forsyth, T. Maguire, and R. Kuffel, "Real time digital simulation for control and protection system testing," in *2004 IEEE 35th Annual Power Electronics Specialists Conference*, vol. 1, pp. 329-335 Vol.1, 2004.

[89] J. H. Chow, J. J. Sanchez-Gasca, R. Haoxing, and S. Wang, "Power system damping controller design-using multiple input signals," *IEEE Control Systems Magazine,* vol. 20, pp. 82-90, 2000.

[90] D. D. Simfukwe and B. C. Pal, "Robust and Low Order Power Oscillation Damper Design Through Polynomial Control," *IEEE Transactions on Power Systems,* vol. 28, pp. 1599-1608, 2013.

[91] X. Xiong, J. Tan, and X. Lin, "Study on Communication Architecture Design of Wide-Area Measurement System," *IEEE Transactions on Power Delivery,* vol. 28, pp. 1542-1547, 2013.

[92] M. Kocvara, M. Stingl, and P. GbR, *PENBMI user's guide (version 2.0).*

[93] R. Majumder, B. Chaudhuri, B. C. Pal, and Q.-C. Zhong, "A unified Smith predictor approach for power system damping control design using remote signals," *IEEE Transactions on Control Systems Technology* vol. 13, pp. 1063-1068, 2005.

[94] M. P. Bahrman and B. K. Johnson, "The ABCs of HVDC transmission technologies," *IEEE Power and Energy Magazine,* vol. 5, pp. 32-44, 2007.